NUMERICAL ANALYSIS OF THE VIBRATION AND ACOUSTIC CHARACTERISTICS OF LARGE POWER TRANSFORMERS

by

Justin James Case

B Eng (Mech) (Hons), B Bus (Finance)

A dissertation submitted in fulfilment

of the requirements for the degree of

Master of Applied Science (Research)

School of Chemistry, Physics and Mechanical Engineering

Science and Engineering Faculty

Queensland University of Technology

Australia

2017

STATEMENT OF ORIGINAL AUTHORSHIP

The work contained in this thesis has not been previously submitted to meet requirements for an award at this or any other higher education institution. To the best of my knowledge and belief, the thesis contains no material previously published or written by another person except where due reference is made.

QUT Verified Signature

10 February 2017

ABSTRACT

The acoustic emissions of large power transformers, being a source of environmental noise pollution, are of concern to communities living in proximity to power substations. Increasingly stringent noise emission limits are therefore placed on transformers by both regulators and utility operators. However, the absence of adequate modelling tools to predict a transformer's noise levels during the design phase means that consistently meeting acoustic specifications is a significant issue for manufacturers.

This thesis has presented a numerical methodology to identify the vibration characteristics and predict the sound pressure levels of a large power transformer. The methodology involves developing the vibro-acoustic finite element model of a transformer and exciting the model with forces that replicate the excitation mechanisms present in a transformer's active part. The characteristics of the transformer assembly's oscillatory motion resulting from the applied forces are then mapped to an external acoustic body, allowing sound pressure levels to be determined.

It is of note that all key structural and fluid bodies influencing a transformer's vibro-acoustic response have been included in the finite element model presented in this thesis. Structural components within the model therefore included the core, the windings, and the tank of the transformer, as well as parts connecting the aforementioned assemblies. Furthermore, the insulation oil within the transformer and the bi-directional fluid-structure interaction between the active part, the oil and the tank have been considered. Such detailed modelling has enabled the prediction of a transformer's vibration and acoustic response characteristics under nominal operating conditions.

The validation of the vibro-acoustic modelling scheme detailed in this thesis has been conducted with appropriate experimental measurements. Specifically, it has been shown that experimentally determined modal parameters and sound pressure levels are in favourable agreement with numerical results. Contrasting simulated and measured sound pressure levels over a 100 Hz to 400 Hz spectrum has also illustrated that the modelling methodology identifies both the local and global trends in a transformer's acoustic behaviour.

The application of the vibro-acoustic modelling methodology with regard to the computer-aided design of transformers has been presented through a sensitivity analysis. From this analysis it is shown that the acoustic behaviour of a transformer is best optimised by increasing the stiffness of the active part, resulting in a more linear acoustic spectrum and lower sound pressure levels. Furthermore, evaluation methods presented in this thesis, including the study of modal mass participation factors, have allowed for the identification of a transformer's complex vibration characteristics that result in elevated noise levels.

The numerical prediction of a transformer's vibration characteristics and acoustic behaviour together with an understanding of the parameters best suited to optimising a unit's acoustic design will better enable transformer manufacturers to consistently produce transformers that meet acoustic targets. Manufactures will therefore be less likely to incur the significant non-conformity costs that may result from exceeding guaranteed noise levels. The acoustic optimisation of large power transformer designs will also benefit persons working or living in proximity to power substations, reducing the adverse health impacts associated with extended periods of noise exposure.

Keywords: Transformer Noise, Finite Element Method, Vibro-Acoustic Modelling, Fluid-Structure Interaction, Resonance, Modal Mass Participation Factor, Modal Damping, Curve-Fitting, Modal Parameter Extraction

ACKNOWLEDGEMENTS

I am most grateful to my supervisor, Dr. Pietro Borghesani, for his encouragement, interest, stimulus and guidance throughout this project. His initiatives have elevated the standard of this project and his enthusiasm has helped to see it through to completion.

Thanks are due to Mr Helmut Pregartner, the Head of Large Power Transformer Noise and Mechanics R&D at Siemens AG, for his valuable advice and support on various issues. I would also like to thank the other members if the Noise and Mechanics R&D team who have provided insight into the field of interest.

I wish to express my gratitude to Mr Martin Stössl, Mr Gerald Leber and again to Mr Helmut Pregartner who have given me the opportunity to conduct my research within the Large Power Transformer Noise and Mechanics R&D team at Siemens AG. I would also like to extend my thanks to the entire Siemens AG Austria, Transformers Weiz R&D department for providing a simulating and enjoyable work environment.

Special thanks are due to my parents for their support during the course of this work. Without them this thesis would not have been completed.

TABLE OF CONTENTS

LIST OF FIGURES

LIST OF TABLES

NOMENCLATURE

Basic Terms, Dimensions and Subscripts

A	Amplitude ratio
a	Acceleration
B	Magnetic flux density through a unit area
c	Speed of sound in a fluid medium
ex	Experimentally determined value
F	Force
i	$\sqrt{-1}$
J	Electric current density
K	Bulk modulus of a fluid
p	Acoustic pressure
m	Mass
N	Number of degrees of freedom
n	Natural frequency
nu	Numerically calculated value
Q	Mass source applied to an acoustic body
r	Number of rigid body modes
T	Transmissibility of a system
t	Instantaneous time value
δr	Virtual displacement
ϵ	Error percentage

ρ	Fluid density
μ	Dynamic viscosity of a fluid
φ	Phase shift of a waveform
ω	Angular frequency

Matrices, Vectors and Scalars

$[\ ]$	Matrix
$\{\ \}$	Column vector
$[\ ]^T; \{\ \}^T$	Transpose of a matrix; vector
$[\ ]^{-1}$	Inverse of a matrix
$[\ ]^*$	Complex conjugate of a matrix
$[\ ]^\dagger$	Gerenalised/Pseudo inverse of a matrix
$[\ \ \ ]$	Diagonal matrix
$[I]$	Identity matrix
$[\ ]_f$	Matix representing the properties of a fluid
$[\ ]_s$	Matix representing the properties of a solid structure

Spatial and Modelling Properties

$[C]$	Viscous damping matrix
$[K]$	Stiffness matrix
$[M]$	Mass matrix
$[R]$	Coupling matrix at the fluid-structure interface
$[\mathrm{k_r}]$	Modal or generalised stiffness matrix

$[\mathrm{m_r}]$	Modal or generalised mass matrix
$\{N\}$	Element shape function
$\{n\}$	Outward normal vector at the fluid boundary
$\{p_e\}$	Nodal pressure vector
$\{\mathrm{q}\}$	Nodal mass source vector
$\{u\}$	Displacement vector
$\{\dot{u}\}$	Velocity vector
$\{\ddot{u}\}$	Acceleration vector
$\{F\}$	Force vector
α	Mass-proportional damping coefficient
β	Stiffness-proportional damping coefficient
ζ_r	Modal damping ratio of the r^{th}mode
Ω_f	Acoustic domain
Γ_f	Acoustic boundary domain

Frequency Response Properties

$[H(\omega)]$	Frequency response matrix
$[L]$	Displacement of masses matrix
$\{s\}$	Displacement transformation vector
$[\Phi]$	Matrix of mass-normalised eigenvectors
$[\Psi]$	Generalised form of the eigenvector matrix

$X(f)$	Fourier transform of the time signal *x(t)*
$x(t)$	Impulse signal in the time domain
Γ_r	Modal participation factor of the r^{th} mode
ϕ_{jr}	The j^{th} element of the r^{th} eigenvector $\{\phi\}_r$

Abbreviations and Units

AC	Alternating current
CAD	Computer-aided design
dB	Decibel
dB(A)	A-weighted decibel
DOF	Degree of freedom
EMA	Experimental modal analysis
FE	Finite element
FEM	Finite element method
FFT	Fast Fourier transform
FRF	Frequency response function
FSI	Fluid-structure interaction
HEM	Hilbert Envelope Method
IFFT	Inverse fast Fourier transform
IFT	Inverse Fourier transform
IRF	Impulse response function
LTP	Large power transformer
MAC	Modal assurance criterion

MSF	Modal scale factor
MDOF	Multiple degree of freedom
SDOF	Single degree of freedom
SPL	Sound pressure level

CHAPTER 1

INTRODUCTION

1.1 BACKGROUND AND MOTIVATION

A power transformer is a device designed to transfer electrical energy between two or more circuits through electromagnetic induction. Serving as critical nodes in the power grid, transformers have become essential in the effective and reliable transmission and distribution of electricity. A diagram of a typical oil-filled transformer is seen in Figure 1-1.

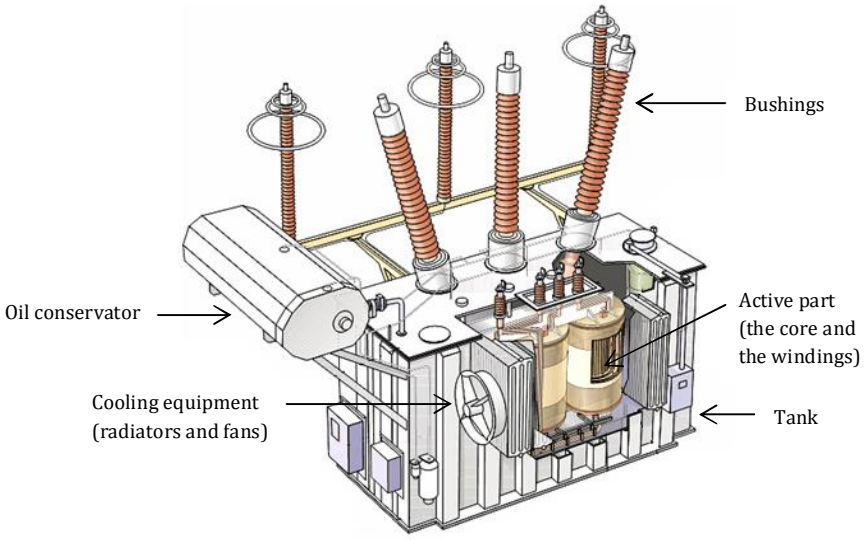

Figure 1-1 Illustration of an oil-filled power transformer [1]

The essential components of an oil-filled transformer, whether it is designed for transmission or distribution purposes, include:

- The active part – comprised of the core and the windings;
- Insulation oil;
- High-voltage and low-voltage bushings; and
- The tank.

Larger oil-filled transformers also generally carry auxiliary cooling equipment, such as fans and radiators, and an oil conservator, which allows for the expansion of the insulation oil within the tank.

Perhaps the best-known effect linked to the operation of a power transformer is the distinctive hum it produces. This characteristic is caused by vibrations in the active part, which result from electromagnetic and magnetostrictive forces in the core and the windings. The noise emissions from large power transformers have become a serious environmental problem for communities living in proximity to power substations and therefore stringent acoustic regulations are increasingly being placed on transformers. Large power transformers typically generate sound pressure levels ranging from 60 dB(A) to 80 dB(A); levels which are widely recognised as unacceptable for 24-hour exposure in a residential environment [2].

A significant issue facing transformer manufacturers is meeting the maximum allowable sound levels specified by noise regulations and utility operators. It is therefore critical that manufacturers are able to accurately identify the acoustic characteristics of a power transformer before production commences. However, this is difficult due to the complex phenomena related to the generation of a transformer's acoustic emissions, as illustrated in Figure 1-2.

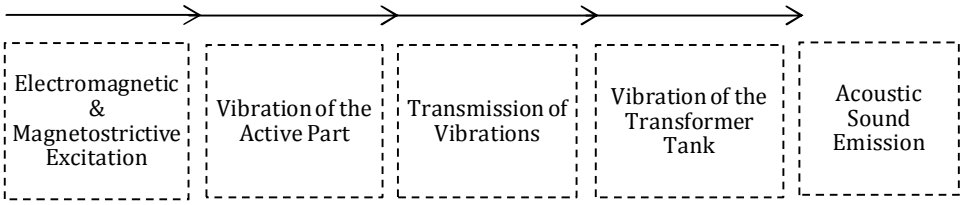

Figure 1-2 Development of the noise emissions from a power transformer (⟶ indicates the progression of events which result in the acoustic emissions of a power transformer)

The inherent uncertainty in the prediction of power transformer noise levels has led to large safety margins in transformer designs. These safety margins introduce additional economic expense for manufacturers in both the design and manufacturing processes. However, failure to meet guaranteed noise levels can result in significant non-conformity costs.

1.2 OBJECTIVES AND SCOPE OF WORK

The aim of this thesis is to develop a numerical methodology that accurately predicts the vibration and acoustic characteristics of a large power transformer. In particular, this thesis is concerned with modelling a transformer's sound radiation and identifying the physical properties that result in elevated noise levels. The four main objectives of this work are set out as follows:

i) To define a set of generic procedures for numerically predicting the vibration characteristics and noise levels of a large power transformer;
ii) To validate the numerical methodology by comparing the simulated vibration characteristics and noise emissions of a transformer with those determined experimentally;
iii) To evaluate and subsequently optimise the vibration and acoustic characteristics of a transformer employing the numerical methodology, replicating the process that may be carried out within the design phase of a transformer; and
iv) To determine the influence of key structural design parameters on the acoustic behaviour of a transformer.

The scope of work covered by this thesis includes the numerical prediction of a transformer's vibration and acoustic behaviour under nominal operating conditions. Specifically, the work is concerned with the vibration and acoustic response of a single-phase, special purpose large power transformer. Within this thesis the term 'large power transformer' (LPT) is used to describe a power transformer with a maximum rated power of 100 MVA or higher; however, it is of note that no industry definition or criterion for what constitutes a LPT exists. The term 'special purpose transformer' is utilised in this work to distinguish between generator-step up and system intertie transformers and all other transformer types.

1.3 SIGNIFICANCE OF THE STUDY

The significance of this study resides in presenting a numerical methodology that will enable transformer manufacturers to evaluate and optimize the acoustic characteristics of LPTs in the design phase. This evaluation and optimisation procedure will centre on sound pressure level estimates and the numerical prediction of a transformer's vibration characteristics that result in elevated acoustic emissions. Such a design tool is of importance to transformer manufacturers as failure to meet acoustic targets specified by regulators and utilities operators can result in considerable non-conformity expenses.

Together with enabling transformer manufacturers to more consistently meet acoustic targets, accurate sound pressure estimates will allow the acoustic safety margins in current LPT design practices to be reduced. These safety margins introduce additional costs in both the design and manufacturing phases. Furthermore, the optimization of LPT designs with respect to acoustic emissions will limit the environmental noise pollution introduced by these pieces of equipment. This would benefit persons working or living in proximity to power substations, reducing the adverse health impacts associated with extended noise exposure.

1.4 NOVELTIES AND AREAS OF SIGNIFICANT CONTRIBUTION

Within this thesis several areas of novel research are presented. These novelties relate to the vibro-acoustic modelling of power transformers and to modal parameter extraction techniques. The current state of the art, as identified in past literature, and the areas of significant contribution within this thesis are described in the following paragraphs. A detailed literature review covering both theoretical topics and past studies is presented in *Chapter 2*; here only a brief statement on the state of the art is reported to highlight the novelty of this thesis.

The vibro-acoustic modelling of power transformers is most comprehensively detailed in the investigations published by Rausch, Kaltenbacher, Landes & Lerch [3] and Kavasoglu [4]. However, both the aforementioned studies omit the transformer core from the respective numerical models and therefore predict only coil-emitted noise emissions. The work presented in this thesis furthers the works of Rausch et al. and Kavasoglu by detailing a vibro-acoustic model that incorporates all key structural and fluid elements (i.e. the core, the windings, the transformer tank and the insulation fluid). This allows the model to predict a transformer's acoustic behaviour under nominal operating conditions, with acoustic emissions resulting from the vibration of both the core and the windings.

A second limitation of the studies performed by Rausch et al. and Kavasoglu is that the prediction and subsequent validation of sound pressure levels is performed exclusively at double the network frequency (being 100 Hz or 120 Hz). When considering the acoustic behaviour of a large power transformer under nominal operating conditions this simplification is not valid. Therefore, the study presented within this thesis is novel in that it predicts and validates acoustic emissions over an extended frequency range. Explicitly, this thesis estimates and validates sound pressure levels over a spectrum which includes the network frequency harmonics considered dominant in the acoustic spectrum of a LPT.

In addition to providing more detailed acoustic predictions, the extended validation spectrum of the vibro-acoustic model employed in this thesis allows for a transformer's key vibration characteristics to be identified and discussed. Such an analysis is presented in this thesis for the first time. Furthermore, numerical indicators including modal mass participation factors are identified as key design-quality parameters. These aforementioned numerical indicators may be used to determine the modes that significantly contribute to excessive noise generation.

Finally, this thesis details the first modal damping analysis of a large power transformer. Due to the limitations of conventional curve-fitting techniques a novel methodology to identify the modal damping behaviour of a complex fluid-filled assembly is also set out and a partial numerical validation of the methodology is given. Additionally, the interpretation and application of the experimentally determined modal damping characteristics to the finite element model of the studied transformer is conducted in a way that has not been presented in past literature.

1.5 ASSUMPTIONS AND APPROXIMATIONS

While attempts have been made to make the numerical prediction of transformer noise presented in this thesis as generic as possible, the modelling process inevitably contains a number of assumptions. These assumptions may to some extent explain the limitations or discrepancies of the results shown in later chapters. The principal assumptions made in this thesis are outlined as follows:

- The discretisation of the model was conducted by means of finite elements;
- Contact between single parts or assemblies have been considered bonded and were therefore modelled with linear bonded contacts;
- The damping nature of the transformer analysed in this thesis is assumed to be that of proportional viscous damping; and
- The electromagnetic and magnetostrictive forces employed to excite the finite element model have been determined analytically by Siemens AG Austria, Transformers Weiz and are assumed to be accurate.

1.6 LAYOUT OF THE THESIS

There are seven chapters in the thesis. Chapter 2 provides a review of past literature and the theoretical framework relevant to the work carried out in this thesis. Chapter 3 details the finite element methodology developed to predict the vibration and acoustic characteristics of a large power transformer operating under nominal conditions. The validation of the numerical methodology is detailed in Chapter 4. Chapter 5 identifies and discusses the vibro-acoustic characteristics of the particular LPT analysed in this thesis and details the computing requirements for the simulations performed. An evaluation of the key structural parameters affecting the acoustic behaviour of a transformer is presented in Chapter 6. Finally, Chapter 7 outlines the significant results obtained from this thesis and discusses the future works to be conducted.

CHAPTER 2

LITERATURE REVIEW AND THEORECTICAL FRAMEWORK

The purpose of this chapter is to provide an overview of the key concepts and to identify the strengths and weaknesses of previous studies relating to the prediction of transformer noise. The chapter begins by introducing the fundamentals of transformer noise including vibration sources, transmission paths and radiated sound. The principal approaches that have been employed in previous investigations to predict transformer noise are then detailed. Within this chapter there is a particular focus on the finite element approach to predict transformer noise and the method's validation through experimental modal analysis (EMA). The analysis of EMA data to determine an oscillating system's modal damping characteristics, thereby allowing the system to be more accurately modelled, is also discussed.

2.1 FUNDAMENTALS OF TRANSFORMER NOISE AND VIBRATIONS

Under nominal operating conditions a transformer's acoustic emissions result from the vibrations of the core and the windings, and the noise generated by auxiliary cooling equipment. Estimation and the subsequent adjustment of the noise produced by cooling equipment, such as fans and pumps, can generally be made through physical measurements and analytical modelling. However, predicting the noise resulting from the vibrations of the core and the windings is significantly more challenging.

The difficulty in predicting the acoustic emissions generated by the vibrations of a transformer's core and windings are the many complex phenomena involved. Specifically, the following aspects must be accounted for:

- The excitation mechanisms in the core and the windings;
- The transmission paths from the active part to the transformer tank; and
- The structural response characteristics of the assembly.

Each of these factors is discussed in further detail within this chapter.

The vibrations of a transformer's active part result from three distinct excitation mechanisms: a magnetostrictive effect in the core; Maxwell forces in the core; and Lorentz forces in the windings [5-7]. Figure 2-1 illustrates these excitation mechanisms within the context of power transformer noise. There is much conjecture about which excitation mechanism in a transformer's active part is the dominant source of acoustic emissions (refer to Refs. [3, 7-10] for conflicting arguments). It is also plausible that the dominant source of noise is dependent on an individual unit's design and operating specifications. This is view supported by Refs. [11, 12].

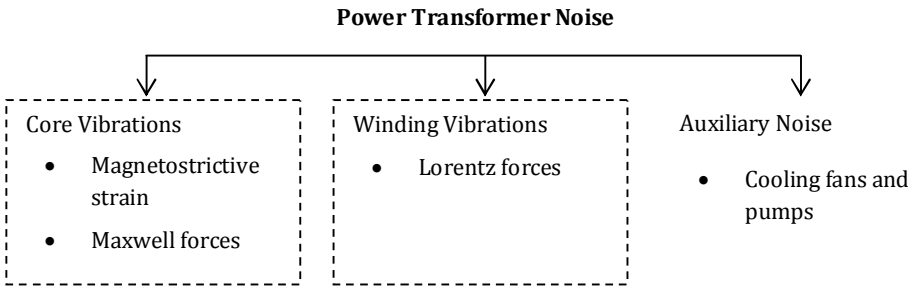

Figure 2-1 Sources of noise emissions from a power transformer (- - - indicates the noise sources considered in this thesis)

Although the dominant source of transformer noise is unclear, the three excitation mechanisms that generate a transformer's acoustic emissions have been studied extensively. Key points of consensus among preceding investigations include:

- The Maxwell forces in the core and the Lorentz forces in the winding act predominantly at double the network frequency; and
- The magnetostrictive strain of the core, due to non-linear saturation of the core material, produces vibrations at even harmonics of the network frequency.

Further detail of the active part's excitation mechanisms and how they characterise the acoustic spectrum of a transformer is provided in *Chapter 3.6*.

The vibrations resulting from the excitation mechanisms in the active part of a transformer are able to reach the tank wall through two transmission paths. Refs. [13-15] have investigated these two transmission mechanisms, being:

- *A direct coupling through mechanical joints*

  A direct coupling of the active part and the tank occurs through mechanical joints, with transmission primarily through the base of the tank on which the active part rests.

- *Indirect transmission through the insulation fluid*

  An indirect coupling through the fluid-structure interaction (FSI) between the insulation liquid, the active part and the tank allows pressure waves generated by the movement of the active part to transmit through the insulation oil to the tank structure.

In addition to acting as a transmission mechanism, the insulation fluid contained within a transformer significantly influences the assembly's frequency response. This is due to the fluid's mass and viscous damping effects as well as the bi-directional coupling between the fluid and the structural elements of a transformer [16, 17].

The transmission of vibrations through the insulation fluid and mechanical joints eventuates in the transformer tank vibrating with oscillatory motion. However, there have been few investigations that specifically examine how the vibration characteristics of a transformer tank affect acoustic emissions. This absence of past research is likely due to: the perception that the tank itself does not have any significant influence on the propagation of noise [12]; and relatively recent advances in computing technology that have allowed for the numerical calculation of a complex structure's vibration characteristics [18].

In Ref. [19] the authors dismiss the notion that the tank has no effect on the propagation of noise. Instead, the authors of Ref. [19] suggest that excessive noise emissions result if the natural frequency of the tank matches the oscillating frequency of the active part, resulting in a resonance event. This understanding that a system's external housing can amplify noise emissions is also in accordance with gearbox and automobile noise studies, such as those presented in Refs. [20-23].

2.2 APPROACHES FOR THE PREDICTION OF TRANSFORMER NOISE

There have been a series of past attempts to model the acoustic characteristics of power transformers. The majority of these previous studies have attempted to develop parametric predictive models (i.e. statistical models formulated from experimental data). These models may broadly be classified into two categories:

- *Correlation between the principal parameters of a transformer and noise levels*

  A number of studies have used measured data to develop acoustic prediction models based on the principal parameters of a transformer, such as core dimensions, tank dimensions and power rating (see Refs. [24-26] as examples).

- *Influence of material properties on the acoustic emissions of a transformer*

  The mechanical properties of specific materials and components within a transformer and how these affect sound radiation levels have been extensively studied. The majority of research in this area has focused on the characteristics of the magnetic core material (see Refs. [27-29] as examples).

The parametric models detailed in past investigations provide an understanding of the factors influencing the noise emissions from power transformers. However, as noted in Ref. [30], acoustic models based on experimental analyses are only able to provide limited information as they focus on a few vibration properties at certain frequencies.

Due to the limitations of statistical techniques, numerical methods have become common in studying the behaviour of transformers. These numerical investigations have developed with the progress of high-powered computing and other technological advances [31]. The numerical techniques that may be employed to study a transformer's behaviour include the finite element method, the finite difference method, the boundary element method, and the point mirroring method, to name a selected few.

Although the three physical fields influencing the sound radiated by a transformer are able to be numerically modelled – namely the electromagnetic, mechanical and acoustic fields – no study has yet to detail a comprehensive calculation scheme to determine the noise emissions of a transformer under nominal operating conditions. However, numerical studies analysing the vibration characteristics of individual components and key structural assemblies within a transformer have been conducted. These numerical analyses have generally employed the finite element (FE) methodology [31].

2.3 FINITE ELEMENT PREDICTION OF TRANSFORMER NOISE

The commercial software package ANSYS® has been used in this thesis to study the vibro-acoustic behaviour of a transformer. Specifically, ANSYS® 16.2 Mechanical software has been employed, which is a finite element analysis tool for linear, nonlinear and dynamic structural analyses. The ANSYS® Mechanical software package also supports coupled structural-acoustics simulations through the integration of acoustic features and by accounting for fluid-structure interaction in the solution process.

The first of the following subchapters details the theoretical basis of the finite element methodology as employed in ANSYS® Mechanical. Specific topics relevant to the FE model presented in this thesis, such as fluid-structure interaction (FSI), are also discussed. The subsequent subchapter then provides a review of relevant past literature that has employed the finite element method in an attempt to predict transformer noise.

2.3.1 THEORETICAL BASIS

The finite element method (FEM) is a numerical technique for finding approximate solutions to differential equations and is used in numerous fields of science and engineering. The central notion behind FEM is to discretise a complex object into components of simple geometry called finite elements. Assembling the equations that describe each of the individual finite elements into a general system of equations provides for a detailed mathematical model of the studied object. The general system of equations can then be solved through numerical methods to obtain an approximate overall solution to the mathematical model [32, 33].

To predict the physical behaviour of systems and structures ANSYS® Mechanical employs the d'Alembert principle [34]. The principle is an interpretation of the classical laws of motion and presents an alternative form of Newton's second law of motion. The advantage of utilising d'Alembert's principle is that a problem in dynamics may be reduced to a problem in statics, such that:

$$F - ma = 0 \qquad \textbf{(2.1)}$$

Where: F is the force acting on a body

m is the mass of the body

a is the acceleration of the body

As seen in Eqn. 2.1, d'Alembert's principle indicates that equilibrium may be considered to result under the action of a real force F and a fictitious force $-ma$. More specifically, the d'Alembert principle states that the sum of the differences between the forces acting on a system of mass particles (or bodies) and the time derivatives of the momenta of the system itself along any virtual displacement consistent with the constraints of the system is zero [35]:

$$\sum_i (F_i - m_i a_i) \cdot \delta r_i = 0 \qquad \textbf{(2.2)}$$

Where: i denotes a particular particle (or body) in the system

δr_i is the virtual displacement of the i^{th} particle (or body)

It is the equation given by d'Alembert's principle together with the discretisation of a continuous structure that ANSYS® Mechanical employs to solve structural dynamics problems. The result is an equation of motion accounting for the mass, damping and stiffness of a body, which is given by [34]:

$$[M] \cdot \{\ddot{u}\} + [C] \cdot \{\dot{u}\} + [K] \cdot \{u\} = \{F(t)\} \qquad \textbf{(2.3)}$$

Where: $[M]$ is the structural mass matrix

$[C]$ is the viscous damping matrix

$[K]$ is the stiffness matrix

$\{\ddot{u}\}$ is the nodal acceleration vector

$\{\dot{u}\}$ is the nodal velocity vector

$\{u\}$ is the nodal displacement vector

$\{F(t)\}$ is the time varying vector of the applied forces

Taking different representations of the time varying force vector in Eqn. 2.3 provides a general classification of the various types of structural dynamics analyses that may be conducted. This leads to three broad categories, being transient, modal and harmonic response, as illustrated in Figure 2-2.

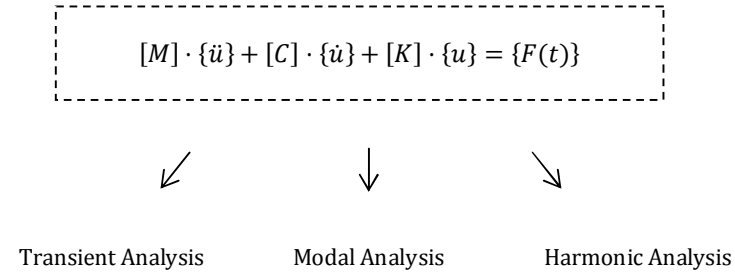

Figure 2-2 Three broad categories of structural dynamics simulations

The dynamic analyses employed in this thesis to determine the vibration and acoustic characteristics of a power transformer are further described in the following paragraphs.

- *Modal Analysis*

  A modal analysis is used to determine the vibration characteristics of a structure through identifying natural frequencies and mode shapes. Therefore, the time varying forces applied to the structure are taken as zero and Eqn. 2.3 may be simplified to:

$$[M] \cdot \{\ddot{u}\} + [C] \cdot \{\dot{u}\} + [K] \cdot \{u\} = 0 \qquad \textbf{(2.4)}$$

  In a mathematical sense the computation of natural frequencies and mode shapes is equivalent with the solution of an eigenvalue problem.

- *Harmonic Response Analysis*

  A harmonic response analysis is employed to solve structural dynamics problems in which applied cyclical loading produces a sustained cyclical response. Within harmonic response analyses the applied loads and displacements vary sinusoidally with the same known frequency although not necessarily in phase. Eqn. 2.3 may therefore be expressed as:

$$[M] \cdot \{\ddot{u}\} + [C] \cdot \{\dot{u}\} + [K] \cdot \{u\} = \left\{F_{max} \cdot e^{i(\omega t + \varphi)}\right\} \quad \textbf{(2.5)}$$

  Where: F_{max} is the amplitude of the force

  ω is the angular frequency

  φ is the phase shift of the force

  Although not employed in this thesis, it is noted that a transient analysis differs from a harmonic response analysis in that any function for the load vector may be specified.

2.3.1.1 Fluid-Structure Interaction in Numerical Analyses

To accurately account for the influence of fluid bodies in numerical analyses the coupling of structural and fluid fields is required. This coupling allows pressure waves in the fluid to be generated by the vibration of a structure and/or structural deformation to result from applied fluid pressure. The coupling of the structural and fluid fields in ANSYS® Mechanical is accomplished by considering the structural dynamics equation, as given in Eqn. 2.3, together with the Navier-Stokes equation of fluid momentum and the flow continuity equation.

Within fluid-structure interaction (FSI) analyses ANSYS® Mechanical simplifies the Navier-Stokes and the flow continuity equations. Assumptions made in this simplification include that the fluid is compressible and that there is no mean flow. The equation resulting from these assumptions, which accounts for the propagation of pressure waves within a fluid body, is given by [36]:

$$\nabla \cdot \left(\frac{1}{\rho_0}\nabla p\right) - \frac{1}{\rho_0 c^2}\frac{\partial^2 p}{\partial t^2} + \nabla \cdot \left[\frac{4\mu}{3\rho_0}\nabla\left(\frac{1}{\rho_0 c^2}\frac{\partial p}{\partial t}\right)\right] = -\frac{\partial}{\partial t}\left(\frac{Q}{\rho_0}\right) + \nabla \cdot \left[\frac{4\mu}{3\rho_0}\nabla\left(\frac{Q}{\rho_0}\right)\right] \quad \textbf{(2.6)}$$

Where:

c	is the speed of sound in a fluid medium	$\left[c = \sqrt{K/\rho_0} \right]$
ρ_0	is the mean fluid density	
K	is the bulk modulus of the fluid	
μ	is the dynamic viscosity	
p	is the acoustic pressure	$[p = p(x, y, z, t)]$
Q	is the mass source in the continuity equation	
t	is the time	

As the viscous dissipation of energy has been taken into account using the Stokes hypothesis[1], the wave equation stated in Eqn. 2.6 is referred to as the lossy wave equation for the propagation of sound in fluids. The discretized structural equation defined in Eqn. 2.3 and the lossy wave equation must be considered simultaneously in FSI problems. The following paragraphs detail how the discretised fluid matrix is derived and presents the coupled fluid-structure matrix utilised in FSI analyses.

[1] Stokes hypothesis states that the average normal stresses on any three mutually perpendicular normal forces in an element of a compressible fluid are equal to zero. Therefore, the second coefficient of viscosity plus two-thirds of the dynamic viscosity is equal to zero [37].

The finite element formulation of the definition of the wave equation is obtained applying the Galerkin procedure to Eqn. 2.6. The wave Eqn. 2.6 is initially multiplied by the weighting function ψ (also referred to as a test function) and integrated over the volume of the acoustic domain to yield the following [36]:

$$\iiint_{\Omega_f} \frac{1}{\rho_0 c^2}\psi \frac{\partial^2 p}{\partial t^2}\, dv + \iiint_{\Omega_f} \nabla\psi \cdot \left(\frac{4\mu}{3\rho_0^2 c^2}\nabla\frac{\partial p}{\partial t}\right) dv \tag{2.7}$$

$$+ \iiint_{\Omega_f} \nabla\psi \cdot \left(\frac{1}{\rho_0}\nabla p\right) dv$$

$$- \oiint_{\Gamma_f} \psi\left(\frac{1}{\rho_0} + \frac{4\mu}{3\rho_0^2 c^2}\frac{\partial}{\partial t}\right)\hat{n}\cdot\nabla p ds$$

$$+ \oiint_{\Gamma_f} \psi\frac{4\mu}{3\rho_0^2}\hat{n}\cdot\nabla Q ds$$

$$= \iiint_{\Omega_f} \psi\frac{1}{\rho_0}\frac{\partial Q}{\partial t} dv + \iiint_{\Omega_f} \nabla\psi\cdot\left(\frac{4\mu}{3\rho_0^2}\nabla Q\right) dv$$

Where: dv is the volume differential of acoustic domain Ω_f

ds is the surface differential of acoustic boundary domain Γ_f

$\hat{n}$ is the outward normal unit vector to the boundary Γ_f

Multiplying a system of partial differential equations (PDEs) by a weighting function and then expressing the PDEs in an integral formulation, as conducted in Eqn. 2.7, is referred to as the weighted residual method. The Galerkin method, as utilised by ANSYS to discredits the wave Eqn. 2.6, employs a specific formulation of the weighting function. A detailed description of the Galerkin finite element method may be found in Ref. [38].

From the equation of momentum conservation, the normal velocity on the boundary of an acoustic element is given by:

$$\frac{\partial v_{n,f}}{\partial t} = \hat{n} \cdot \frac{\partial \bar{v}}{\partial t} = -\left(\frac{1}{\rho_0} + \frac{4\mu}{3\rho_0^2 c^2}\frac{\partial}{\partial t}\right)\hat{n} \cdot \nabla \mathrm{p} + \frac{4\mu}{3\rho_0^2}\hat{n} \cdot \nabla \mathrm{Q} \tag{2.8}$$

Substituting the definition provided in Eqn. 2.8 into Eqn. 2.7 gives the "weak" form of acoustic wave equation, notated as [36]:

$$\begin{aligned} &\iiint_{\Omega_\mathrm{f}} \frac{1}{\rho_0 c^2}\psi \frac{\partial^2 p}{\partial t^2}\, dv + \iiint_{\Omega_\mathrm{f}} \nabla\psi \cdot \left(\frac{4\mu}{3\rho_0^2 c^2}\nabla\frac{\partial p}{\partial t}\right) dv \\ &\quad + \iiint_{\Omega_\mathrm{f}} \nabla\psi \cdot \left(\frac{1}{\rho_0}\nabla p\right) dv + \oiint_{\Gamma_f} \psi \frac{\partial v_{n,f}}{\partial t}\,\mathrm{ds} \\ &\quad = \iiint_{\Omega_\mathrm{f}} \psi \frac{1}{\rho_0}\frac{\partial Q}{\partial t} dv + \iiint_{\Omega_\mathrm{f}} \nabla\psi \cdot \left(\frac{4\mu}{3\rho_0^2}\nabla \mathrm{Q}\right) dv \end{aligned} \tag{2.9}$$

Considering that the normal acceleration of a fluid particle can be presented using the normal displacement of the fluid particle, such that,

$$\frac{\partial v_{n,f}}{\partial t} = \hat{n} \cdot \frac{\partial^2 u_f}{\partial t^2} \tag{2.10}$$

Where: u_f is the displacement of the fluid particle

the weak form of the acoustic wave equation in Eqn. 2.9 may then be expressed as:

$$\iiint_{\Omega_f} \frac{1}{\rho_0 c^2} \psi \frac{\partial^2 p}{\partial t^2}\, dv + \iiint_{\Omega_f} \nabla\psi \cdot \left(\frac{4\mu}{3\rho_0^2 c^2} \nabla \frac{\partial p}{\partial t}\right) dv + \iiint_{\Omega_f} \nabla\psi \cdot \left(\frac{1}{\rho_0} \nabla p\right) dv + \oiint_{\Gamma_f} \psi \frac{\partial^2 u_f}{\partial t^2} ds = \iiint_{\Omega_f} \psi \frac{1}{\rho_0} \frac{\partial Q}{\partial t} dv + \iiint_{\Omega_f} \nabla\psi \cdot \left(\frac{4\mu}{3\rho_0^2} \nabla Q\right) dv \quad \textbf{(2.11)}$$

The definition given in Eqn. 2.11, which contains the fluid pressure p and the fluid displacement u_f as the dependent variables, can be discretised and notated in matrix form. The generic discretisation process of a weak form integral to reach the matrix formulation, as presented in Ref. [38], involves the following process:

i) Representation of the domain of calculation V by a set of n finite elements V^e $(e = 1 \dots n)$;

ii) Approximation of the solution function and the test function on each element as a combination of the corresponding values at the element nodes, weighted by a shape function $N_i(x)$:

$$u^e(x,t) = \sum_i N_i(x)\, u_i(t) \quad \textbf{(2.12)}$$

$$\psi^e(x) = \sum_i N_i(x)\, \psi_i \quad \textbf{(2.13)}$$

Where $u_i(t)$ are nodal variables of the solution function

ψ_i are nodal variables of the test function

N_i is the interpolation (or shape) function linking the solution at coordinates x with the solution the in node i

Employing Eqn. 2.12 and Eqn. 2.13, the discretised elementary weak form of Eqn. 2.11 may be determined. Assembling of the set of elementary contributions then results in the discretised global wave equation matrix form of Eqn. 2.11. This final global form is presented in Eqn. 2.14, where the dependency of all the terms on the test function has been eliminated.

$$\left[M_f\right]\{\ddot{p}_e\} + \left[C_f\right]\{\dot{p}_e\} + \left[K_f\right]\{p_e\} + \bar{\rho}_0[R]^T\{u_{f,e}\} = \{F_f\} \qquad \textbf{(2.14)}$$

Where:

$\left[M_f\right] = \bar{\rho}_0 \iiint_{\Omega_f} \frac{1}{\rho_0 c^2}\{N\}\{N\}^T dv$ is the acoustic fluid mass matrix

$\left[C_f\right] = \bar{\rho}_0 \iiint_{\Omega_f} \frac{4\mu}{3\rho_0^2 c^2}[\nabla N]^T[\nabla N]\, dv$ is the acoustic fluid damping matrix

$\left[K_f\right] = \bar{\rho}_0 \iiint_{\Omega_f} \frac{1}{\rho_0}[\nabla N]^T[\nabla N]\, dv$ is the acoustic fluid stiffness matrix

$[R]^T = \oiint_{\Gamma_f}\{N\}\{n\}^T\{N'\}^T\, ds$ is the acoustic fluid boundary matrix

$\{F_f\} = \bar{\rho}_0 \iiint_{\Omega_f} \frac{1}{\rho_0 c^2}\{N\}\{N\}^T dv\ \{\dot{q}\}$

$+\bar{\rho}_0 \iiint_{\Omega_f} \frac{4\mu}{3\rho_0^2}[\nabla N]^T[\nabla N] dv\ \{q\}$ is the acoustic fluid load vector

$\{p_e\}$ is the nodal pressure vector

$\bar{\rho}_0$ is the acoustic mass fluid constant

$\{N\}$ is the element shape function[2] for pressure

$\{N'\}$ is the element shape function[2] for displacements

$\{n\}$ is the outward normal vector at the fluid boundary

$\{q\}$ is the nodal mass source vector

[2] The element shape function is the function that interpolates the solution between discrete values obtained at the mesh nodes. Low order polynomials are typically chosen as shape functions. The degree of the polynomial representing the shape function is dependent on the number of nodes of the element employed.

Simulations that incorporate both structural and fluid fields, and the coupling between them, require mass, damping and stiffness matrices that describe both fields. This culminates in a coupled fluid-structure matrix given by [39]:

$$\begin{bmatrix} M_s & 0 \\ \rho_0 R^T & M_f \end{bmatrix} \begin{Bmatrix} \ddot{u} \\ \ddot{p} \end{Bmatrix} + \begin{bmatrix} C_s & 0 \\ 0 & C_f \end{bmatrix} \begin{Bmatrix} \dot{u} \\ \dot{p} \end{Bmatrix} + \begin{bmatrix} K_s & -R \\ 0 & K_f \end{bmatrix} \begin{Bmatrix} u \\ p \end{Bmatrix} = \begin{Bmatrix} F_s \\ F_F \end{Bmatrix} \qquad \textbf{(2.15)}$$

Where: $_s$ denotes the properties of a solid structure

$_f$ denotes the properties of a fluid

The extra diagonal term $-R$ of the stiffness matrix in Eqn. 2.15 transfers the affect of the fluid pressure to the coupled solid structure while the extra diagonal term $\rho_0 R^T$ of the mass matrix represents the affect of the structure's inertial forces on the second derivative of the fluid pressure. The bi-directional coupling in FSI analyses, as given by Eqn. 2.15, therefore requires a single layer of finite elements at the interface between the fluid and structural fields that have both pressure and displacement degrees of freedom.

With regard to Eqn. 2.15 it is of note that the global mass and global stiffness matrices of the coupled fluid-structure matrix are asymmetric (i.e. the off-diagonal terms are not transposes of each other). Solving for the nodal pressure and displacements, which requires the inversion of the asymmetric matrix, therefore requires a significant amount of computing resources.

To reduce computational requirements, under the assumptions of a linear harmonic analysis a symmetric matrix formulation for FSI problems may be achieved. For linear harmonic analyses Eqn. 2.15 can be reduced to an expression without differentials as,

$$\begin{bmatrix} -\omega^2 M_s + i\omega C_s + K_s & -R \\ -\omega^2 \rho_0 R^T & -\omega^2 M_f + i\omega C_f + K_f \end{bmatrix} \begin{Bmatrix} u \\ p \end{Bmatrix} = \begin{Bmatrix} F_s \\ F_f \end{Bmatrix} \tag{2.16}$$

A symmetrical formulation of Eqn. 2.16 may then be accomplished by defining a transformation variable for the nodal pressures such that,

$$\dot{q} = i\omega q = p \tag{2.17}$$

and substituting Eqn. 2.17 into Eqn. 2.16 so that the system of equations becomes:

$$\begin{bmatrix} -\omega^2 M_s + i\omega C_s + K_s & -i\omega R \\ -i\omega R^T & \dfrac{\omega^2 M_f}{\rho_0} + \dfrac{i\omega C_f}{\rho_0} + \dfrac{K_f}{\rho_0} \end{bmatrix} \begin{Bmatrix} u \\ q \end{Bmatrix} = \begin{Bmatrix} F_s \\ \dfrac{i}{\omega \rho_0} F_f \end{Bmatrix} \tag{2.18}$$

Eqn. 2.18 presents a symmetric fluid-structure matrix formulation that can be inverted and solved for the vectors of the structural nodal displacements u and the transformation variable for nodal pressures q, faster than the unsymmetric formulation in Eqn. 2.15. The nodal pressures p can then be calculated using Eqn. 2.17.

As previously noted, the fluid-structure interaction detailed by the formulations in Eqn. 2.15 and Eqn. 2.18 account for the two-way coupling between structural bodies and fluids. This mechanism is significant if a structure is radiating into a heavier-than-air medium such as water, or if the structure is lightweight. In such cases the acoustic field is dissipated by the induced vibration of the structure, which has the effect of damping the vibration and acoustic response of the system [39].

2.3.1.2 Numerical Error Associated with the Finite Element Method

As a numerical technique, the finite element method provides only an approximate solution rather than an exact answer. The two primarly types of errors associated with finite element analyses are modelling and discretisation errors. The former arises from an incorrect decription of the boundary value problem – being geometric and material properties, loading, applied boundary conditions and the analysis type. The latter arises from the creation of the mesh. Numerical errors, which arise from the use of numerical methods, may also be significant if the model is ill-conditioned or if there is a lack of computing power.

2.3.2 PAST FINITE ELEMENT STUDIES OF TRANSFORMER NOISE

There have been a series of past investigations employing the finite element method to studying the vibration characteristics of individual transformer components. These studies have considered the structural response of the windings [40-42], the core [42-44], the active part (i.e. the core and the windings) [30, 45], and the tank [46]. However, the limited scope of the aforementioned analyses and the absence of acoustic elements limit their ability to qualitatively or quantitatively predict the noise emissions of a transformer.

To overcome the shortcomings of empirical prediction formulas and numerical structural vibration analyses in the prediction transformer noise, two past investigations have presented multi-physics finite element models. These studies are the most comparable to that which is presented in this thesis and they are therefore discussed in further detail.

- M. Rausch, M. Kaltenbacher, H. Landes, and R. Lerch, *Numerical computation of the emitted noise of power transformers*, 2001 (full citation in Ref. [3])

  Ref. [3] is the earliest study which has employed a vibro-acoustic FE model to determine a power transformer's noise emissions. Much of this paper focuses on the theoretical basis and governing equations behind the physical fields. In this sense the work presented in Ref. [3] is an application of the preceding theoretical papers published by the contributing authors (see Refs. [47, 48]).

  The principal shortcoming of the vibro-acoustic model presented in Ref. [3] is the omission of the transformer core. This has led to numerous simplifications and assumptions, which prevent the model from predicting a transformer's acoustic emissions under nominal operating conditions. Limitations of the vibro-acoustic model presented in Ref. [3] include:

  - The vibration characteristics of the transformer core, which are noted in Refs. [7, 28, 44, 49-51] to significantly affect the overall sound pressure level of a transformer, are overlooked;
  - Only the acoustic emissions at double the line frequency are considered, being those at 100 Hz in the study conducted in Ref. [3]. This is a simplification that does not hold true in reality due to the significant sound emissions from a transformer at even harmonics of the line frequency [10, 15, 52]; and
  - The omission of the transformer core has necessitated the use of spring elements to support the winding blocks within the numerical model presented in Ref. [3]. However, the values assigned to these spring elements have not been experimentally validated.

Following their initial paper, the authors of Ref. [3] presented the vibro-acoustic computation scheme again in Ref. [53]. This second paper further detailed the application of a vibro-acoustic simulation, describing how it may be employed to understand the influence of various components on a transformer's sound radiation levels. However, the numerical model in Ref. [53] is identical to that in Ref. [3] and as such has the same shortcomings.

- M. Kavasoglu, *Load controlled noise of power transformers: 3D modelling of interior and exterior sound pressure field*, 2010 (full citation in Ref. [4])

  A similar investigation to that presented in Refs. [3, 53] was carried out in Ref. [4], a thesis published by the KTH Royal Institute of Technology. The investigation in Ref. [4] appears to be carried out on the same FE model presented in Refs. [3, 53]. As such, the principal limitation of the study in Ref. [4] is the omission of the transformer core. This leads to identical shortcomings noted of the preceding works, including assumptions that have not been validated and only the prediction of the coil emitted noise at a single point on the acoustic frequency spectrum. The study in Ref. [4] is also published in Ref. [54],

In addition to the limitations previously noted of Refs. [3, 4, 53, 54], the investigations did not conduct a detailed experimental modal analysis of the assembly. Such an analysis would have allowed for greater validation of the modelling procedure and subsequent vibration and acoustic estimates. As noted in Ref. [12], the simulation of any structural system that results in an acoustic response should begin with a numerical modal analysis validated by experimental results.

2.4 EXPERIMENTAL MODAL ANALYSIS

Experimental Modal Analysis (EMA) is the process of experimentally extracting the vibration characteristics of a structure, being the natural frequencies, mode shapes and modal damping. The purpose of the EMA results presented in this thesis are to correlate a transformer's measured vibration response to that simulated through numerical methods. The validated numerical modal may then be used to:

- Predict the response of the structure with complex excitation forces applied;
- Provide response information at points where physical measurements were not taken; and
- Analyse how the vibro-acoustic characteristics of a transformer are affected by modifications to key structural elements.

Within this thesis the fast Fourier transforms (FFTs) of the impulse response data (i.e. frequency response functions), which are the basis of EMA, have been provided by Siemens AG Austria, Transformers Weiz and were accepted as a starting point for this investigation. The design of the experiments and the measurement choices therefore did not form part of this thesis. Furthermore, Siemens AG Austria, Transformers Weiz had previously analysed the EMA data to determine the mode shapes and natural frequencies of the transformer studied in this thesis. As such, only the theoretical basis of EMA and modal damping extraction are further discussed in this chapter. Methods to correlate EMA results to numerical modal predictions are also presented.

Two commercial software packages were used in the EMA conducted by Siemens AG Austria, Transformers Weiz. Brüel and Kjær Pulse software was utilised for acquiring raw data and performing the spectral analysis. The Me'Scope software package was employed for extracting the experimental modal parameters, including the natural frequencies and the mode shapes of the studied transformer.

2.4.1 THEORETICAL BASIS

The basis for experimentally determining the vibration characteristics of a system is the frequency response function (FRF). The function, defined as the ratio of the Fourier-transformed response to the Fourier-transformed input force, allows the bias of the force spectral distribution to be removed from the response measurement; therefore describing the unbiased structural response of a system [55]. To introduce modal parameter extraction methods and numerical model validation techniques, a derivation of the FRF assuming viscous damping is provided. The derivation is based on that provided in Ref. [56].

The equation of motion for a discrete linear system (or a system in which the finite element approach has been applied such that the response is considered at a series of discrete locations) has been notated in Eqn. 2.3. Considering the case where the structure is excited sinusoidally by a set of forces all at the same frequency, ω, but with various amplitudes and phases, such that:

$$\{F(t)\} = \{\mathrm{F}\}\, e^{i\omega t} \qquad \textbf{(2.19)}$$

and assuming that a solution exits in the form:

$$\{u(t)\} = \{\mathrm{U}\}\, e^{i\omega t} \qquad \textbf{(2.20)}$$

Where: {F} is the force applied at each degree of freedom in the system

{U} is the resultant displacement at each degree of freedom in the system

{F}, {U} are $N \times 1$ vectors of the time-dependent complex amplitudes

N is the number of degrees of freedom

the equation of motion expressed in Eqn. 2.3 becomes:

$$([\mathrm{K}] + i\omega[\mathrm{C}] - \omega^2[M])\{U\}\, e^{i\omega t} = \{F\}\, e^{i\omega t} \qquad \textbf{(2.21)}$$

or, rearranging to solve for the unknown responses,

$$\{U\} = ([\mathrm{K}] + i\omega[\mathrm{C}] - \omega^2[M])^{-1}\,\{\mathrm{F}\} \qquad \textbf{(2.22)}$$

which may be expressed as,

$$\{U\} = [\mathrm{H}(\omega)]\,\{\mathrm{F}\} \qquad \textbf{(2.23)}$$

Where: $[\mathrm{H}(\omega)]$ is the $N \times N$ frequency response matrix for the system and constitutes its modal response

The general element in the frequency response matrix $\mathrm{h_{jk}}(\omega)$, defined as the displacement at coordinate j due to a single harmonic excitation force applied at coordinate k with a frequency of ω, is notated as follows:

$$\mathrm{h_{jk}}(\omega) = \frac{\{\mathrm{U}\}_\mathrm{j}}{\{\mathrm{F}\}_\mathrm{k}} \qquad \textbf{(2.24)}$$

Before preceding with the deviation of the FRF and relating the modal parameters to the system matrices it is important to note that the modal model possess orthogonality properties. These properties may be stated as,

$$[\Psi]^\mathrm{T}[\mathrm{M}][\Psi] = \left[\ \mathrm{m_r}\ \right] \qquad \textbf{(2.25)}$$

and,

$$[\Psi]^\mathrm{T}[\mathrm{K}][\Psi] = \left[\ \mathrm{k_r}\ \right] \qquad \textbf{(2.26)}$$

Where: $[\Psi]$ is the generalised eigenvector matrix

$\left[\ \mathrm{m_r}\ \right]$ is the modal or generalised mass matrix

$\left[\ \mathrm{k_r}\ \right]$ is the modal or generalised stiffness matrix

A proof of the orthogonality properties of the generalised mass and stiffness matrices is presented in Ref. [56].

If the eigenvector matrix $[\Psi]$ is normalised with respect to the mass matrix then the mass-normalised eigenvectors $[\Phi]$ have the particular property that,

$$[\Phi]^{\mathrm{T}}[M][\Phi] = [\mathrm{I}] \tag{2.27}$$

and therefore,

$$[\Phi]^{\mathrm{T}}[K][\Phi] = \begin{bmatrix} \ddots & \\ & \omega_r{}^2 \end{bmatrix} \tag{2.28}$$

Where: $[\mathrm{I}]$ is the identity matrix

$\begin{bmatrix} \ddots & \\ & \omega_r{}^2 \end{bmatrix}$ is comprised of eigenvalues ω_1 to ω_N.

The relationship between the mass-normalised mode shape for mode r $\{\phi\}_{\mathrm{r}}$ and the generalized form $\{\Psi\}_{\mathrm{r}}$ is given by $\{\phi\}_{\mathrm{r}} = \frac{1}{\sqrt{\mathrm{m_r}}}\{\Psi\}_{\mathrm{r}}$.

Returning to Eqn. 2.23 it may be stated that,

$$[\mathrm{H}(\omega)]^{-1} = ([\mathrm{K}] + i\omega[\mathrm{C}] - \omega^2[M]) \tag{2.29}$$

Premultiplying the above definition by $[\Phi]^{\mathrm{T}}$ and postmultiplying both sides by $[\Phi]$,

$$[\Phi]^{\mathrm{T}}[\mathrm{H}(\omega)]^{-1}[\Phi] = [\Phi]^{\mathrm{T}}([\mathrm{K}] + i\omega[\mathrm{C}] - \omega^2[M])[\Phi] \tag{2.30}$$

and assuming proportional damping in the form $[\mathrm{C}] = \alpha[\mathrm{M}] + \beta[\mathrm{K}]$ (i.e. Rayleigh damping), Eqn. 2.29 may be notated as:

$$[\Phi]^{\mathrm{T}}[\mathrm{H}(\omega)]^{-1}[\Phi] = [\omega_r{}^2] + i\omega\left(\alpha[\mathrm{I}] + \beta[\omega_r{}^2]\right) - \omega^2 \tag{2.31}$$

Where: α is the mass-proportional damping coefficient

β is the stiffness-proportional damping coefficient

Noting that [C] is a linear combination of [M] and[K] and therefore $[\Phi]^{\mathrm{T}}[\mathrm{C}][\Phi]$ is also orthogonal, the left-hand side of Eqn. 2.31 is orthogonal and the r^{th} item is,

$$([\Phi]^{\mathrm{T}}[\mathrm{H}(\omega)]^{-1}[\Phi])_{r^{th}\ item} = {\omega_r}^2 + 2i\omega_r\omega\zeta_r - \omega^2 \qquad \textbf{(2.32)}$$

Where: ζ_r is the modal damping ratio of the r^{th}mode, defined as,

$$\zeta_r = \frac{1}{2}\left(\frac{\alpha}{\omega_r} + \beta\omega_r\right) \qquad \textbf{(2.33)}$$

As the mass-normalised eigenvector matrix $[\Phi]$ has orthogonality properties with respect to the mass, stiffness and viscous damping matrices, it can be noted that $[\Phi]^{\mathrm{T}} = [\Phi]^{-1}$. Therefore, the frequency response matrix $[\mathrm{H}(\omega)]$ can be related to the modal frequency, mode shapes and damping as,

$$[\mathrm{H}(\omega)] = [\Phi]\begin{bmatrix} \ddots & & \\ & \frac{1}{{\omega_r}^2 + 2i\omega_r\omega\zeta_r - \omega^2} & \\ & & \ddots \end{bmatrix}[\Phi]^{\mathrm{T}} \qquad \textbf{(2.34)}$$

Resulting from the orthogonality of the matrices in Eqn. 2.34, each row of the equation in is independent and represents a single degree of freedom system. The FRF $\mathrm{h_{jk}}(\omega)$ is therefore given by,

$$h_{jk}(\omega) = \frac{\{\mathrm{U}\}_{\mathrm{j}}}{\{\mathrm{F}\}_{\mathrm{k}}} = \sum_{r=1}^{N} \frac{\phi_{jr}\,\phi_{kr}}{{\omega_r}^2 + i2\omega_r\omega\zeta_r - \omega^2} \qquad \textbf{(2.35)}$$

Where: ϕ_{jr} is the j^{th} element of the r^{th} einvector $\{\phi\}_r$
(i.e. the relative displacement at that point during vibration in the r^{th} mode)

N is the number of degrees of freedom (or modes)

The expression in Eqn. 2.35 has defined the receptance FRF $h_{jk}(\omega)$ as the ratio between the harmonic displacement response and the harmonic force. Similarly, the acceleration $a(t) = \ddot{u}(t)$ can be used as the response parameter, noting that it is customary to measure acceleration during experimental testing. In this form the FRF $h_{jk}(\omega)$ would be given as,

$$h_{jk}(\omega) = \frac{\{\ddot{U}\}_j}{\{F\}_k} = -\omega^2 \sum_{r=1}^{N} \frac{\phi_{jr}\,\phi_{kr}}{{\omega_r}^2 + i2\omega_r\omega\zeta_r - \omega^2} \qquad \textbf{(2.36)}$$

With respect to Eqn. 2.35 and Eqn. 2.36 it can be seen that:

- The FRF relates the modal parameters to the system matrices; and
- The system's vibration response is a summation of the contribution of all the system's modes.

The process of identifying the modal parameters from FRF data is commonly referred to as curve-fitting or modal parameter extraction.

2.4.2 MODAL DAMPING EXTRACTION

Modal damping is a fundamental feature required to fully describe an oscillating system, noting that damping exists in all vibratory systems that experience energy dissipation. Ref. [57] provides a comparison of several curve-fitting methods for extraction of the modal parameters from FRF data, with a particular focus on modal damping estimates. For the purpose of the work conducted in this thesis an overview of the Hilbert Envelop Method (HEM) is provided.

- *Hilbert Envelop Method (HEM)*

  The smooth curve outlining the amplitude of a rapidly oscillating signal that varies gradually with time is referred to as the signal's envelope. The envelope is an important characteristic of a time-domain signal as it allows the instantaneous attributes of the series to be determined. By utilizing the Hilbert transform, which provides an analytic signal from a real data sequence, the rapid oscillation of a signal can be removed. A representation of the data sequence's envelope is thus constructed.

  The Hilbert transform is employed to compute a time signal $\tilde{h}(t)$ from the original time signal $h(t)$, where $\tilde{h}(t)$ retains the amplitudes of spectral components but the phases are altered by $\pi/2$ such that:

$$h(t) = Ae^{-\zeta t} \sin \omega_n t \quad \textbf{(2.37)}$$

$$\tilde{h}(t) = -Ae^{-\zeta t} \cos \omega_n t \quad \textbf{(2.38)}$$

Where: A is the amplitude of the complex exponential

ζ is the damping factor

ω_n is the angular frequency

t is the instantaneous time value

The magnitude of the analytic signal $\hat{h}(t)$, which describes the Hilbert envelope, can be directly calculated from $h(t)$ and $\tilde{h}(t)$ as follows:

$$\left|\hat{h}(t)\right| = \sqrt{h(t) + i\,\tilde{h}(t)} \quad \textbf{(2.39)}$$

Where: $$\left|\hat{h}(t)\right| = Ae^{-\zeta \omega_n t} \quad \textbf{(2.40)}$$

From Eqn. 2.40 it can be determined that the logarithm of the Hilbert envelope gives a first order polynomial whose slope is the negative of the damping coefficient. This may be expressed as:

$$\zeta = -\log\left(\left|\hat{h}(t)\right|/A\right)/\omega_n \qquad \textbf{(2.41)}$$

Figure 2-3 shows the impulse response of an SDOF system and how its envelope can be obtained by means of a Hilbert transform.

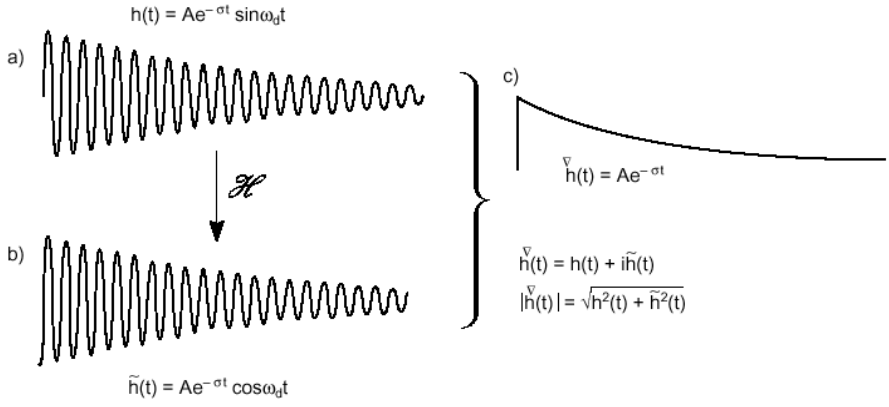

Figure 2-3 *Envelope computation of the impulse-response function with use of the Hilbert transform [58]*

With regard to the HEM, it should be noted that if a one-sided spectrum is inverse transformed to the time domain, the resulting time signal is analytic. Therefore the imaginary component of the computed signal is automatically the Hilbert transform of the real part and its modulus is the envelope [57]. Since the Hilbert transform corresponds to a convolution with a hyperbolic function, it cannot produce a sudden step as illustrated in Fig. 2-3 but a little away from the initial part of the response the estimated envelope is accurate [59].

The description of the HEM provided so far in this chapter applies only to SDOF systems. When applying the HEM to MDOF systems, individual resonance peaks are bandpass filtered in a signal's frequency domain and inverse transformed to give the equivalent SDOF impulse response function [57]. The HEM is then applied as previously discussed. Of note is that the HEM may provide inaccurate modal damping ratio estimates when structures have high modal densities and therefore exhibit heavily coupled modes.

2.4.3 CORRELATION OF EXPERIMENTAL AND NUMERICAL MODAL RESULTS

The primary application of EMA results in this thesis is to validate the employed FE computation methodology. In practice, the accuracy of a FE model is limited by uncertainties relating to geometric and material properties, boundary conditions and loading applied to the model. Reliable vibration and acoustic predictions can therefore only be made if the numerical model is validated with experimental results.

The correlation of finite element and experimental results is usually conducted within the context of finite element model updating. However, as this thesis is concerned with developing a numerical methodology to be utilised with the design phase, no model updating will be conducted. The correlation of numerical and experimental results is therefore used as a tool to validate the modelling methodology employed. Several correlation methods are detailed as follows:

- *Natural frequency correlation*

  The simplest and most frequently employed approach to correlate two modal models is through the direct comparison of natural frequencies. If the experimental values and the numerical results lie on a straight line with a gradient of one when plotted against each other the data is perfectly correlated. A percentage difference between the experimental and numerical modes can also be defined as:

$$\epsilon_{\omega_j} = \frac{\omega_{nu_j} - \omega_{ex_j}}{\omega_{nu_j}} \times 100 \qquad \textbf{(2.42)}$$

  Where: ϵ_{ω_j} is the error percentage between experimental and numerical natural frequencies at mode *j*

  ω_{nm_j} is the numerical natural frequency at mode *j*

  ω_{ex_j} is the experimental natural frequency at mode *j*

- *Direct mode shape correlation*

  In addition to comparing natural frequencies, mode shapes may also be directly compared by plotting numerical modes against those determined experimentally. The modal scale factor (MSF) allows for modal vectors to be compared and contrasted by normalising all estimates of the same modal vector, taking into account magnitude and phase differences. Once two different modal vector estimates are scaled similarly, elements of each vector can be averaged, differentiated, or sorted to provide an indication of the error vector superimposed on the modal vector [60]. The modal scale factor is defined as:

$$MSF(\phi_{nu}, \phi_{ex}) = \frac{\{\phi_{nu}\}^T\{\phi_{ex}\}^*}{\{\phi_{nu}\}^T\{\phi_{ex}\}^*} \quad \textbf{(2.43)}$$

  Where: ϕ_{nu} is the numerically determined mode shape

  ϕ_{ex} is the experimentally determined mode shape

  $\{\}^*$ denotes an complex conjugate column vector

  If a numerical and an experimental vector are considered to represent the same mode, the numerically computed vector and the MSF may also be used to complete the experimental modal vector [60]. It is of note that in almost all cases the experimental data set is incomplete as measurements are taken at selected locations and in particular directions.

- *The Modal Assurance Criterion*

  The function of the Modal Assurance Criterion (MAC) is to provide a measure of consistency (i.e. the degree of linearity between estimates of a modal vector) [61]. It is one of the most popular tools for the quantitative comparison of modal vectors. The MAC is calculated as a normalised scalar product of the two sets of vectors $\{\phi_{nu}\}$ and $\{\phi_{ex}\}$ as follows:

$$MAC_{jk} = \frac{\left|\{\phi_{nu}\}_j^T \{\phi_{nu}\}_k^*\right|^2}{\left(\{\phi_{nu}\}_j^T \{\phi_{nu}\}_j^*\right)\left(\{\phi_{ex}\}_k^T \{\phi_{ex}\}_k^*\right)} \quad \textbf{(2.44)}$$

  A MAC value of one indicates that the two modes are perfectly correlated while a value of zero indicates that there is no correlation at all.

- *Frequency response function correlation*

  In addition to contrasting modal parameters, a direct comparison of FRFs may be conducted to determine the correlation between numerically and experimentally determined data. To compare numerical and experimental transfer functions a visual inspection is often sufficient to determine agreement. Additionally, employing the Euclidean norm of the FRF vectors measured at discrete frequencies allows for an error indication to be computed as [62]:

$$\epsilon_{H_{jk}} = \frac{\left\|(H_{nu})_{jk} - (H_{ex})_{jk}\right\|}{\left\|(H_{nu})_{jk}\right\|} \quad \textbf{(2.45)}$$

Based on the MAC technique and on the concept of frequency shifting, Ref. [63] proposed to measure the correlation between experimental and numerically determined FRFs by using the Frequency Domain Assurance Criterion (FDAC) as,

$$FDAC(\omega_A, \omega_A, j) = \frac{\left|\{H_A(\omega_A)\}_j^T \{H_X(\omega_X)\}\right|^2}{\left(\{H_A(\omega_A)\}_j^T \{H_A(\omega_A)\}_j\right)\left(\{H_X(\omega_X)\}_j^T \{H_X(\omega_X)\}_j\right)} \quad \textbf{(2.46)}$$

Where: j corresponds to the measured column of $[H]$

ω_A is the frequency at which $\{H_A\}$ is calculated

ω_X is the frequency at which the FRF was measured experimentally

The FDAC measure can be viewed as an equivalent to MAC in the frequency domain. As with the MAC criterion, a value of zero indicates no correlation between the FRFs considered while a value of one indicates perfect correlation.

CHAPTER 3

FINITE ELEMENT MODEL

OF THE TRANSFORMER

This chapter presents the finite element modelling methodology employed in this thesis to determine the vibration and acoustic characteristics of a large power transformer. The boundary conditions and electromagnetic and magnetostrictive forces applied to the finite element model are also discussed in detail. The steps taken in the development of the FE prediction tool are shown in Figure 3-1. For a review of the theoretical constructs of the finite element methodology refer to C*hapter 2.4.1.*

The finite element computation scheme presented in this chapter can be divided into the following four steps:

- Modelling the active part, namely the core and the windings;
- Modelling the tank and auxiliary components;
- Defining acoustic bodies and fluid-structure interaction in the FE model; and
- Application of excitation forces to the FE model.

The above modelling steps are further discussed in the following subchapters. The final part of this chapter details the damping characteristics applied to the FE model, as determined from the FRF data provided by Siemens AG Austria, Transformers Weiz.

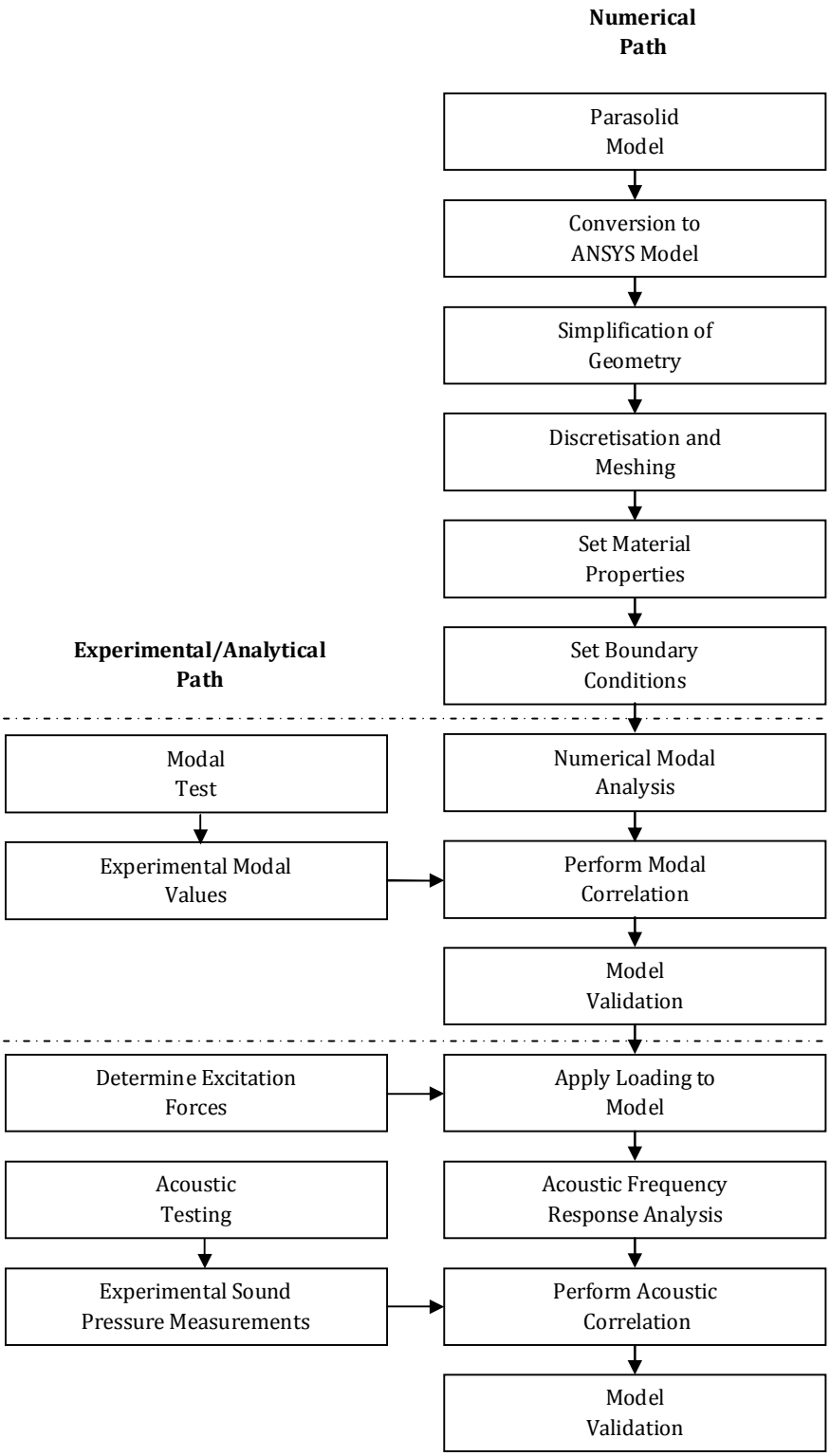

Figure 3-1 Steps in the development of the finite element tool to predict the vibration and acoustic characteristics of a power transformer

3.1 SPECIFICATIONS OF THE TRANSFORMER

The transformer analysed within this thesis is a single-phase, special purpose transformer. A single-phase unit has been studied to simplify the electro-magnetic loading conditions applied to the model, whereby reducing a potential error source in the numerical model. It is anticipated that simulating a three-phase transformer, provided that the loading conditions of the model are accurately calculated, will not affect the validity of the vibro-acoustic modelling methodology presented in this thesis.

The single-phase transformer studied in this thesis features a two-limb core design, which decreases the magnitude of potential short-circuit forces by reducing the ampere-turns per height. The two-limb core design has been adopted due to the high rating of the unit. Siemens AG Austria, Transformers Weiz have provided the computer-aided design (CAD) model of the transformer. An illustration of the unit from the CAD model is shown in Figure 3-2.

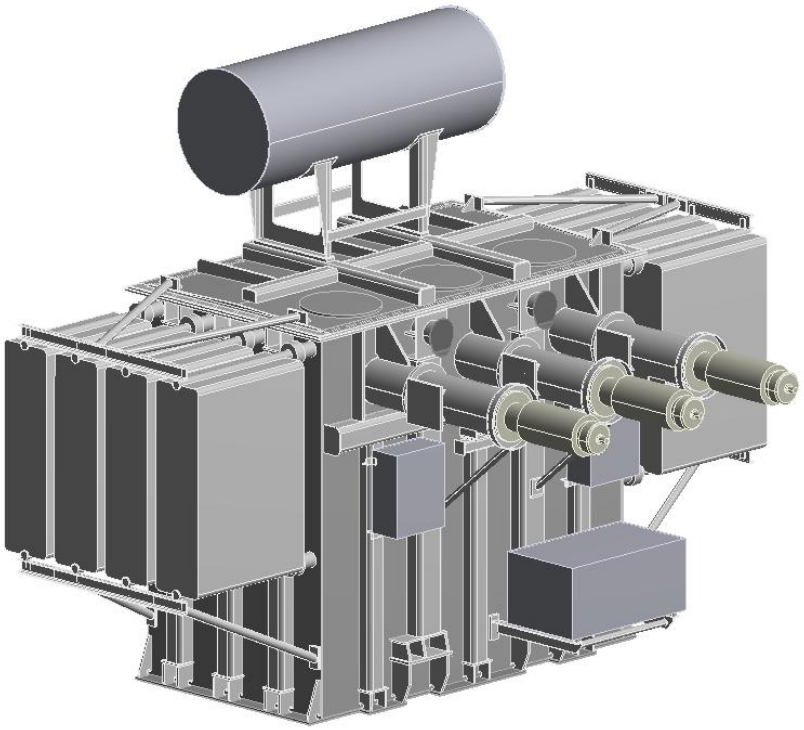

Figure 3-2 Geometry of the transformer assembly

Due to the sensitive commercial nature of the data presented in this thesis, including vibration characteristics and sound pressure measurements, the exact technical specifications of the transformer will not be stated. However, the basic geometric parameters of the transformer are given in Table 3-1.

Table 3-1 Geometric parameters of the transformer

Part	**Approximate Dimensions** (m)	**Approximate Mass** (kg)
Transformer tank	• 4.0 (l) *x* 2.0 (w) *x* 3.5 (h)	19, 000
Core *(single-phase, two-limb design)*	• 3.3 (l) *x* 2.7 (h) • $Ø_{limb}$ = 0.3	19, 000
Windings	• 1.6 (h) • $Ø_{winding}$ = 1.6	28, 000
Radiators	-	5, 500
Conservator	-	1, 500
Bushings	-	1, 400
Insulation fluid	-	18, 000

3.1.1 SIMPLIFICATION OF THE COMPUTER-AIDED DESIGN MODEL

The illustration of the transformer shown in Figure 3-2 is a simplified copy of the original computer-aided design model. Simplification of the model, which suppresses parts and features not likely to influence the accuracy of analysis results, has been carried out to increase computational performance both in terms of mesh size and mesh quality. The simplification methods that have been employed within this thesis are detailed in Table 3-2.

Table 3-2 Model Simplification Methodology

Feature Type	Simplification Methodology
Fasteners	The fasteners connecting bodies, i.e. bolts, nuts and screws, have been suppressed when simplifying the CAD model. The connection between bodies and components connected with fasteners has been considered as a bonded contact. Surfaces held together with adhesives or surfaces welded together have also been considered as exhibiting the characteristics of a bonded contact.
Holes	Holes, such as those created for the bolted connections, have been filled. Holes that were filled have a diameter of less than 20 mm and are not in proximity to boundary conditions or applied loads.
Chamfers	Chamfers not in proximity to boundary conditions or applied loads and with an edge length of less than 20 mm have been suppressed in the model.
Rounds	Rounds not in proximity to boundary conditions or applied loads and with a radius of less than 5 mm have been suppressed in the model.

3.2 MODELLING OF THE TANK

There are several reasons for modelling the tank of the transformer. The most significant of these is the need to identify the situations where vibrations propagating from the active part excite a natural frequency of the tank structure. At these inherent natural frequencies the tank can amplify the vibrations propagating from the active part. This phenomenon, referred to as a resonance, results in elevated sound radiation levels.

To discretise the transformer tank three-dimensional solid elements, namely Solid185 and Solid186, have been employed. The quadratic displacement properties of these elements lend them to modelling complex geometry. The discretised tank structure is illustrated in Figure 3-3.

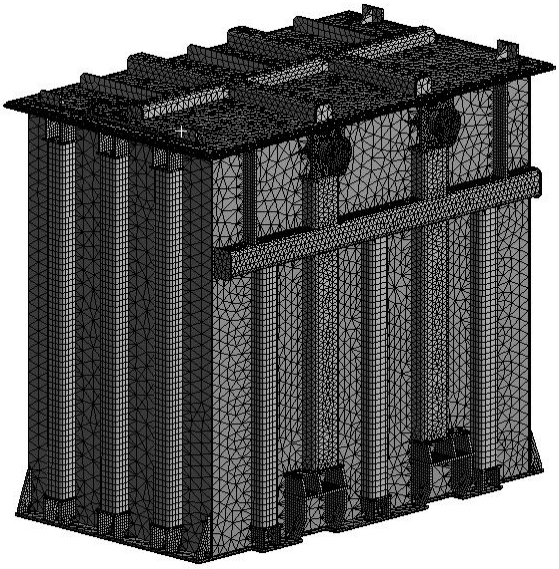

(a)

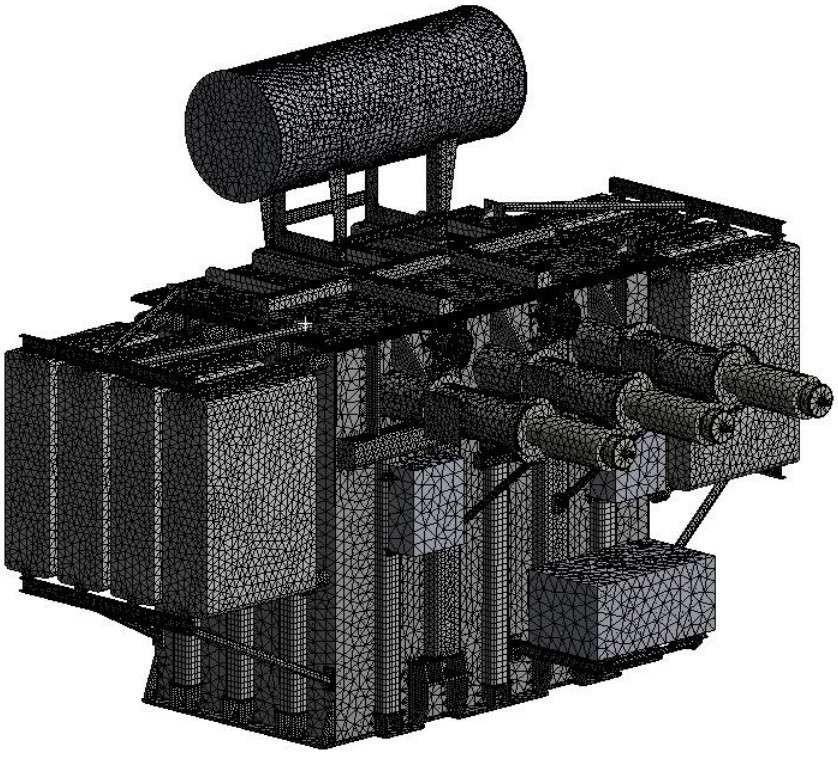

(b)

Figure 3-3 Finite element model of (a) the transformer tank and (b) the transformer tank with auxiliary equipment

Within the finite element model the connections between the tank, the bushings, the conservator and the auxiliary equipment have been modelled as bonded contacts. The bonded contacts replicate the fasteners and welded joints that connect these structural elements. To replicate the test setup of the transformer an elastic support has been modelled on the base of the transformer tank. The value of the elastic support was calculated from the mechanical properties and dimensions of the rubber mat positioned under the transformer during testing.

3.3 MODELLING OF THE ACTIVE PART

The core and the windings are the two principal components that comprise the active part of a transformer. Additional components in the active part assembly include press plates, press rings, support blocks and tie-rods, which act primarily to maintain clamping pressure on the core and the windings. As with the tank structure, solid elements Solid185 and Solid186 have been employed to discretise the active part assembly. The finite element model of the active part is illustrated in Figure 3-4.

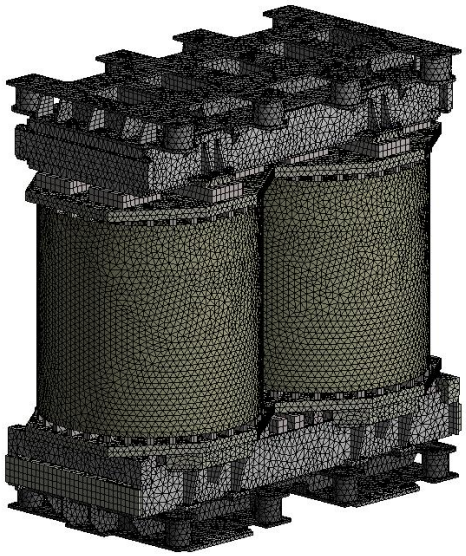

Figure 3-4 Finite element model of the active part

As seen in Figure 3-4, a significant focus of the modelling procedure employed in this thesis has been to incorporate all key structural elements into the finite element model of the active part. Creating such a detailed model, whereby all components that comprise the active part are mechanically coupled, has negated the use of fictitious spring elements or other constraints[3]. Although not illustrated in Figure 3-4, it is of note that the active part is also directly coupled to the base of the tank.

Within the numerical model of the active part fasteners have been suppressed and the connections between components held together with fasteners or adhesives have been modelled as bonded contacts. Furthermore, bonded contacts have been used between the windings, the press rings and the press plates. The bonded contact between these aforementioned elements replicates the rigid clamping system that maintains pressure on the winding assembly over the life of the transformer[4].

Several materials and components within the active part assembly display anisotropic mechanical behaviour (i.e. they exhibit directionally dependent mechanical properties). To accurately account for the structural response of the active part the anisotropic material properties of these parts have been accounted for in the FE model. The anisotropic materials and components within the active part are further described in the following paragraphs.

[3] Fictitious spring elements have been required in previous finite element studies investigating the acoustic emissions of power transformer. These spring elements have been required to constrain the active part within the tank as no mechanical coupling between the active part and the tank has been modelled (see Ref. [3] and Ref. [4]).

[4] In order to withstand the mechanical stresses during lifting, transportation, operation and short circuits events the winding assembly of a transformer must be appropriately clamped. Clamping is generally conducted by applying a force to the press ring and then filling the gap created between the press ring and the clamping plate with insulation material.

- *Winding block assembly*

  Transformer windings are manufactured from paper insulated copper conductors and pressboard spacers. Depending on the specifications of the unit and manufacturer preferences, these conductors may be in the form of individual strip conductors, bunched conductors or continuously transposed cable conductors. The complexity of the windings makes accurate geometric modelling impractical. Therefore, within this study the winding block has been considered as a homogeneous body.

  The mechanical properties of the homogeneous winding block have been determined from measurements relating the deflection of the winding to the forces applied during the assembly process. These measurements were provided by Siemens AG Austria, Transformers Weiz. From this data the elastic modulus of the windings in the pressing plane has been determined. In the radial plane the windings were assumed to have an elastic modulus equal to that of copper.

- *Electrical steel*

  The purpose of a transformer core is to provide a low-reluctance path for the magnetic flux that links the primary and secondary windings. The majority of modern transformer cores are therefore produced from grain-orientated steel, which reduces hysteresis losses, increases permeability and also increases resistivity [52]. However, as a result of the grain-orientation, core steels exhibit anisotropic properties. The properties of the core material utilised within this thesis have been taken from values published by electrical steel producers.

- *Clamping rings*

  Clamping rings are an integral component of a transformer's active part, designed to prevent the windings from sustaining permanent distortion or damage during short-circuit events. The clamping rings of the unit analysed in this thesis were produced from densified cellulous pressboard layers and adhesive. This construction results in weaker mechanical properties in the radial plane. The anisotropic material properties of this production method have been determined by Siemens AG Austria, Transformers Weiz through experimental measurements.

3.4 ACOUSTIC BODIES AND FLUID-STRUCTURE INTERACTION

The oil within a transformer is vital to its effective operation, especially so in larger units. This is due to the dual roles that the fluid performs, acting as a coolant and as an insulator. The energy losses of a transformer manifest themselves primarily as heat, and efficient cooling is therefore required in order to limit the maximum operating temperature. Furthermore, the oil helps to insulate components of the transformer assembly that are at different electrical potentials from one another. Through the impregnation of various porous components the oil also adds to the efficiency of solid insulation.

In this study the insulation oil has been considered as an acoustic domain. This has allowed for the bi-directional coupling of fluid and structural elements, creating an indirect transmission path between the active part and the tank structure. Fluid elements Fluid220 and Fluid221 have been employed to model the acoustic body representing the insulation oil. These three-dimensional solid elements exhibit quadratic pressure behaviour and are therefore suited to modelling the fluid medium and the fluid-structure interface.

In addition to the acoustic domain representing the insulation oil, the finite element prediction of sound radiation has required the oscillations of the transformer tank to be applied to an external acoustic body. Specifically, the nodal velocities from the transformer's external surfaces, which resulted from excitation of the finite element model, have been interpolated and mapped to an acoustic mesh. Figure 3-5 illustrates the nodal velocity vectors of the transformer tank. The forces applied to excite the FE model, replicating the electromagnetic and magnetostrictive forces in the active part, are further described in *Chapter 3.7*.

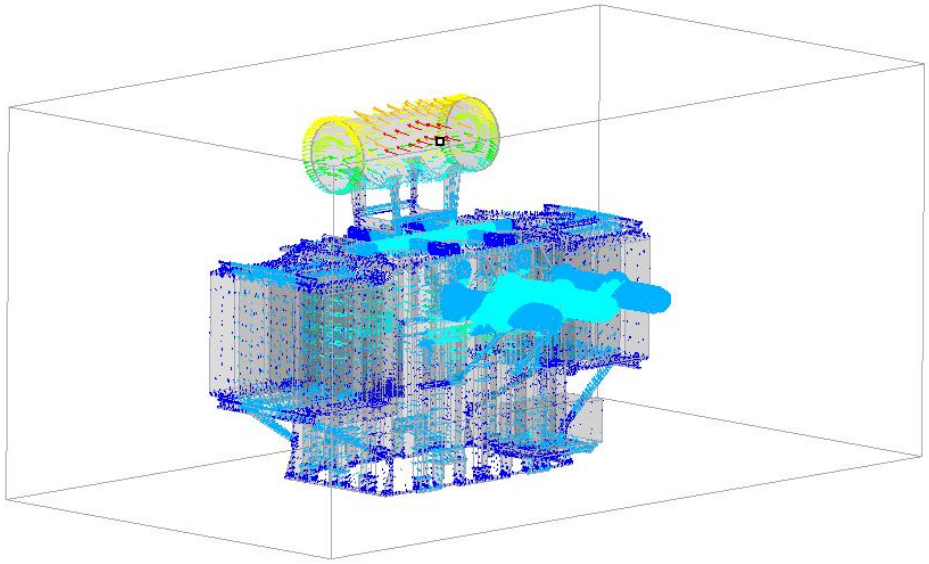

Figure 3-5 Nodal velocity vectors mapped to the acoustic body surrounding the transformer tank

As opposed to the bi-directional fluid-structure interaction between the insulation fluid, the active part and the tank, a single direction coupling has been modelled between the tank and the external acoustic body. This single direction coupling is assumed to be valid, as the air surrounding the transformer tank does not affect the amplitude or other vibration characteristics of the tank. Furthermore, neglecting the acoustic effect on the structure and therefore defining a one-way coupling from the structural to the acoustic field has provided a more computationally efficient analysis.

The acoustic finite element domain surrounding the transformer has been modelled to geometrically and physically replicate the transformer's environs. Specifically, the acoustic body aims to reproduce the test laboratory in which the experimental noise measurements of the unit were obtained. Fluid221 elements were used to model the external acoustic body surrounding the transformer.

3.5 EXCITATION MECHANISMS

The electromagnetic and magnetostrictive forces that act of a transformer's active part have been extensively studied. Detailed mathematical descriptions and calculation procedures of these forces are found in many textbooks, with Refs. [7, 64, 65] being a selected few. Therefore, comprehensive mathematical formulations and calculations of the electromagnetic and magnetostrictive forces will not be presented in this thesis. Instead this chapter will focus on the characteristics of the excitation mechanisms in a transformer's active part and how these characteristics influence the acoustic behaviour of a transformer.

The electromagnetic and magnetostrictive forces applied to excite the FE model in this thesis have been calculated with Siemens AG's internal noise prediction tool. The calculation tool accounts for both the physical description of the forces and the specific design characteristics of the active part, such as dimensions and material grades. The three excitation mechanisms that generate the vibrations of the active part are Maxwell and magnetostrictive forces, acting on the core, and Lorentz forces in the windings.

3.5.1 EXCITATION MECHANISMS IN THE CORE

The vibrations of the core, which produce acoustic emissions referred to as no-load transformer noise, result from alternating flux in the active part. The alternating flux causes magnetostrictive forces in the ferromagnetic core sheets and Maxwell forces at corner joints and air-gaps. The amplitudes of these magnetic and magnetostrictive forces are dependent on both the flux density in the core sheets and the material properties of the magnetic core steel. Further descriptions of these two forces acting on the transformer core are given as follows:

- *Maxwell forces*

  Maxwell forces act on the boundaries between two magnetic media with different permeabilities. In transformer cores these forces are therefore typically associated with air-gap regions and joints. The amplitude of the Maxwell forces can be calculated by the surface integration of the local force density based on the Maxwell stress tensor as [5, 66]:

$$F = \frac{1}{\mu_0} \oint_A \left(B(B\,n) - \frac{1}{2} B^2 n \right) dA \qquad \textbf{(3.1)}$$

  Where:

  μ_0 is magnetic constant permeability of free space

  B is the magnetic flux density flowing through the closed surface area A

  n is a unit vector normal to surface A

  dA is the area differential of the closed surface area A around the domain of interest

From Eqn. 3.1 it can be determined that the Maxwell forces act predominantly at twice the power frequency. This is due to the forces being proportional to the squared magnetic flux density in the core sheets. Therefore, assuming that the structural response of a transformer is linear, the sound radiation resulting from Maxwell forces in the core is dominant at twice the network frequency.

- *Magnetostrictive strain*

  Magnetostriction refers to the change in the dimensions of a magnetic material when it is subjected to a magnetic field. The dimensional change results from the rotation of uniform magnetic domains – regions within a magnetic material that have uniform magnetisation – under an applied magnetic field. Within a transformer core the magnetostrictive strain reaches saturation twice per cycle of the network frequency [6].

  Magnetostriction exhibits hysteretic behaviour (i.e. time based dependence) with respect to the applied magnetic field [67]. This complex hysteretic behaviour reflects the nonlinear change of the magnetic domains within a magnetic material during AC magnetisation. Magnetostrictive strain curves in the time domain illustrating this phenomenon are shown in Figure 3-6 at differing induction levels. The measurements provided in Figure 3-6 were recorded during quality assurance measurements performed on generic transformer core material.

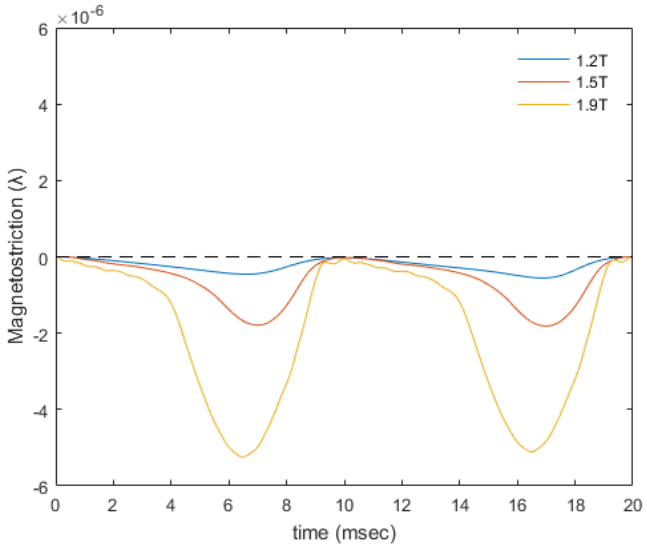

Figure 3-6 Magnetostrictive effect in SiFe sheets at differing induction levels (Source: Siemens AG Austria, Transformers Weiz)

The nonlinear characteristics of the magnetostrictive strain occurring in transformer core steel result in the sound radiation from magnetostriction containing even harmonics of the network frequency. The significance of each of these harmonics is dependent on the induction level in the core.

3.5.2 ELECTROMAGNETIC FORCES IN THE WINDINGS

The electromagnetic excitation of a transformer's windings, which produce acoustic emissions referred to as load noise, results from the interaction between the current carrying winding loops and the magnetic stray flux. These forces, referred to as Lorentz forces, are determined by the current amplitude and the magnitude of the magnetic stray flux at the winding location such that:

$$F = J \times B \qquad \textbf{(3.2)}$$

Where: F is the Lorentz force

J is the electric current density

B is the magnetic flux density

As with Maxwell forces, the Lorentz forces are dominant at twice the power frequency. This is due to the Lorentz forces being proportional to the squared winding current [6, 52, 68]. The sound radiation resulting from Lorentz forces is therefore prevalent at twice the network frequency, assuming that a transformer's structural response is linear.

3.5.3 SUMMARY OF THE CHARACTERISTICS OF THE EXCITATION MECHANISMS

From the preceding descriptions of the excitation mechanisms in a transformer's active part it can be summarised that:

- The Maxwell forces in the core and the Lorentz forces in the windings act predominantly at twice the line frequency; and
- The non-linear characteristics of the magnetostrictive strain in a transformer's core results in significant mechanical forces at even harmonics of the network frequency.

Higher harmonics in the acoustic spectrum of a transformer may also result from the presence of nonlinear magnetic stray flux in the active part and the nonlinear behaviour of the windings and other components.

Past literature on the transformer noise characteristics [67, 69, 70] identifies the first three even harmonics of the line frequency as being dominant in the sound radiated by transformers (i.e. assuming a network frequency of 50 Hz the noise emissions of a transformer may be considered dominant at 100 Hz, 200 Hz and 300 Hz). This notion is further supported by the typical acoustic frequency spectrum of a transformer, as illustrated in Figure 3-7. It can therefore be concluded that a noise prediction tool to estimate acoustic emissions of a transformer operating under nominal conditions must incorporate the first three even harmonics of the network frequency.

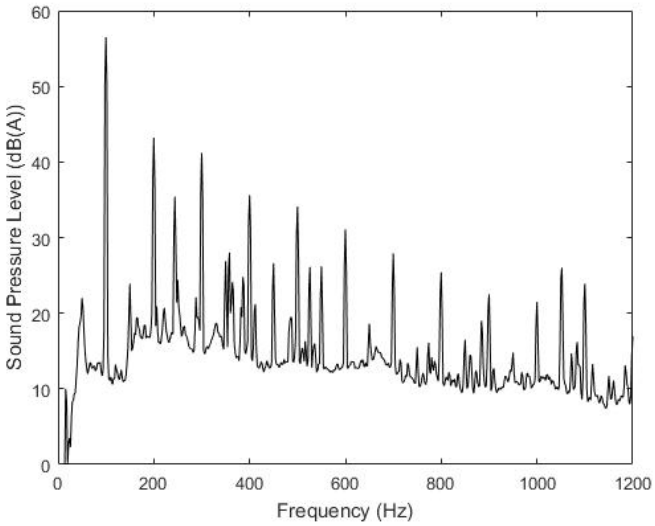

Figure 3-7 Typical acoustic spectrum produced by a 50 Hz power transformer (Source: Siemens AG Austria, Transformers Weiz)

3.5.4 MODELLING OF THE FORCES APPLIED TO THE NUMERICAL MODEL

Within this study multiple mono-harmonic linear simulations (i.e. simulations at discrete frequencies in which the FE model is excited with sinusoidal forces that produce a harmonic response) across a 100 Hz to 400 Hz frequency spectrum have been performed to determine the vibration and acoustic response of the numerically modelled transformer. This approach has been adopted as it is able to identify the distance of the assembly's resonance peaks from the mechanical excitation frequencies in the active part, being 100 Hz or 120 Hz and higher harmonics thereof. A prediction of this distance between the resonance frequencies and the excitation frequencies is critical in understanding the risk of high noise emissions from a transformer.

The multiple mono-harmonic simulation approach employed in this thesis accounts for variation in the natural frequencies' of a transformer arising from both model uncertainty and manufacturing variability. A simulation approach with fixed multi-harmonic excitation would only have provided three noise prediction points over the 100 Hz to 400 Hz range of interest (being at the dominant harmonics of the excitation mechanisms). Furthermore, a fixed-multi-harmonic simulation would not have accounted for any variability between numerical and experimental natural frequencies.

The forces employed in this thesis to excite the FE model at each discrete excitation frequency replicate the fundamental frequency component of the Maxwell, Lorentz and magnetostrictive forces present in the transformer's active part. These aforementioned forces have been applied to the surfaces of the active part geometry on which they primarily act. As such and where valid, Lorentz forces have been applied to the windings, Maxwell forces have been applied to the core joints, and Magnetostrictive strain has been applied to the electrical core sheets. Further discussion on the characteristics of these forces has been provided previously in *Chapter 3.5.3*.

Although not considered in this thesis, the multiple mono-harmonic simulation approach may also be employed to estimate a transformer's total noise levels under nominal operating conditions. This total noise prediction would require the non-linearity of the excitation mechanisms to be accounted for, which has not been considered in this thesis. Specifically, the discrete amplitudes of the electromagnetic and magnetostrictive forces at the first three even harmonics of the network frequency would need to be determined and applied within the numerical model.

Employing the multiple mono-harmonic simulation approach, the prediction of a transformer's total operational acoustic emissions would be made through the summation the sound pressure levels determined at each simulation frequency. Therefore, the total sound pressure of transformer accounting for measurements at the network frequency's first three even harmonics would be determined by:

$$L_{\Sigma} = 10\log_{10}\left(10^{\frac{L_1}{10\ dB}} + 10^{\frac{L_2}{10\ dB}} + 10^{\frac{L_3}{10\ dB}}\right)\ dB \qquad \textbf{(3.3)}$$

Where: L indicates individual the sound pressure levels at each of the dominant harmonics

It is of note that employing Eqn. 3.3 is similar to conducting a multi-harmonic simulation to compute a single total sound pressure level estimate.

Within this thesis the operational acoustic characteristics of the analysed transformer are not stated due to the sensitive commercial nature of the data. However, ad hoc acoustic measurements for the validation of the finite element model over a range that incorporates the first three even harmonics of the network frequency are presented in *Chapter 4.3*. The validation of the numerical vibro-acoustic model represents a key novelty of this thesis.

3.6 MODAL DAMPING

Damping exists in all oscillatory systems that experience energy dissipation, having the effect of diminishing the system's vibration in the neighbourhood of a resonance. Damping also affects the transmissibility of vibrations through a system, i.e. the ratio between the vibration output and imposed vibration input. Accurate modelling of the damping loss factor in vibro-acoustic predictions is therefore critical in order to account for the correct transmissibility of vibrations and sound.

As opposed to the mass and stiffness matrices in finite element models, the damping matrix of an assembly cannot be practically evaluated from structural materials and member sizes. Instead modal damping is determined from dynamic tests and experimental results. To fully describe the vibration response of the transformer analysed within this thesis, the modal damping characteristics of both the active part and the oil-filled tank assembly have been determined through the evaluation of experimental modal analysis (EMA) results.

The EMAs of the active part and the oil-filled tank assembly were conducted by means of roving impact hammer tests. A detailed theoretical description of this method can be found in Refs. [71, 72]. Siemens AG Austria, Transformers Weiz performed the EMAs of the active part and the tank assembly and provided the relevant data utilised within this thesis. Of note is that no EMA was conducted on the active part of the specific transformer modelled and analysed within this thesis. Therefore, data from an EMA conducted on the active part of a similar unit has been utilised.

Following the evaluation of damping from EMA results, this chapter will detail how the modal damping characteristics of the transformer have been accounted for in the FE model. The most common formulation to numerically model modal damping in dynamic FE simulations is that of Rayleigh damping. Expressed in matrix form, Rayleigh damping is a linear combination of the mass and stiffness matrices of the structure:

$$[C] = \alpha\,[M] + \beta\,[K] \qquad \textbf{(3.4)}$$

Where: $[C]$ is the viscous Rayleigh damping matrix

$[M]$ is the mass matrix

$[K]$ is the stiffness matrix

α is the mass-proportional damping coefficient

β is the stiffness-proportional damping coefficient

In this thesis it has been assumed that damping is in the form of Rayleigh damping (i.e. mass and stiffness proportional damping). Therefore the modal damping investigations detailed in the following subchapters are conducted with the objective of determining the Rayleigh damping coefficients alpha and beta.

3.6.1 MODAL DAMPING OF THE ACTIVE PART

The most common approach to describing the damping characteristics of a system is through the modal damping ratio. This parameter, usually denoted by zeta, ζ, provides a mathematical means of expressing the level of damping in a system relative to the system's critical damping[5]. In this investigation the half-power bandwidth method has been employed to determine the damping of the active part. The aforementioned methodology is the most widely used frequency domain approach for determining a system's damping behaviour.

The half-power bandwidth method utilises the frequency response curve from a forced vibration test to determine of the modal damping ratio. Employing the half-power bandwidth methodology the modal damping ratio is computed from:

$$\zeta = \left(\frac{\omega_2 - \omega_1}{\omega_n}\right)/2 \qquad \textbf{(3.5)}$$

Where: ζ is the modal damping ratio

ω_n is the natural frequency

ω_1, ω_2 are points on the frequency response curve that that relate to the maximum response multiplied by $1/\sqrt{2}$

[5] A system's critical damping refers to the damping required to return a perturbed system to its equilibrium position in the shortest possible time without any oscillation

In this study the FRF data describing the vibration characteristics of the active part had qualities well suited to the use of the half-power bandwidth method. These qualities included:

- Clearly defined and isolated modes within the frequency response function, which allowed for the accurate identification of the half-power points; and
- A high resolution of the frequency response function, with measurements taken at 0.25 Hz intervals. This allowed for accurate identification of the normalised acceleration magnitude of the FRF functions at resonance peaks.

Applying the half-power bandwidth method at resonance peaks along the measured frequency spectrum has allowed for to the modal damping characteristics of the active part to be determined. For the purposes of this study the damping characteristics have been determined between 100 Hz and for 400 Hz, matching the frequency spectrum over which numerical vibration and acoustic analyses of the transformer have been performed.

Illustrations of the half-power bandwidth methodology as applied to the resonance peaks measured at 192 Hz and 346 Hz are presented in Figure 3-8(a) and Figure 3-8(b), respectively. Figure 3-8(c) shows the Rayleigh damping curve determined from the modal damping ratios calculated at 192 Hz and 346 Hz. The Rayleigh damping curve in Figure 3-8(c) has been computed from the definition provided in Eqn. 3.16.

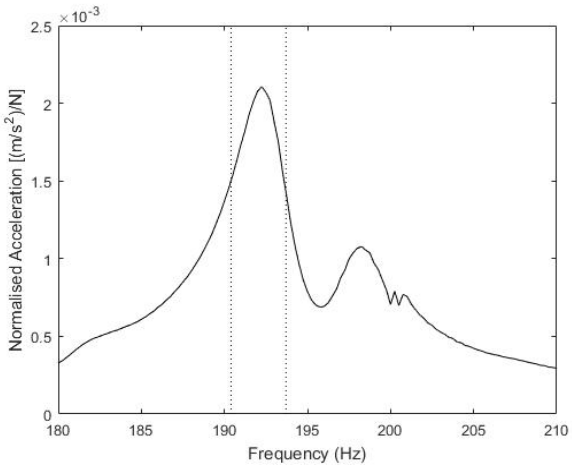

(a)

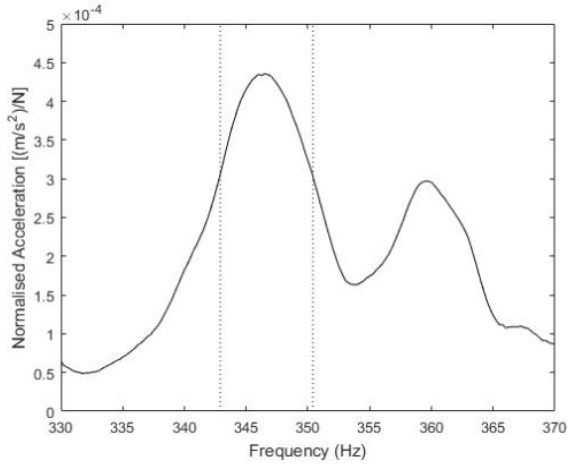

(b)

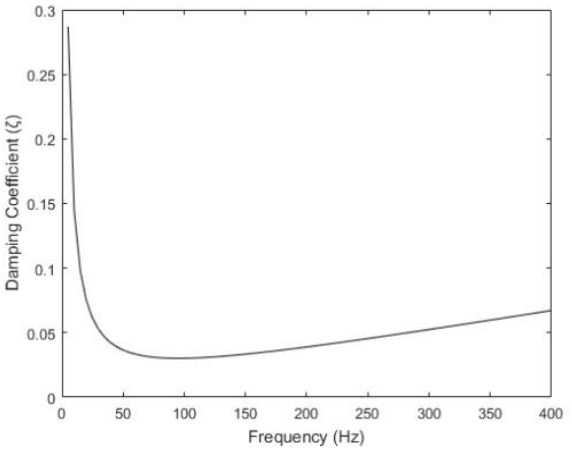

(c)

Figure 3-8 Half-power points on an FRF employed to calculate the damping ratios of the active part at (a) 192 Hz and (b) 346 Hz (c) and the resulting Rayleigh damping curve

3.6.2 MODAL DAMPING OF THE TANK STRUCTURE

Conventional curve-fitting methods such as the half-power bandwidth method and the Hilbert Envelope Method (HEM) determine the modal damping characteristics of a system at isolated resonance peaks. However, the complexity of the transformer assembly studied in this thesis, with a high modal density and therefore heavily coupled modes, has nullified conventional curve-fitting approaches. A novel adaptation of the HEM, herein referred to as the *adapted damping estimation technique*, is therefore employed in this thesis[6].

To determine the studied transformer's modal damping characteristics, the novel damping technique estimates modal damping within defined bandwidths as opposed to at isolated resonance peaks. The adapted damping estimation technique assumes that a single principal resonance, which occurs at an unknown frequency, dominates within each defined bandwidth. All other resonance peaks that occur within the bandwidth are therefore considered as noise. Under this assumption the prevailing resonance in each band dominates the decay of the time domain impulse response. The unknown frequency of the dominant resonance is approximated by the geometric mean value of the band (the centre frequency).

The adapted damping estimation technique is further detailed in the following paragraphs with a mathematical description followed by a numerical justification. An overview of the methodology as applied to the EMA data of the oil-filled transformer assembly analysed within this thesis is also presented.

[6] The Hilbert Envelope Method is used as the theoretical foundation of the adapted damping estimation technique due to its relative simplicity and its high level of accuracy in comparison to other methods (refer to Ref. [73] for a comparison of curve-fitting techniques).

- *Mathematical Description*

  Within this thesis the damping characteristics of the transformer assembly were calculated within one-third octave bands. However, other bandwidths, depending on the vibration characteristics of the structure analysed, may have been employed. The one-third-octave bandwidth delineation of the FRF signal is notated by:

$$\Delta f_k = \left[h_k/2^{\frac{1}{6}}, h_k\, 2^{\frac{1}{6}}\right];\ h_{k+1} = \ h_k\, 2^{\frac{1}{3}} \qquad \textbf{(3.6)}$$

  Where: Δf_k is the frequency band

  h_k is the geometric mean of the frequency band

  As an adaption of the Hilbert Envelop Method, the modal damping estimation was conducted in the time domain. This required the inverse fast Fourier transform (IFFT) of the FRF to be taken, such that:

$$x(t) = IFFT(X(f) \cdot I(f; \Delta f_k)) \qquad \textbf{(3.7)}$$

  Where: $x(t)$ is the impulse signal in the time domain

  $X(f)$ is the Fourier transform of the complex series *x(t)*

  The term $I(f; \Delta f_k)$ in Eqn. 3.7 acts as an indicator function (ideal filter), allowing only the frequency data points within the given one-third-octave bandwidth to pass through the IFFT algorithm. The remaining FRF data points, which fall outside the band, return a zero value, such that:

$$I(f; \Delta f_k) = \begin{cases} 1\ if\ f \in \Delta f_k \\ 0\ otherwise \end{cases} \qquad \textbf{(3.8)}$$

  The time domain vector resulting from Eqn. 3.7 therefore retains the original length of the FRF vector.

Since the FRF function $X(f)$ inverse transformed to the time domain in Eqn. 3.7 is one-sided (no negative frequency component) the resulting time signal is analytic. Furthermore, it can be assumed that the analytic signal may be mathematically approximated as a simple harmonic oscillation in the form,

$$x_a(t) = e^{-\zeta \omega_n t} \sin(\omega_n t) \tag{3.9}$$

Where: x_a is the analytic signal

ζ is the damping factor

ω_n is the angular frequency ($\omega_n = 2\pi f_n$)

Taking the absolute value of the analytic signal results in an exponential function that describes the signal's envelope. This may be notated as:

$$|x_a(t)| = Ke^{-\zeta \omega_n t} \tag{3.10}$$

Where: K is a constant

The natural logarithm of Eqn. 3.10 represents the envelope of the analytic signal as a linear function:

$$\log(|x_a(t)|) = \log(K) - \zeta \omega_n t \tag{3.11}$$

The function in Eqn. 3.11 is a first order polynomial. Therefore, identifying the coefficients of the first order polynomial that best fit the function, in a least-squares sense, provides an estimate of $-\zeta \omega_n$.

The calculation of the modal damping ratio ζ is computed assuming that the frequency of the dominant resonance within each defined band is equal to the geometric mean value of the band of interest. Although this assumption may lead to highly approximate modal damping ratios for each band, it is considered that fitting the Rayleigh damping coefficients to a number of damping estimates calculated over the frequency spectrum provides a reasonably accurate approximation of the proportional damping behaviour of the studied system. The fitting of the Rayleigh damping coefficients to the calculated modal damping ratios is further detailed in Chapter 3.6.3.

- *Numerical Justification*

  In the absence of an empirical validation, a numerical study of the adapted damping estimation technique has been conducted. An analytical study and a full empirical validation will form part of the future works to be conducted following this thesis. Further detail of these future works is provided in *Chapter 7*. The numerical study, which considers only mass-proportional damping, provides an indication of the error distribution associated with the methodology. The effect of the frequency response function's bandwidth delineation on the accuracy of the methodology is also considered.

The partial numerical validation of the adapted damping estimation technique was conducted by creating a random FRF to which the technique was applied. The random FRF featured a fixed number of resonance peaks n with the position in the frequency domain ω_n and the amplitude and phase of the resonances being randomly assigned. The damping at each of the n resonance peaks was imposed in the form: $\zeta_n = \frac{1}{2}\left(\frac{\alpha}{\omega_n} + \beta\omega_n\right)$. Specific features of the random FRF used within this thesis included:

- 400 random resonance peaks were generated with uniform distribution along a frequency spectrum from 0 Hz to 1600 Hz;
- The damping factor at each resonance peak was obtained with regard to mass-proportional Rayleigh damping, such that

$$\zeta(f) = \frac{1}{2\omega_n}\,\alpha \qquad \textbf{(3.12)}$$

  ($Note$: β is set to zero in Eqn. 3.12)
- A second random vector with uniform distribution U [0,1] determined the relative significance of each resonance.

Considering the above three points, the random generation of the FRF can be notated mathematically as:

$$\text{FRF}\,(f) = \sum_{n=1}^{n} \frac{g_n}{\left[1 - \left({}^{\omega}/_{\omega_n}\right)^2\right] + 2i\,\zeta_n\left({}^{\omega}/_{\omega_n}\right)} \qquad \textbf{(3.13)}$$

Where:

g_n is the magnitude of resonance n

ω/ω_n is the angular frequency vector of the FRF normalised to the angular frequency at which the resonance n occurs

ζ_n is the damping factor at resonance point n

Variables within the generation of the random FRF included the number of resonance peaks, the sampling rate, the number of samples taken and the mass-proportional damping factor. These variables were assigned values of, or considered representative of, those in the FRF of the oil-filled transformer assembly. The values of the variables employed in the random FRF generation and further explanation of these values is provided in Table 3-3.

Table 3-3 Variables employed in the generation of the random FRF

Parameter	**Value**	**Relation to the experimental case**
Sampling rate	4096	The value utilised during the experimental modal analysis of the transformer assembly
Number of samples taken	4096	The value utilised during the experimental modal analysis of the transformer assembly
Mass-proportional damping	50	Considered representative of the mass-damping value of the transformer, with the oil contained within the transformer tank having a significant mass-damping effect
Natural frequencies generated	400	Considered representative of the transformer's high modal density

The error estimate associated with the adapted damping estimation technique was determined by comparing:

- the known damping within the randomly generated FRF; and
- the damping value computed when applying the adapted damping estimation technique to the randomly generated FRF.

Figure 3-9 provides an illustration of this comparison between the estimated damping and the damping imposed on the FRF.

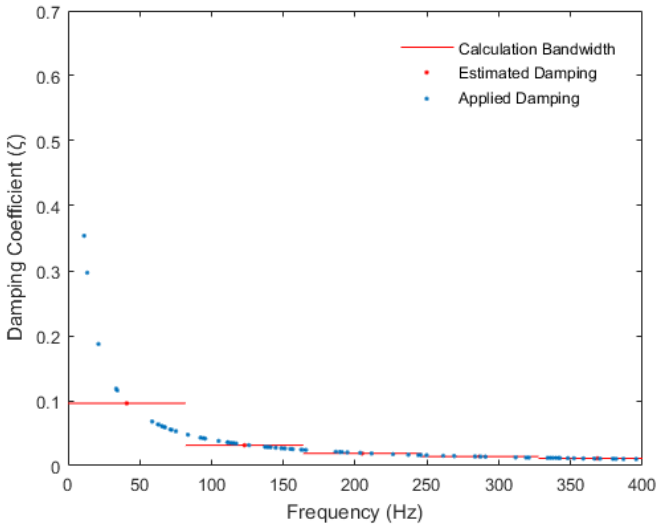

Figure 3-9 *Estimated damping in comparison to applied damping – 0 Hz to 400 Hz*

For the purposes of this investigation, the error estimate of the adapted damping estimation technique was conducted over a range from 0 Hz to 400 Hz. This encompasses the range considered dominant in a transformer's noise spectrum. Furthermore, with the length of the random FRF exceeding that of the analysis range, the effects of resonance peaks partially within the within the analysis spectrum were accounted for. The occurrence of these partial peaks is realistic and likely has the effect of increasing the error associated with the adapted damping estimation technique.

As a base case for studying the adapted damping estimation technique the 0 Hz to 400 Hz analysis spectrum of the randomly generated FRF signal was delineated into five constant-size frequency bands. Within each frequency band the initial 500 samples of the time-domain signal have then been considered in estimating the modal damping factor. To provide an error distribution of the methodology the random FRF generation and the subsequent application of the adapted damping estimation technique was iterated 100 times. Figure 3-10 illustrates the resulting error distribution.

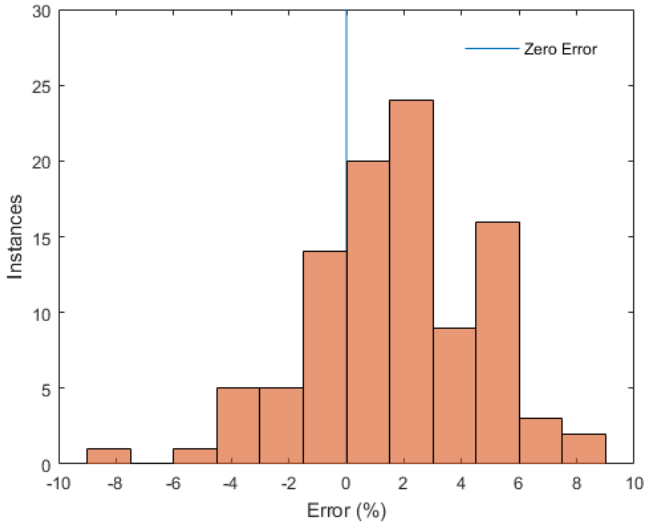

Figure 3-10 *Error distribution of the applied damping methodology with the 0 – 400 Hz analysis spectrum delineated into five bands (base case)*

As seen in Figure 3-10, considering the base case parameter values, the curve fitting methodology provides a good estimate of the random FRF's damping characteristics. Specifically, the average error associated with the 100 iterations of the damping estimation presented in Figure 3-10 was determined to be 1.64 %.

In addition to the base case, the average error of the adapted damping estimation technique with differing bandwidth delineations of the FRF signal has been considered. Specifically, the average error associated with the technique when delineating the FRF signal into four, five and six frequency bands over the 0 Hz to 400 Hz analysis spectrum has been analysed. The results from these analyses, with each analysis considering 100 iterations to provide an average error, are presented in Table 3-4.

Table 3-4 Effect of frequency bands on the accuracy of damping estimates

Number of Frequency Bands	**Average Error**[a]
4	1.23 %
5 (base case)	1.64 %
6	0.20 %

Note: [a] Due to the signal generation being a random process the results presented are not reproducible; however, they provide an understanding of key trends

From the results presented in Table 3-4 it is apparent that increasing the number of bands into which the analysis spectrum is divided significantly reduces the average error. This is likely a result of less spectral noise being introduced into the impulse response functions when taking the IFFTs within each band. By delineating the analysis spectrum into smaller frequency bands the adapted damping estimation technique also more closely replicates conventional curve-fitting methods, which determine damping estimates at isolated resonance peaks.

At this point it is worth noting that the numerical study of the applied damping estimation technique has identified that taking the IFFT of the frequency domain FRF signal likely introduces an error factor. This source of error has also been noted in previous studies. The error arises from the 'spectral leakage' of the transformed signal from one period into the following period. This is caused by:

- The IFFT not recreating the impulse response of the original time signal but rather a repeated pulse train response; and
- The non-casual spreading of IFFT signal – with the pulse arriving before the impulse and continuing after it.

Of significance in this study is that the spectral leakage appears to be exaggerated when taking an IFFT across a defined frequency band of a FRF as opposed to across the complete FRF signal. This aforementioned phenomenon is illustrated in Figure 3-11.

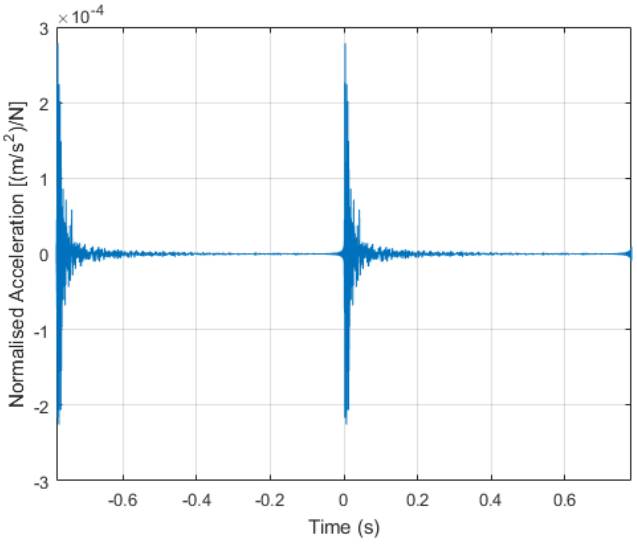

(a)

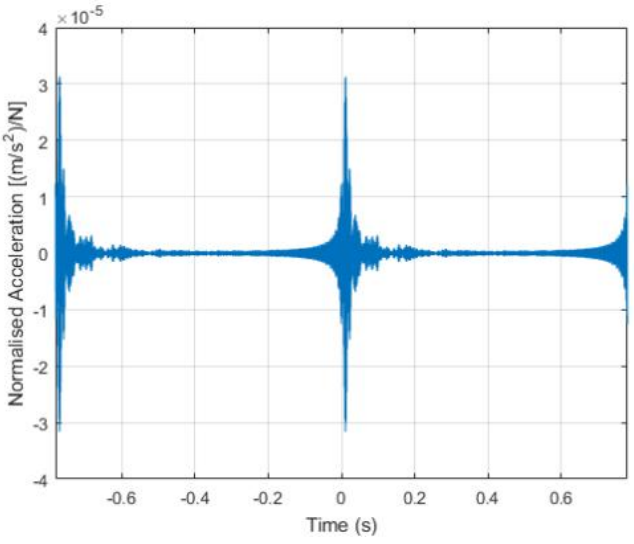

(b)

Figure 3-11 *Spectral leakage when taking the IFFT of (a) a complete FRF signal and (b) a defined a frequency band of the complete FRF signal*

To gain an insight into the practical application of the novel damping estimation technique detailed in this chapter, the error associated with the estimated damping factors should be observed within the context of a system's transmissibility. This parameter relates the amplitude of a system's vibration response to the amplitude of the excitation vibration applied. The transmissibility factor, being dependent on the damping ratio, the frequency of vibration and the natural frequencies of the system, is mathematically notated as:

$$T = \left|\frac{A_0}{A_i}\right| = \sqrt{\frac{1 + \left(2\zeta\frac{f_v}{f_n}\right)^2}{\left[1 - \left(\frac{f_v}{f_n}\right)^2\right]^2 + \left[2\zeta\frac{f_v}{f_n}\right]^2}} \qquad \textbf{(3.14)}$$

Where:

T is the transmissibility factor

A_0 is the amplitude of the vibration response

A_i is the amplitude of the vibration input

f_v is the frequency of the excitation vibration

f_n is the natural frequency of the system

From Eqn. 3.14 it is observed that when the excitation frequency is equal to that of a system's natural frequency the transmissibility factor is at a maximum. It can also be shown that, for small values of ζ, when the excitation and natural frequencies of a system coincide the transmissibility can be approximated as [74]:

$$T(f_v = f_n) = \frac{\sqrt{1 + 4\zeta^2}}{2\zeta} \approx \frac{1}{2\zeta} \qquad \textbf{(3.15)}$$

To illustrate how the damping factor affects the transmissibility of a system three modal damping ratios have been selected, being 4.95 %, 5.50 % and 6.05 %. An illustration of a system's transmissibility with these damping factors applied is shown in Figure 3-12. The 10 % difference between the modal damping ratios is representative of the maximum error considered to be present in the novel curve-fitting methodology (refer to Figure 3-10 for a plot of the error distribution).

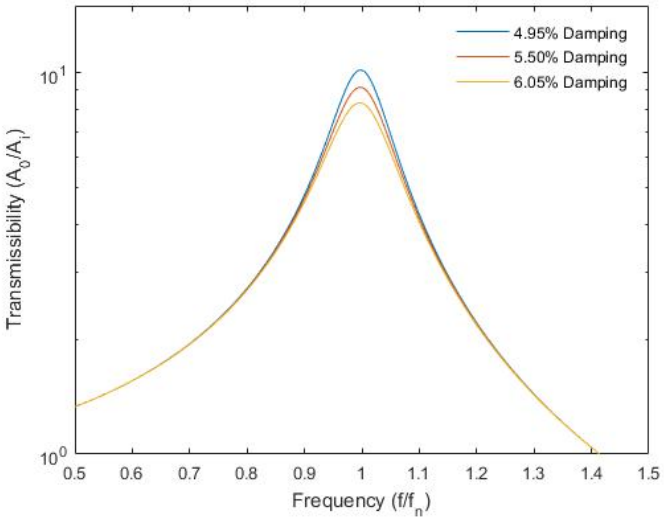

Figure 3-12 *Transmissibility functions with modal damping at 4.95 %, 5.50 % and 6.05 %*

Eqn. 3.15 and Figure 3-12 illustrate that when a forcing frequency is in proximity to a system's natural frequency the structure's damping properties influence the transmission of vibrations through the system. However, a slight difference between the excitation frequency and the system's natural frequency significantly reduces the dependence of a system's transmissibility on the damping properties.

Considering this characteristic of the transmissibility function, together with the absence of conventional curve fitting methodologies and largely accurate damping estimates provided by the novel methodology detailed, it may be concluded that the adapted damping estimation technique is appropriate to provide an approximation of the transformer assembly's modal damping over the frequency range of interest.

- *Application of the Damping Methodology*

  An illustration of the adapted damping estimation technique as applied to a single FRF signal generated during the experimental modal analysis of the transformer analysed with this study is provided in Figure 3-13. The figure illustrates the linear best-fit trend line, which allows the calculation of the damping factor ζ from the expression given in Eqn. 3.11.

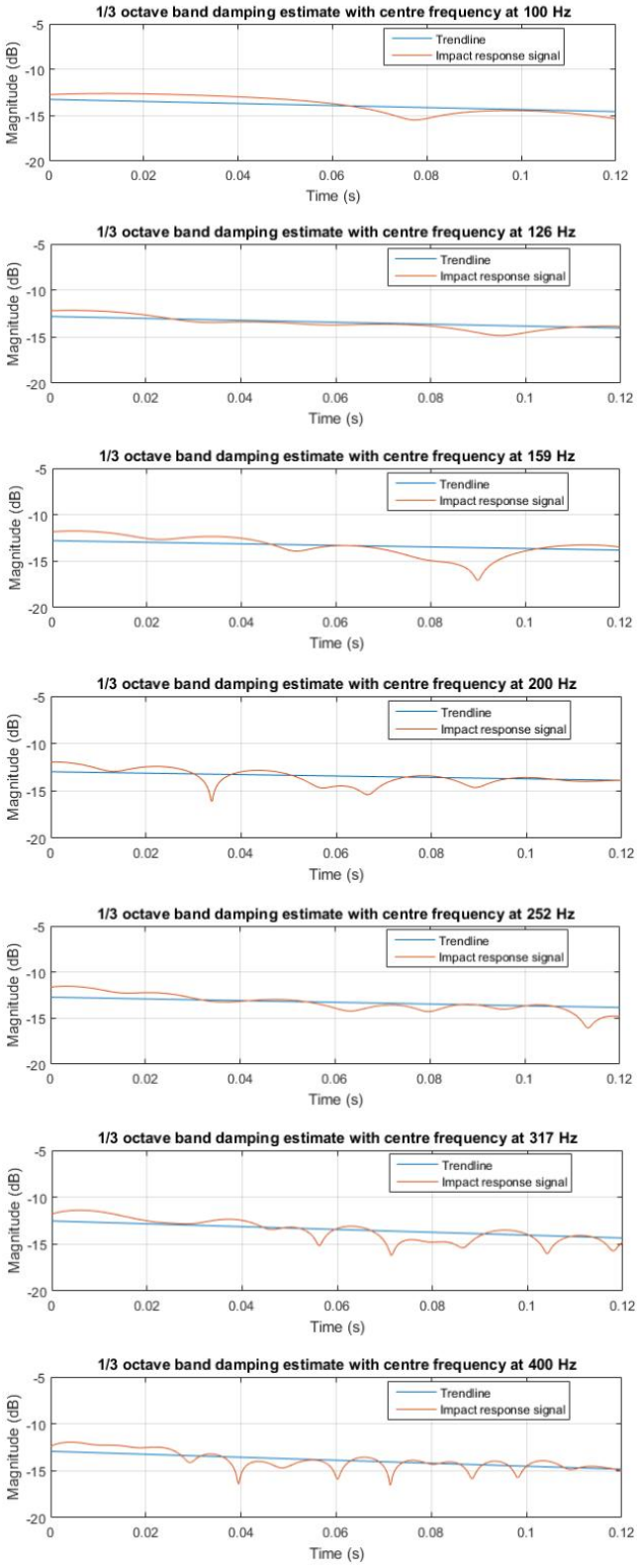

Figure 3-13 Transformer assembly damping estimates in 1/3 octave bands

3.6.3 MODAL DAMPING IN THE FINITE ELEMENT MODEL

The modal damping characteristics of the transformer modelled in this thesis have been accounted for in the FE model employing the Rayleigh damping formation (refer to Eqn. 3.3 for a mathematical description of Rayleigh damping). The Rayleigh mass and stiffness proportional damping coefficients, α and β, have conventionally been evaluated from damping ratios and natural frequencies corresponding to two reference modes of vibration as:

$$\begin{bmatrix}\zeta_i\\ \zeta_j\end{bmatrix} = \frac{1}{2}\begin{bmatrix}\frac{1}{\omega_i} & \omega_i\\ \frac{1}{\omega_j} & \omega_j\end{bmatrix}\begin{bmatrix}\alpha\\ \beta\end{bmatrix} \qquad \textbf{(3.16)}$$

Where: i, j denote the two reference modes of vibration

It is well known that calculating the Rayleigh damping coefficients using the expression in Eqn. 3.16 results in erroneous modal damping ratios except for the two reference modes of vibration considered. This error is a significant source of inaccuracy in estimation of system's structural response [75]. Therefore, in this investigation a Moore-Penrose pseudoinverse matrix has employed, allowing the Rayleigh damping coefficients to be fitted to a number of reference modes over the frequency spectrum.

The use of the pseudoinverse matrix allows for the computation of a best-fit solution, in a least-squares sense, to a system of linear equations that lack a unique solution. Therefore, the use of the inverse matrix has allowed for better estimate of the Rayleigh damping coefficients over the frequency spectrum under consideration. The estimation of Rayleigh damping coefficients employing the Moore-Penrose pseudoinverse matrix is notated as:

$$\begin{bmatrix}\alpha\\ \beta\end{bmatrix} = 2\begin{bmatrix}\frac{1}{\omega_i} & \omega_i\\ \vdots & \vdots\\ \frac{1}{\omega_n} & \omega_n\end{bmatrix}^{+}\begin{bmatrix}\zeta_i\\ \vdots\\ \zeta_n\end{bmatrix} \qquad \textbf{(3.17)}$$

Where: $[\,]^{+}$ denotes a Moore-Penrose pseudoinverse matrix

Utilizing Eqn. 3.17 the Rayleigh damping coefficients were determined independently for the oil-filled tank assembly and the active part. The modal damping ratios $\zeta_i \ldots \zeta_n$, to which the Rayleigh damping factors have been fitted, were determined from experimental modal analyses results as discussed in *Chapter 3.6.1* and *Chapter 3.6.2*.

The computed Rayleigh damping coefficients of the active part and the transformer tank were applied to the respective structural assemblies for which α and β had been determined. Of note is that the damping characteristics of the fluid were not accounted for by manual input of α and β coefficients. Instead ANSYS accounted for the damping characteristics of the fluid employing the acoustic properties of the fluid body, as notated in Eqn. 2.15.

Differences between the damping matrix formulation in FSI simulations and the experimental setup employed to determine the damping characteristics of the transformer may have lead to slight differences between the damping characteristics determined experimentally and those exhibited by the numerical model. However, these differences have been considered of negligible influence.

CHAPTER 4

VALIDATION OF THE NUMERICAL MODEL

As discussed in *Chapter 2*, the accuracy of finite element models is limited by uncertainties relating to geometric and material properties, boundary conditions and loading applied to the model. The validation of finite element models through the comparison of experimental and numerical results is therefore necessary. Within this thesis experimental modal analysis results have allowed for the validation of the structural finite element model while measured sound pressure levels have been employed to validate the acoustic noise predictions. The following subchapters discuss the structural and acoustic validation of the vibro-acoustic model in further detail.

4.1 MODAL VALIDATION OF THE ASSEMBLY

The structural dynamics characteristics of the numerical transformer model detailed in *Chapter 3* have been validated by comparing numerically computed modal parameters to those determined experimentally. The experimental modal parameters employed in this validation procedure were extracted from impact hammer tests conducted with tri-axial accelerometers positioned at 197 points on the transformer. Therefore, the experimental modal model consisted of 591 degrees of freedom. In comparison, the numerical model comprises in excess of 9.5 million degrees of freedom.

The significant difference in the number of degrees of freedom between the modal models has resulted in the numerical model computing a considerably greater number of modes than were determined experimentally. Validating the numerical model through methods such as the modal assurance criterion (MAC) is therefore impractical. In particular, MAC may mistakenly indicate unity when the experimental modal vector is incompletely measured (i.e. too few response stations have been included in the experimental determination of the modal vector). In such cases the incompleteness of the experimental modal vector results in the comparison of two uncorrelated modes.

In this thesis the structural validation of the finite element model has been conducted by comparing experimental and numerical natural frequencies at modes shapes that exhibit visual correlation. This simplistic comparison method has been adopted due to limitations associated with the incomplete experimental modal model, as discussed in the preceding paragraph. Also of note is that because experimental modal measurements were taken on the external surfaces of the tank, the shape of the tank at natural frequency points has therefore formed the basis of visual comparisons made in this thesis.

Due to the complexity of mode shapes occurring at higher frequencies numerical and experimental modes have been compared at the lower end of the frequency spectrum during this validation procedure. The comparison of modes in lower frequency ranges, where modes are characterised by greater global deformation, has also decreased the probability of comparing uncorrelated mode shapes. The natural frequencies of the first six correlated experimental and numerical modes are presented in Table 4-1.

Table 4-1 Natural frequencies of the transformer tank

Mode No.	Experimental Analysis	Numerical Analysis
1	11 Hz	10.24 Hz
2	17 Hz	20.03 Hz
3	25 Hz	25.87 Hz
4	29 Hz	32.33 Hz
5	39 Hz	39.31 Hz
6	46 Hz	42.02 Hz

The averaged difference between natural frequencies of the six correlated modes as identified in Table 4-1 is 2.9 %. Noting that no model updating has been conducted – as the computation scheme presented in this thesis is intended to be used in the design phase of a transformer – this represents a very high degree of correlation. Figure 4-1 illustrates the distribution of the numerical verses experimental natural frequencies.

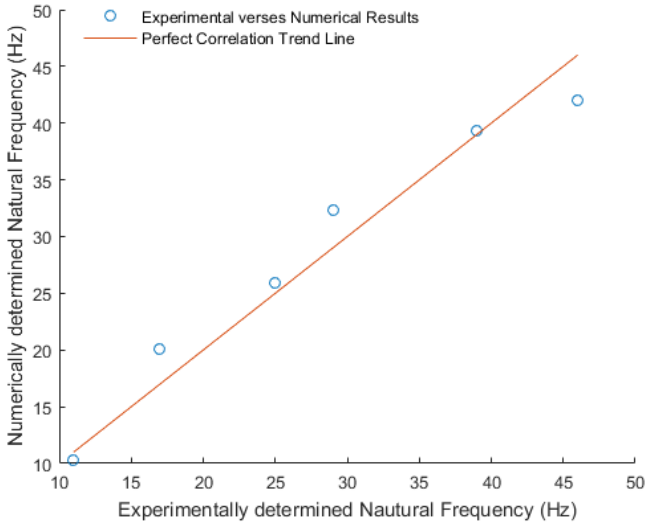

Figure 4-1 Numerical verses experimental natural frequencies of the correlated modes with trend line indicating perfect correlation

The correlated numerical and experimental mode shapes of the transformer at ~11 Hz, ~25 Hz and ~39 Hz are illustrated in Figure 4-2, Figure 4-3 and Figure 4-4, respectively. For illustrative purposes, only the deformation of the tank has been presented; however, for both the numerical and experimental modal analyses the transformer was fully assembled, as presented in Figure 3-3(b) and Figure 3-4.

In addition to modal parameter correlation, the comparison of FRFs may have been utilised to validate the structural dynamics characteristics of the numerical model. However, this correlation method has been dismissed as a result of two factors. The primary reason that FRFs have not been compared is the complexity of transformer assembly, with a high modal density and heavily coupled modes, making the correlation of FRFs a difficult task. Furthermore, the computing requirements to calculate a numerical FRF with a sampling frequency matching that of the experimental FRF would be excessive. The computing requirements of the numerical analyses employed within this thesis are further discussed in *Chapter 5.4.*

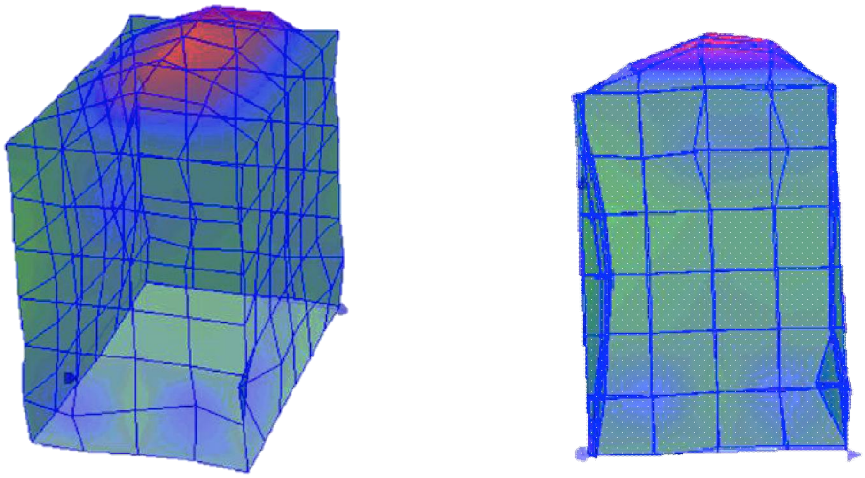

(a)

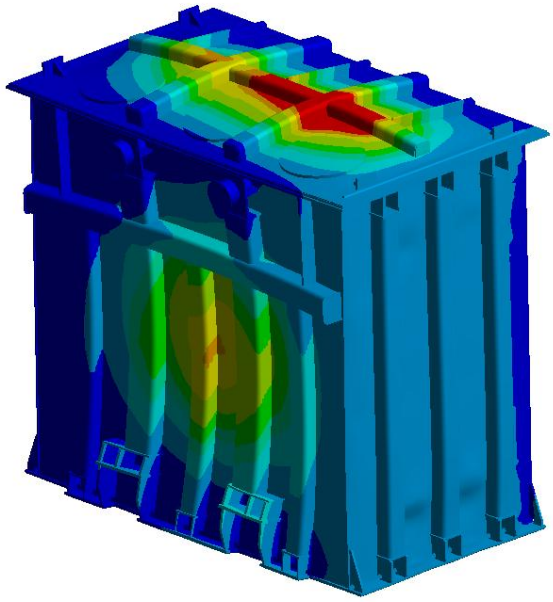

(b)

Figure 4-2 Comparison of (a) the experimental mode shape at 11 Hz and (b) the experimental mode shape of the transformer at 10.24 Hz

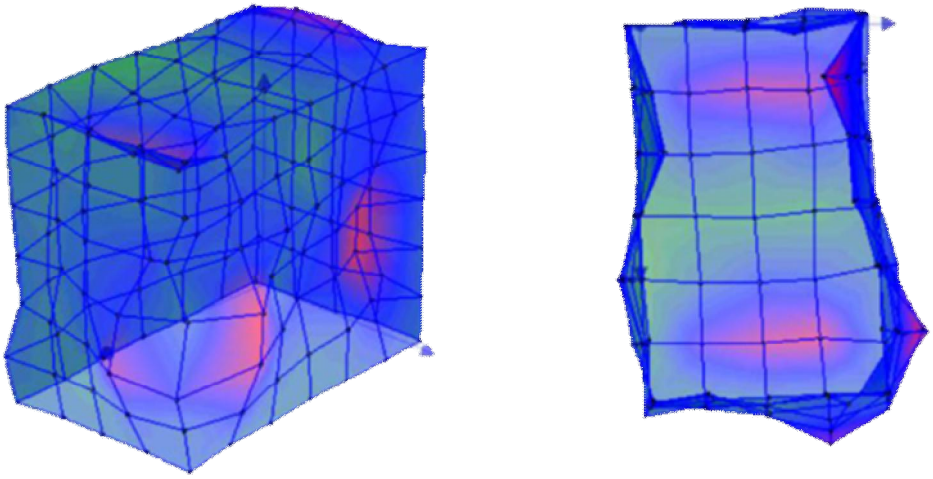

(a)

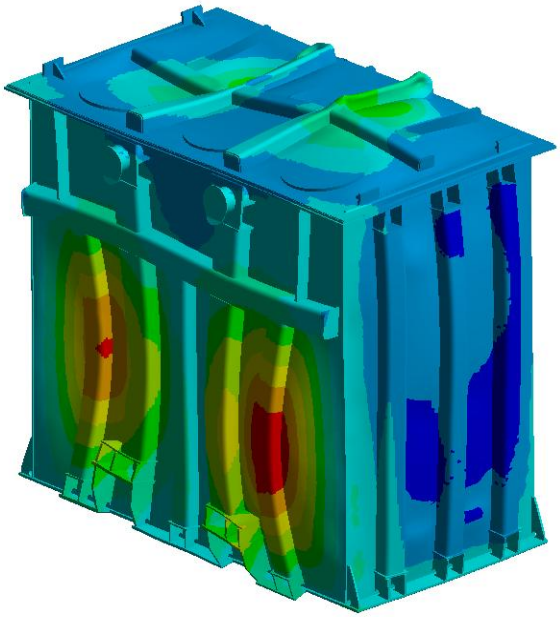

(b)

Figure 4-3 Comparison of (a) the experimental mode shape at 25 Hz and (b) the experimental mode shape of the transformer at 25.87 Hz

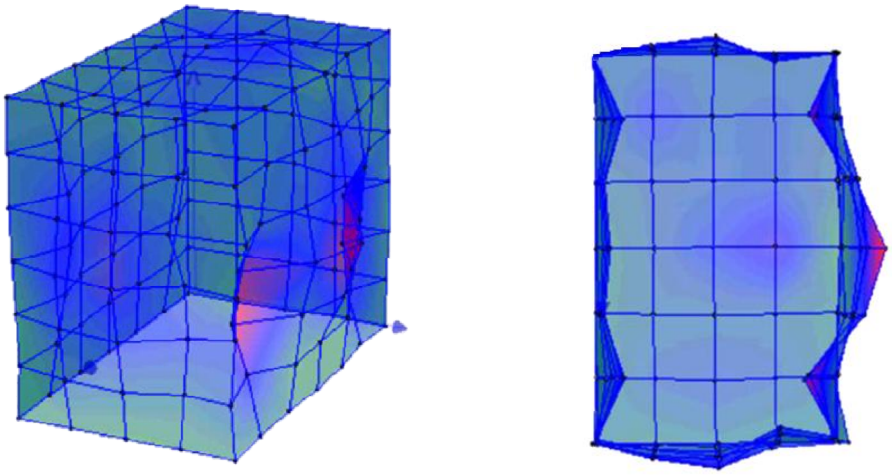

(a)

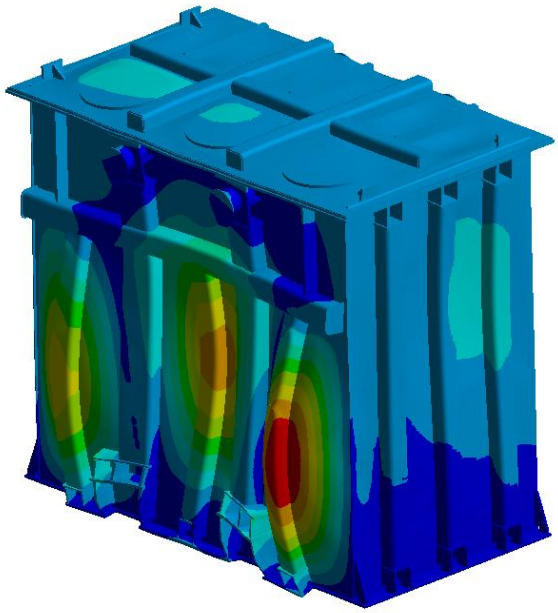

(b)

Figure 4-4 Comparison of (a) the experimental mode shape at 39 Hz and (b) the experimental mode shape of the transformer at 39.31 Hz

4.2 ACOUSTIC VALIDATION OF THE NUMERICAL MODEL

The acoustic validation of the numerical simulation has acted to validate all preceding steps in the modelling of the transformer. The validation has been conducted by directly comparing experimentally and numerically determined sound pressure levels over a spectrum from 100 Hz to 400 Hz. This validation approach is opposed those employed in comparable preceding studies, which validated acoustic results at a single frequency point of interest.

Validation of the numerical model from 100 Hz to 400 Hz is significant, as has been discussed in detail in *Chapter 3.6*. This is because the spectral range is inclusive of the network frequency's first three even harmonics, which are considered dominant in a LPTs acoustic response. Furthermore, validation over the aforementioned frequency spectrum will allow for future works to estimate the total audible noise levels of a transformer under nominal operating conditions employing the computational scheme presented in this thesis.

4.2.1 SOUND PRESSURE LEVEL MEASUREMENTS

The sound pressure level measurements of the transformer analysed in this thesis were provided by Siemens AG Austria, Transformers Weiz. The measurements, which have been carried out in the Transformers Weiz test laboratory, were taken in accordance with:

IEC 60076-10 Power Transformers – Part 10: Determination of Sound Levels

In agreement with IEC 60076-10 [76] sound measurements were taken at one-third and two-third-heights of the transformer. Furthermore, as no cooling equipment was in operation during the measurements, sound pressure levels were determined at a distance of 0.3 metres from the radiating surfaces.

With respect to the sound pressure level measurements of the studied transformer it should be noted that a narrow-band measurement method has been employed. Specifically, the fast Fourier transformation (FFT) frequency analysis method, as described in *IEC 60067-10,* has been used. This method provides constant bandwidth acoustic measurements across a defined spectrum. When performing the acoustic measurements of the transformer studied within this thesis a bandwidth resolution of 2 Hz was employed.

The FFT narrow-band method uses an FFT algorithm to transform the measured digital sound pressure versus time spectrum to a sound pressure versus frequency spectrum. The bandwidth of the spectrum therefore depends on the sampling rate of the analogue-to-digital converter. As noted in *IEC 60067-10*, when employing a narrow-band measurement method the summation of sound levels for the first 10 bands containing frequencies equal to twice the rated frequency and multiples thereof is adequate to approximate total sound levels for most transformers. The summation of sound pressure levels can be calculated as follows:

$$L_{Ai} = 10log_{10}\left(\sum_{v=1}^{v_{max}} 10^{0,1L_{Av}}\right) \qquad \textbf{(4.1)}$$

Where:

L_{Ai} is the sound pressure level at rated voltage and rated frequency

L_{Av} is the sound pressure level (or sound intensity level) measured over the chosen bandwidth, Δf, centred on a frequency equal to $2f_v$, at rated voltage and rated frequency

f is the rated frequency

v is the sequence number (1, 2, 3, etc.) of multiples of even harmonics of the rated frequency;

$v_{max} = 10$

During the acoustic measurements conducted on the transformer studied in this thesis, the unit was excited under load conditions at a series of discrete electrical frequencies ranging from 50 Hz to 200 Hz. The excitation of the unit resulted in mechanical forces acting on the active part at twice the applied electrical frequency and higher harmonics thereof. A detailed review of the excitation forces in a transformer's active part can be found in *Chapter 3.6*.

For comparison of the experimental sound pressure levels and the numerical predictions, the experimental sound levels were evaluated at a single point on the acoustic frequency response spectrum. Specifically, the sound pressure levels were evaluated at the second harmonic of the electrical excitation frequency, which is also the fundamental frequency of the Maxwell, Lorentz and magnetostrictive excitation forces that act on the core and the windings. The electrical excitation frequencies, fundamental frequency of the excitation forces, the frequency at which the sound pressure levels were determined and the measured sound pressure levels are presented in Table 4-2.

Table 4-2 Electrical excitation frequency and corresponding sound pressure level measurement points and values

Measurement Point	**Electrical Excitation Frequency** (Hz)	**Fundamental Frequency of the Excitation Forces** (Hz)	**Sound Pressure Level Evaluation Frequency** (Hz)	**Sound Pressure Level** (dB)
1	50	100	100	42.44
2	60	120	120	44.74
3	70	140	140	48.18
4	80	160	160	51.68
5	90	180	180	41.38
6	100	200	200	40.06
7	110	220	220	38.11
8	120	240	240	38.87
9	130	260	260	39.88
10	140	280	280	36.86
11	150	300	300	37.07
12	160	320	320	37.79
13	170	340	340	37.37
14	180	360	360	37.33
15	190	380	380	46.11
16	200	400	400	50.48

With regard to the acoustic measurements presented in Table 4-2, it should be noted that although the unit was excited under load conditions, the results are not representative of load noise acoustic measurements. This is because the acoustic measurements have been evaluated at a single point on the acoustic frequency response spectrum i.e. the second harmonic of the electrical excitation frequency.

The industry definitions of load and no-load noise generally relate to total noise levels instead of noise levels at an individual frequency component. Sound emissions at higher harmonics of the excitation frequency are therefore considered in the calculation of load and no-load noise. It is also important to note that, as previously discussed in *Chapter 2.1* and *Chapter 3.5*, load and no-load noise levels may be dominated by different harmonics of the excitation frequency.

As sound levels at only a single harmonic of the excitation frequency have been evaluated in this thesis it has been considered inappropriate to contrast results under load and no-load conditions. Such results would have no context within the industry interpretation of load and no-load transformer noise. The viewpoint taken to not contrast load and no-load noise measurements has also been carried forward to the following sections of this thesis, which present numerically predicted noise levels.

4.2.2 SOUND PRESSURE LEVEL PREDICTIONS

The sound pressure level predictions of the transformer analysed in this thesis were determined employing the computation scheme detailed in *Chapter 3*. For the validation of the numerical model simulations at 16 discrete frequencies across a 100 Hz to 400 Hz spectrum were conducted. These simulations allowed for the vibration and acoustic response of the numerical model to be determined. The forcing frequencies of these 16 simulations matched the second harmonic of the 16 electrical excitation frequencies applied to the transformer during experimental testing. Therefore, noting that the experimental results were evaluated at the second harmonic of the electrical excitation frequency, an acoustic frequency response spectrum with 16 corresponding experimental and numerical measurement points has been created.

To ensure similarity between experimental and simulated results the numerical sound pressure levels were calculated on acoustic surfaces surrounding the transformer that approximated the experimental measurement area. It is also of note that validation of the numerical model though a numerical frequency point to experimental frequency point comparison allowed the non-linearity of the excitation forces and structural elements to be disregarded. A comparison of experimental and predicted sound pressure levels is illustrated in Figure 4-5.

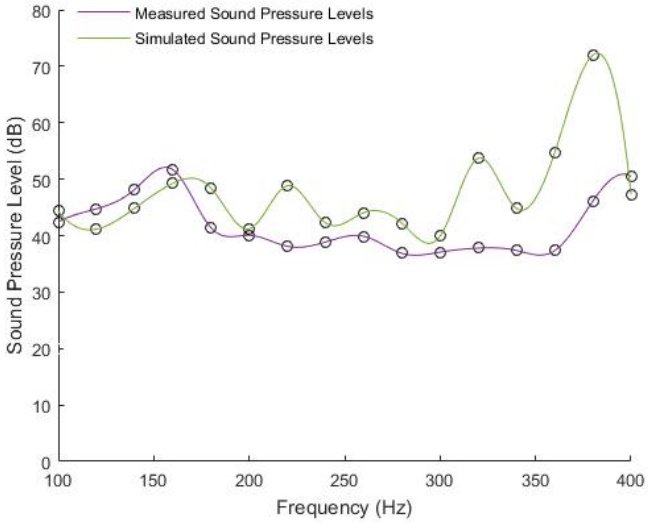

Figure 4-5 Comparison of measured and predicted sound pressure levels at 16 corresponding measurement points

From Figure 4-5 it appears that there is a high degree of correlation between the numerical and experimental sound pressure levels. At double the 50 Hz (60 Hz) network frequency, being the fundamental frequency of the Maxwell, Lorentz and magnetostrictive forces in the active part, the error between experimental and numerical sound pressure levels is 1.91 dB (3.60 dB). The average error at the first three even harmonics of the network frequency, which are the frequencies considered dominant in the acoustic response spectrum of a LPT, is 1.96 dB (5.72 dB).

The numerical and experimental acoustic results of the studied transformer remain in favourable agreement across all measurement points within the 100 Hz to 300 Hz (100 Hz to 360 Hz), with an average error of 2.48 dB (4.86 dB) over this spectrum. However, above this frequency range of interest the error between numerical and experimental results increases. The total error across the 100 Hz to 400 Hz analysis spectrum considered in this thesis is 5.67 dB.

The sound pressure level results presented in Figure 4-5 are comparable to those presented in preceding studies. Specifically, the results are comparable to those presented in Ref. [3], which contained a 1.5 dB difference between simulated and experimental values (at the single 100 Hz validation point considered) and those presented in Ref. [4], which included a 6.61 dB error (again at a single frequency point). The numerical sound pressure levels presented in this thesis are therefore considered accurate, as the aforementioned preceding studies have predicted only coil-emitted noise at a single frequency point.

Further examination of Figure 4-5 illustrates that the predicted sound pressure levels exhibit the local and global trends of the transformer's acoustic behaviour. The global behaviour is characterised with the sound pressure levels increasing between 100 Hz and 160 Hz and again between 360 Hz and 400 Hz. Additionally, the peaks in sound pressure, which may be attributed to natural frequencies of the transformer being excited, illustrate the frequency-localised characteristics of the unit.

The final point of note regarding Figure 4-5 is that the numerical results show higher correlation to measured sound pressure levels at the lower frequency points within the 100 Hz to 400 Hz analysis spectrum. This is of significance as lower frequencies in the spectrum considered are generally more dominant in the acoustic response of a large power transformer. Refer to Figure 3-7 for an illustration of this characteristic.

As the numerical vibro-acoustic methodology proposed in this paper is intended for use in the design process, computing time is a significant consideration. As such, a simplified acoustic prediction simulation was run, with the transformer assembly comprising of the active part, the tank and the insulation fluid while excluding the conservator, radiators, bushings and other auxiliary equipment. The results of this simulation, with a comparison to the results from the fully assembled transformer model, are presented in Figure 4-6.

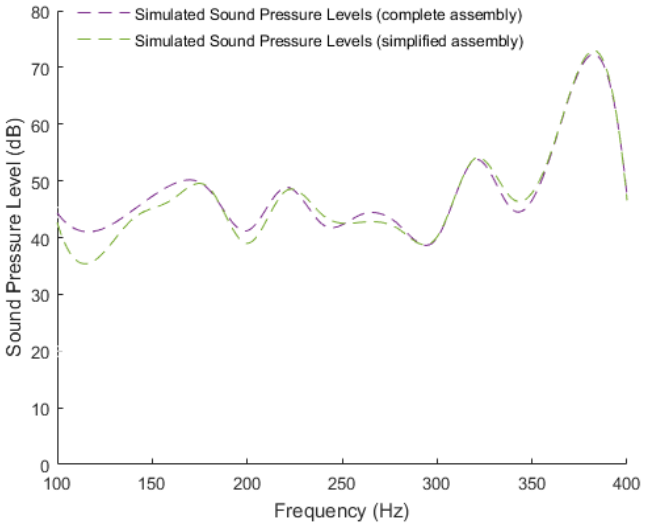

Figure 4-6 Comparison of predicted sound pressure levels calculated with the simplified numerical transformer assembly and the complete numerical transformer model

The results in Figure 4-6 illustrate that the simplified numerical model provides sound pressure level estimates in favourable agreement with those from the numerical analysis of the complete transformer assembly. Further comparison of the simplified and complete numerical models is provided in *Chapter 5.1*. A discussion of the computing requirements for the simplified and complete simulations is given in *Chapter 5.4*.

4.3 CONCLUSIONS

This chapter has detailed the validation of the numerical transformer model presented in *Chapter 3*. Experimental modal analysis results have allowed for the validation of the structural finite element model by direct comparison of numerical and experimental mode shapes and corresponding natural frequencies. The numerical results have shown favourable agreement with experimental measurements, the average difference between the modal frequencies of the first six correlated numerical and experimental modes being 2.9 %.

Following the validation of the structural model, measured sound pressure levels were employed to validate the acoustic noise predictions. Specifically, 16 frequency points across a 300 Hz spectrum from 100 Hz to 400 Hz have been analysed employing the numerical model, corresponding to the 16 frequencies at which experimental sound pressure levels were evaluated. Validation of the numerical model though a numerical frequency point to experimental frequency point comparison has allowed the non-linearity of the excitation forces and structural elements to be disregarded.

Comparison of the numerical and experimental sound pressure level results over the analysis spectrum showed a high degree of correlation. At the first three even harmonics of the 50 Hz (60 Hz) network frequency, being the harmonics which are considered dominant in the sound radiation of a transformer, comparison between numerical and experimental measurements resulted in an average error of 1.96 dB (5.72 dB). The accuracy of these results is in line with comparable preceding studies. Furthermore, comparison of the acoustic prediction and measured sound pressure levels has illustrated that the applied methodology identifies both the global and local acoustic behaviour of the transformer over the analysis spectrum.

The error margins relating to the respective numerical models presented in this chapter have been provided in Table 4-3. The error values stated in Table 4-3 are average error values accounting for all corresponding experimental and numerical data points considered in the modal and acoustic models.

Table 4-3 Model Validation Methods and Corresponding Error Margins

Model Validation Method	**Model Error**
Modal Validation	2.9 %
Acoustic Validation	5.67 dB
Acoustic Validation (*simplified transformer)*	4.95 dB

CHAPTER 5

DISCUSSION

Through the comparison of experimental and numerical results it has been shown that the computation scheme described in *Chapter 3* is able to predict a transformer's acoustic emissions with a level of accuracy in line with comparable preceding investigations. Additionally, the inclusion of all key structural and fluid elements together with validation over a 100 Hz to 400 Hz spectrum has allowed for the first time a detailed insight into the vibration and acoustic characteristics of a transformer. This chapter identifies these vibration and acoustic characteristics and provides methods for identifying them during the design process. The computing requirements for the numerical simulations employed within this thesis are also discussed.

5.1 INCREASED FREQUENCY SAMPLING TO PROVIDE DETAILED ACOUSTIC CHARACTERISTICS

Following the acoustic validation of the finite element model, sound pressure level predictions were made at frequency points where physical measurements had not been not been taken. This has allowed for a more detailed image of the studied transformer's acoustic behaviour to be constructed. Specifically, sound pressure level predictions have been made at 10 Hz intervals across the 100 Hz to 400 Hz analysis spectrum. This is opposed to the 20 Hz intervals at which acoustic measurements were performed to validate the numerical model, as presented in *Chapter 4.2.1*. The refined acoustic spectrum is presented in Figure 5-1.

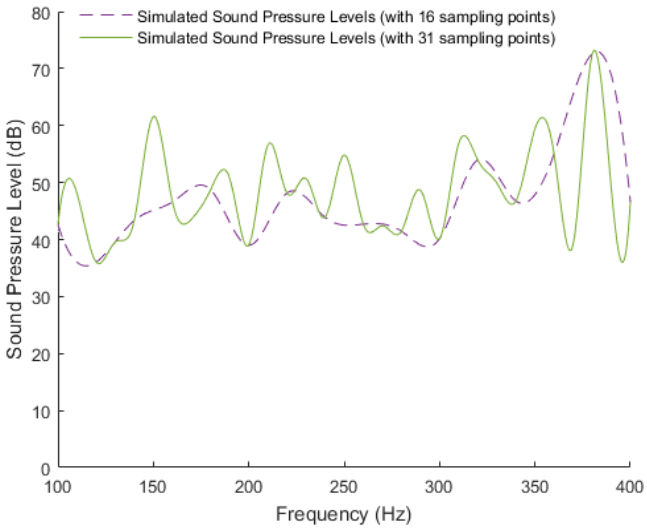

Figure 5-1 Comparison of the transformer's acoustic behaviour as identified by sound pressure levels determined at 10 Hz and 20 Hz intervals

Figure 5-1 illustrates that increasing the number of frequency sampling points provides a higher resolution frequency response spectrum. This is of importance as predicting the distance of resonance peaks from 100 Hz (120 Hz) and higher harmonics thereof is critical in understanding the risk of high noise emissions from a transformer. The aforementioned frequencies and their higher harmonics are of significance as they are the frequencies at which the excitation forces in the active part occur.

When determining if a numerically predicted resonance peak is likely to produce high noise emissions from a manufactured transformer a confidence interval should be accounted for. This confidence interval allows for differences between the numerical and experimental resonance frequencies, noting that the numerical model is an idealized representation of the physical unit. In particular, the numerical model does not account for variables including manufacturing tolerances, assembly process variances and non-linear material properties.

The significance of a high resolution acoustic spectrum is clearly depicted in Figure 5-1. As shown, the refined acoustic spectrum identifies a resonance peak at 150 Hz, made visible through elevated sound pressure levels (being approximately 10 dB above other sound level predictions made in proximity). This elevated noise level estimation is in favourable agreement with the elevated noise level determined experimentally at 160 Hz. The difference between the experimental and numerical resonance peak may be accounted for by the variables identified in the preceding paragraph.

In addition a more providing a more detailed acoustic frequency response of the studied transformer, the increased sampling of sound pressure levels has been employed to further validate the simplified model presented in *Chapter 4.3*. Figure 5-2 provides a comparison of sound pressure levels calculated at 10 Hz intervals with the simplified and the complete numerical models. The simplified model included the active part, the tank and the insulation fluid but excluded the conservator, radiators, bushings and other auxiliary equipment.

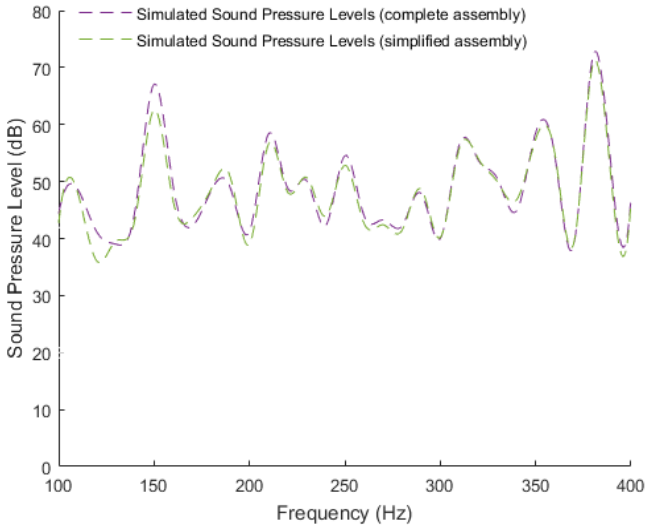

Figure 5-2 Comparison of predicted sound pressure levels at 10 Hz intervals calculated with the simplified numerical transformer assembly and the complete numerical transformer model

The calculated sound pressure levels presented in Figure 5-2 again illustrate that the simplified numerical model provides acoustic estimates in favourable agreement with those of the complete transformer assembly. From these results it is concluded that simplified numerical models can be employed within the design process to reduce modelling, discretisation and simulation time. A discussion of the computing requirements for the complete and simplified simulations is presented in *Chapter 5.4*.

5.2 EXCITATION MECHANISMS AND ACTIVE PART VIBRATION CHARACTERISTICS

Past literature [7, 28, 44, 49-51] has identified that the noise levels of a transformer are significantly influenced by the vibration characteristics of the active part and in particular the core. This connection between vibration characteristics and sound generation is a consequence of the active part's modes being excited by electromagnetic and magnetostrictive excitation forces. The excitation of the assembly's modes results in an amplification of vibrations, leading to elevated noise levels. Despite being identified as a source of excessive noise generation in past literature, this thesis presents for the first time a rigorous validation of this correlation.

The likelihood of an active part's mode being excited by electromagnetic and magnetostrictive forces is analyzed in this chapter through determination of the assembly's modal mass participation factors. The modal mass participation factor is a measure of the mass displaced by an individual mode shape; therefore, modes with high modal mass participation factors are expected to involve large areas of the transformer and are likely to be excited by internal forces. A mathematical description of the modal participation factor, as presented in Ref. [77], is given below.

Noting that a system's generalised mass matrix $[m_r]$ is given by,

$$[m_r] = [\Psi]^T[M][\Psi] \quad \textbf{(5.1)}$$

Where: $[\Psi]$ is the eigenvector matrix

$[M]$ is the mass matrix

and a matrix describing the displacement of the masses resulting from a unit displacement spectrum in each of the Cartesian directions may be defined as,

$$[L] = [\Psi]^T[M]\{s\} \quad \textbf{(5.2)}$$

Where: $\{s\}$ is a displacement transformation vector that expresses the displacement of each structural DOF due to static application of a unit movement in each of the Cartesian directions

The modal participation factor for the r^{th} mode may then be defined as:

$$\Gamma_r = \frac{[L]_r}{[m_r]_r} \quad \textbf{(5.3)}$$

Where: Γ_r is the modal participation factor of the r^{th} mode

As discussed in *Chapter 2.4*, if the eigenvector matrix $[\Psi]$ is mass-normalised, with the resulting matrix denoted as $[\Phi]$, then $[m_r] = [I]$.

With regard to Eqn. 5.3 it is of note that that modal mass participation factors are analysed within a translational or rotational direction of motion. In ANSYS® Mechanical these factors are calculated in the global *x*-, *y*-, and *z*-axes. Due to the movement of magnetic flux through the core, electromagnetic forces acting in the vertical plane were considered most likely to excite the two-limb core design of the transformer analysed in this investigation.

The numerical model employed to determine the modal mass participation factors of the active part in this thesis has not directly account for fluid-structure interaction. The fluid-structure coupling has been omitted due to the excessive computing power it required. A 20 % reduction in the calculated natural frequencies has therefore been introduced. This factor accounts for the added-mass and viscous damping effects associated with the submersion of the active part in mineral oil.

The factor used to relate the numerically calculated natural frequencies to the resonances of the submerged active part has been determined from experimental measurements. The measurements, which were provided by Siemens AG Austria, Transformers Weiz, contrast the vibration response of a transformer core in air and submerged in mineral oil. The factor employed in this thesis is also in favourable agreement with analytical approximations, determined from the expressions found in Ref. [78] and Ref. [79]. Figure 5-3 presents the updated natural frequencies of the model and the corresponding modal mass participation factors, normalised to the largest within the set.

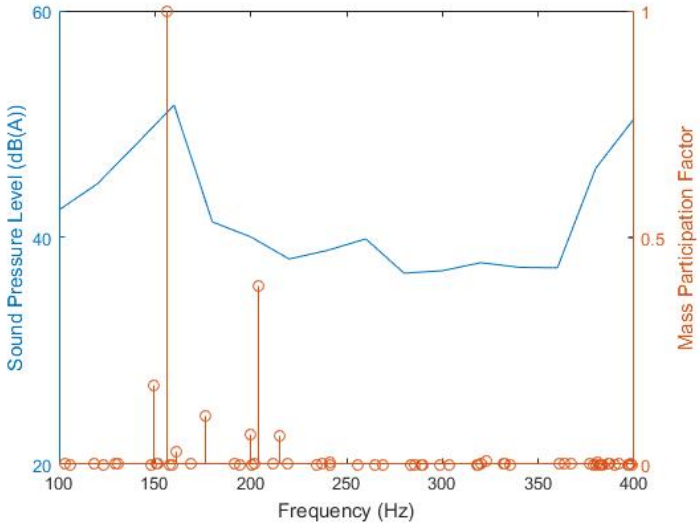

Figure 5-3 Modal mass participation factor of active part modes in the vertical plane (○ indicates the natural frequency and mass participation factor of a numerically calculated mode)

From Figure 5-3 it may be predicted that the sound radiation levels significantly increase when the transformer is excited at 160 Hz. This agrees favourably with measured sound pressure levels, which have also been illustrated in Figure 5-3. Furthermore, contrasting the measured sound pressure levels and the mass participation factor's of the active part illustrates that the numerical parameter is able to provide a qualitative acoustic estimate over the entire frequency spectrum.

5.3 RESONANCE EFFECTS AND EXCESSIVE SOUND RADIATION

In addition to modal excitation of the active part, resonances of the tank may also lead to elevated sound levels. However, due to the complexity and size of large power transformers, predicting such resonances is challenging. This is particularly true at higher frequencies, with the occurrence of closely grouped modes characterised by multiple local deformations on the transformer tank. Such modes do not generally contribute significantly to the overall noise level of a transformer.

To gain insight into the presence of global modes shapes on the transformer tank at higher frequency ranges a series of forced excitation simulations have been conducted employing the numerical model detailed in *Chapter 3*. These forced excitation simulations followed an identical procedure to that used to predict the acoustic characteristics of the transformer. The forced excitation simulations conducted in proximity to 400 Hz have identified a mode shape characterised by the global deformation of the tank cover.

In addition to the global mode shape of the tank occurring at approximately 400 Hz, the frequency spectrum illustrated in Figure 5-3 indicates that the active part has a high modal density between 360 Hz and 400 Hz. A number of active part modes (represented by circles in Figure 5-3) may therefore be excited by electromagnetic and magnetostrictive forces within this frequency range. The abovementioned observations indicate that the high noise emissions of the transformer studied in this thesis between 350 to 400 Hz likely resulted from the coincidence of:

i) A mode shape of the active part being excited by electromagnetic and magnetostrictive forces; and
ii) A global mode shape of the tank being excited by vibrations propagating from the active part.

The shape of the tank at approximately 400 Hz, characterised by the global deformation of the tank cover, is illustrated in Figure 5-4.

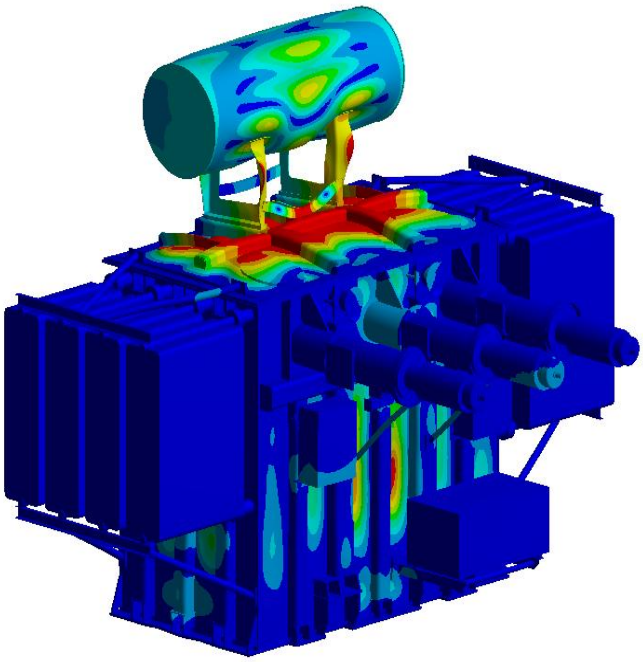

Figure 5-4 Mode shape exhibiting global deformation of the tank cover at approximately 400 Hz

5.4 COMPUTING REQUIREMENTS

Noting that the computation scheme presented in this thesis has focused on its use within the design phase of a transformer, computing requirements and simulation time are significant factors. From a design perspective, the numerical prediction tool should not require excessive simulation time, allowing for the model to be iteratively updated and an optimised solution achieved. The computing specifications used for the various numerical simulations within this investigation were as follows:

- Processors: Intel Xeon CPU E5 2867W v3 @ 3.10 Hz
- Available Memory: 256 GB
- Drive Type: Solid State

With respect to the drive type, for technical computing loads solid states drives provide up to 7.3 times increased performance when compared to HDD drives [80].

Modal and harmonic response analyses are the two dynamic structural response simulations that have been conducted within this thesis. The computation time for each for these analyses may be normalised as follows:

- Modal analysis – minutes per calculation of a single mode within a defined frequency spectrum; and
- Harmonic response analysis – minutes per simulation of the acoustic sound pressure level at a single frequency point.

Based on these normalisation factors, Table 5-1 presents the approximate computing time for the dynamic structural response simulations performed.

Table 5-1 Computing specifications

Analysis	**Reference**	**Approximate computing time**
Modal analysis – complete transformer assembly	Chapter 4.2	300 minutes per mode
Modal analysis – active part with fluid-structure interaction	Chapter 5.1	Greater than 100 minutes per mode [a]
Modal analysis – active part without fluid-structure interaction	Chapter 5.1	0.37 minutes per mode
Harmonic response analysis – complete transformer assembly	Chapter 4.3	120 minutes per frequency point
Harmonic response analysis – simplified transformer assembly	Chapter 4.3	80 minutes per frequency point

Note: [a] the simulation was aborted before completion due to excessive computing time

From the computing times presented in Table 5-1 it is apparent that performing a fully coupled fluid-structure interaction modal analysis not likely to be feasible in the design phase. This is due to the significant computing requirements of the asymmetric matrix formulation in such simulations. However, performing a structural modal analysis of the active part and analytically accounting for the added-mass effect of the fluid within the design process is realistic. As presented in *Chapter 5.3*, this analytical correction allows for an accurate quantitative estimate of noise levels and the identification of modes that may significantly influence the acoustic characteristics of a transformer.

In addition to a modal analysis of the active part, the computing requirements detailed in Table 5-1 illustrate that employing forced excitation harmonic response analyses to aid in transformer design is feasible. It has also been shown in *Chapter 5.2* that simplification of the transformer assembly – whereby removing all auxiliary equipment, including the conservator, the radiators and the bushings – reduces the computing time by approximately 33 % while not significantly influencing the accuracy of the results. Furthermore, the forced excitation harmonic response simulations presented in this thesis have also been shown to identify the global modes of the tank structure.

CHAPTER 6

SENSITIVITY ANALYSIS

This chapter presents a sensitivity analysis to better understand the influence of selected parameters on a transformer's vibro-acoustic characteristics. It is anticipated that the understanding gained from this analysis may aid in the acoustic optimisation of a transformer during the design phase. The parameters within this study have been selected on the basis that they do not affect a transformer's electrical behaviour. Parameters that have been analysed include the stiffness of the active part, the number of stiffening ribs on the tank walls, the transmissibility of vibrations between the active part and the tank and the dimensions of the tank.

The sensitivity analysis has been conducted by changing selected parameters within the numerical transformer model presented and validated in the preceding chapters. Of note is that the simplified numerical model – consisting of the active part, the tank and the insulation fluid but excluding the conservator, the radiators, the bushings and other auxiliary equipment – has been employed in these analyses. This is due to the reduced simulation time associated with the simplified model. All acoustic results presented in this chapter have been calculated at 10 Hz intervals over an analysis spectrum from 100 Hz to 400 Hz.

6.1 Influence of Active Part Stiffness

The stiffness of the active part is an important parameter as it influences the assembly's structural dynamics characteristics, with these characteristics known to significantly affect the acoustic behaviour of a transformer. As noted in Ref. [44], decreasing in the stiffness of the core results in closer spacing between the active part's natural frequencies. The higher modal density therefore increases the likelihood of an active part mode being excited, eventuating in higher noise levels.

Within this parametric study the stiffness of the active part has been increased in an effort to lower the assembly's modal density within the frequency spectrum of interest. Specifically, the Young's moduli of both the core material and the windings have been increased by 15 %. The resulting acoustic characteristics of the transformer, with a comparison to results calculated with original numerical model, are presented in Figure 6-1.

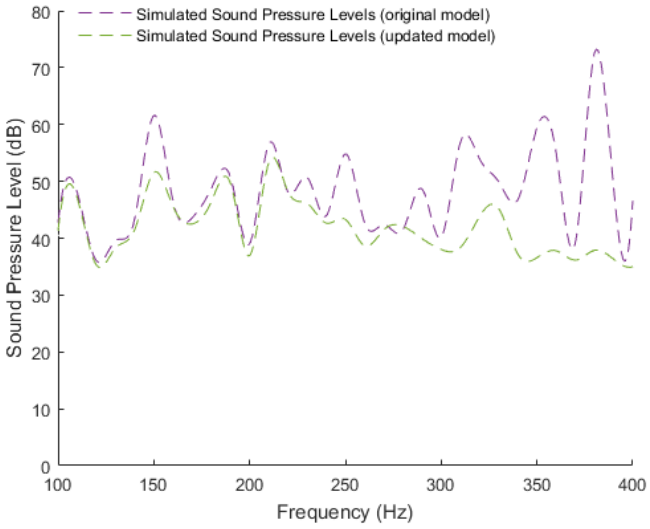

Figure 6-1 Influence of active part stiffness on the acoustic behaviour of a transformer

It is shown in Figure 6-1 that the transformer's acoustic characteristics are influenced by the stiffness of the active part. In particular, as predicted by the study in Ref. [44], increasing the stiffness of the active part has resulted in a more linear acoustic spectrum. This indicates a lower modal density of the assembly and subsequently fewer natural frequencies being excited over the analysed frequency spectrum. This is particularly true at the higher frequency ranges of the spectrum considered.

The second trend illustrated in Figure 6-1 is the notably lower noise levels calculated when the stiffness of the active part is increased. This suggests that, in addition a lower modal density, increasing the active part's stiffness has had the effect reducing the amplitude of the assembly's vibrations. The application of this result has already been implemented in shunt reactor cores, which are designed as very stiff structures to eliminate excessive vibrations [7].

Increasing the stiffness of the active part to optimise a transformer's vibration and acoustic characteristics may be carried out in numerous ways. As identified in Ref. [44], the laminations of the core significantly affect the structure's flexibility (with an increase in lamination material decreasing the stiffness of the core). Therefore, the degree of lamination applied to the core sheets and the properties of the laminating material may be optimised to provide a stiffer core. Additional methods that may be employed to increase the stiffness of the active part include further tensioning of the tie rods and increasing the clamping pressure applied to the windings.

6.2 INFLUENCE OF STIFFENING RIBS

The second parameter analysed within this chapter with respect to the acoustic emissions of a power transformer is the number of stiffening ribs placed on the tank walls. The addition of stiffening ribs is a technique frequently employed to stiffen a structure, thereby reducing the structure's vibration levels and subsequent noise radiation levels. However, as noted in Refs. [81, 82], increasing the number of ribs on a structure does not assure a systematic reduction in radiated sound power. This is due to variations in the sound radiation efficiency resulting from stiffened structures.

Within this parametric study additional stiffening ribs have been added to those already present on the tank walls. The U-shaped stiffeners included in the original design fulfil the duel purposes of increasing the tank's vacuum pressure withstand capabilities (necessary as oil-filling of a transformer is carried out under vacuum) and reducing the assembly's acoustic emissions. Within this parametric study, an additional two stiffening ribs were placed on each of the tank walls. The updated layout of the tank is illustrated in Figure 6-2.

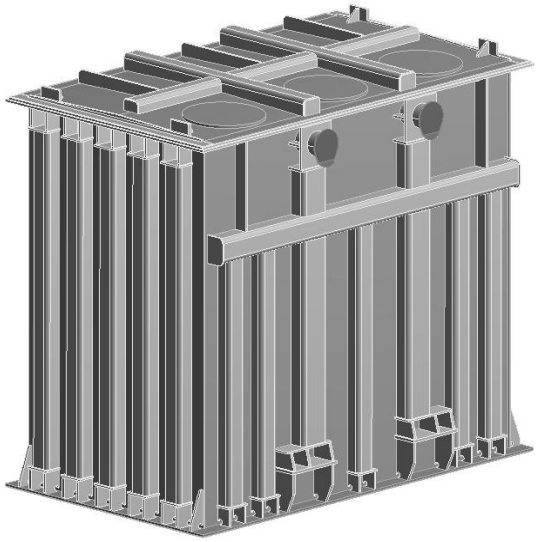

Figure 6-2 Updated tank layout of tank with additional stiffening ribs

The simulation with additional stiffening ribs of the tank wall has been conducted only to understand the degree of influence these elements have on the transformer's acoustic response. Therefore, the ideal placement of the additional ribs to reduce vibrations has not been considered. Such calculation schemes are presented in Refs. [81, 83]. The acoustic characteristics of the transformer with additional stiffening ribs and a comparison to results calculated with the original numerical model is presented in Figure 6-3.

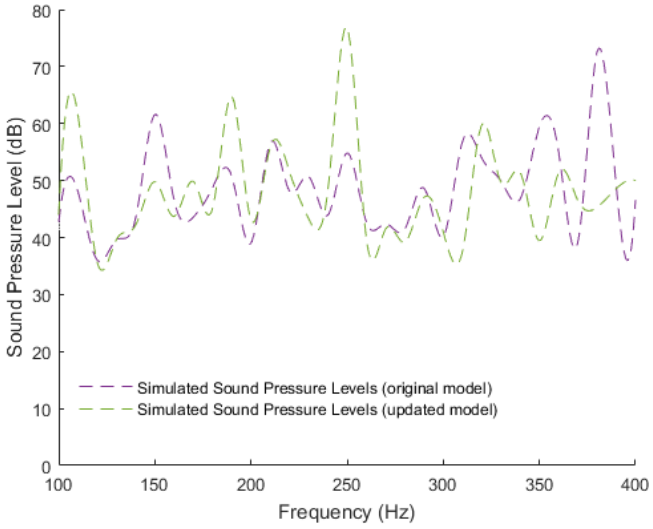

Figure 6-3 Influence of stiffening ribs on the acoustic behaviour of a transformer

With additional stiffening ribs on the tank the acoustic behaviour of the transformer has been significantly altered, as shown in Figure 6-3. In particular, the results appear to show that some natural frequencies of the assembly have been amplified while others damped by the alterations made to the tank layout. This occurrence, which is particularly visible at lower frequencies, may be attributed to 'stopping' and 'passing' bands introduced by the additional stiffeners. Further reading on the formation of these bands may be found in Refs. [20, 82, 84].

Reducing the acoustic emissions from a power transformer by optimising the number and the positioning of stiffening ribs on the tank walls would require a detailed algorithm. Such a study, as applied to a constant speed gearbox, has been conducted in Ref. [20]. The reduction of a transformer's noise emissions would however require a significantly more detailed algorithm than that employed in Ref. [20]. This is due to the complexity and individuality of transformer tank designs.

6.3 INFLUENCE OF THE DIRECT TRANSMISSION PATH BETWEEN ACTIVE PART AND TANK

As with stiffening ribs, vibration-damping pads are often used to minimise structure borne vibrations. In transformers, such pads are generally employed to isolate the active part, being the source of vibrations, from the base of the tank. However, in oil-filled transformers isolating the active part from the tank base only limits one transmission part, as the vibrations are still able to travel indirectly from the active part to the tank structure through the fluid medium.

To quantify the acoustic effects of isolating the active part from the base of the tank in an oil-filled transformer a simulation with additional damping applied to material elements connecting the active part and the tank has been conducted. Specifically, a constant damping factor of 0.3 has been applied to the rubber compound that connects the active part to the base of the transformer tank. The rubber compound measures 27 mm in height. The results of the simulation are illustrated in Figure 6-4.

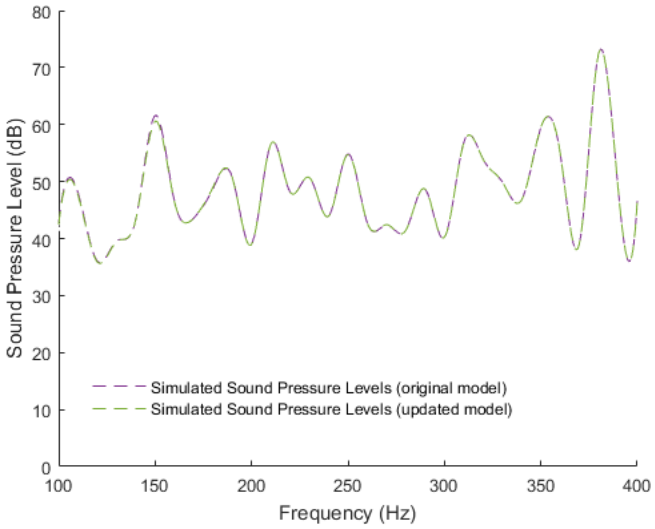

Figure 6-4 Influence of the direct vibration transmission path between the tank and the active part of a transformer

As seen in Figure 6-4 additional damping applied to the connection between the active part and the tank structure has had a limited influence on the acoustic characteristics of the studied transformer. The average decrease in the acoustic emissions of the transformer with additional damping measures 0.1 dB across the 31 corresponding simulation points[9]. Therefore, it appears that the primary transmission path from the active part to the tank of the transformer is through the fluid medium. It should also be noted that no assertion is made in this thesis as to the probability of being able to achieve additional damping of 0.3 between the active part and tank of a transformer.

6.4 INFLUENCE OF TANK DIMENSIONS

The final parameter studied within this chapter is the influence of tank dimensions on a transformer's acoustic response. Tank dimensions are generally calculated with regard to the dimensions of the active part, the eddy current losses in the tank walls (which result from magnetic field leakage) and material costs. These factors make altering the dimensions of the tank more complicated than the parameters previously discussed.

To identify how tank dimensions influence a transformer's acoustic response the length of the tank in the numerical model has been increased by approximately 10 %. It is noted that due to the elongation of the tank the placement of the stiffening ribs relative to the four corners of the tank has also been altered. The acoustic characteristics of the transformer with an elongated tank and a comparison to those sound pressure levels calculated with the original numerical model are presented in Figure 6-5.

[9] The greatest vibration damping effect has been noted in the lower frequency ranges of the numerical simulation. Specifically, between 100 Hz and 150 Hz an average decrease of 0.3 dB is calculated across the six simulation points. Above 150 Hz it is likely that the stiffness damping coefficient applied globally to the numerical model (refer to *Chapter 3.6.3*) becomes dominant and therefore the localised constant damping applied to the elements connecting the active part of and the base of the tank has minimal effect.

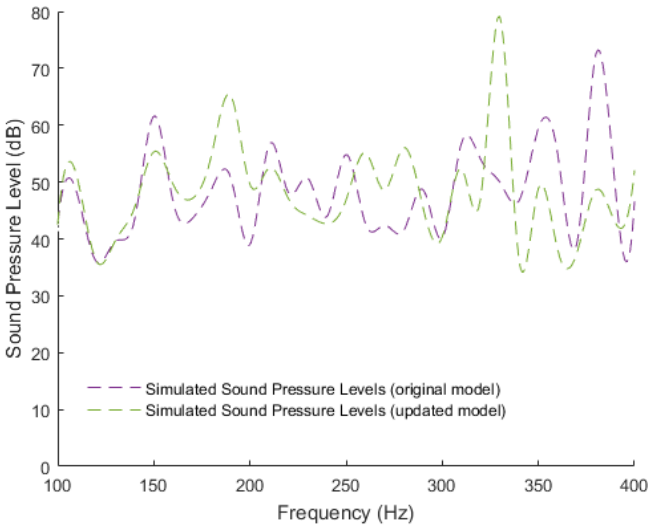

Figure 6-5 Influence of tank dimensions on the acoustic behaviour of a transformer

From Figure 6-5 is it apparent that the elongation of the transformer tank has influenced the acoustic response of the unit. However, there is no clear correlation between acoustic response of the original design and the updated assembly. Furthermore, from the results presented in Figure 6-5 it cannot be concluded whether the change in acoustic characteristics is due to the increased oil volume within tank, the tank's revised structural design or a combination of these aforementioned factors.

6.5 CONCLUSIONS

This chapter has detailed a sensitivity analysis to better understand influence of selected parameters on the sound pressure levels and vibration characteristics of a large power transformer. Four parameters selected on the basis that they do not influence the electrical behaviour of the unit have been considered, being: the stiffness of the active part; the number of stiffening ribs placed on the tank walls; the transmissibility of vibrations between the active part and the tank; and the dimensions of the tank. The analysis was conducted by changing the selected parameters within the numerical model presented and validated in the preceding chapters of this thesis.

From the analyses presented within this chapter it has been seen that the stiffness of the active part is the parameter best suited to optimise the acoustic behaviour of a transformer. Specifically, increasing the active part's stiffness has been shown to result in a more linear acoustic spectrum with lower sound pressure levels. These results indicate that the increased stiffness has had the effect of reducing the assembly's modal density while also eliminating excessive vibrations.

CHAPTER 7

CONCLUSIONS AND FUTURE WORK

7.1 CONCLUDING REMARKS

This thesis has presented the vibro-acoustic model of a large power transformer, which allows the vibration and acoustic characteristics of the unit to be determined. The model has been discretised and solved using the finite element method and accounts for the bi-directional fluid-structure interaction between the active part, the insulation fluid and the tank. Although a series of previous investigations have employed the finite element method to predict the vibration characteristics of individual transformer components, the narrow scope of these previous analyses and the absence of acoustic elements limit their ability to qualitatively or quantitatively predict the complex acoustic characteristics of a power transformer.

The two most comparable studies to that presented in this thesis, being those detailed in Ref. [3] and Ref. [4], are limited by the omission of the transformer core. This omission has led to simplifications and assumptions that do not allow for the prediction of a transformer's acoustic behaviour under nominal operating conditions. The shortcomings of the models presented in Refs. [3, 4] include:

- The vibration characteristics of the transformer core, which may significantly affect a transformer's overall sound pressure levels, are overlooked;
- Only the acoustic emissions at double the line frequency are considered, being those at 100 Hz. This is a simplification that does not hold true in reality due to the significant sound emissions from a transformer at even harmonics of the line frequency; and
- The omission of the core structure has necessitated the use of spring elements to support the winding blocks within the numerical models presented in Refs. [3, 4]. However, the values assigned to these spring elements have not been experimentally validated.

The vibro-acoustic modelling methodology adopted in this thesis has attempted to address the limitations in preceding works. Specifically, all key structural elements (i.e. the core, the windings, and the tank, as well as the significant components connecting these assemblies) and the insulation fluid have been incorporated into the numerical model. Furthermore, validation of the acoustic predictions has been conducted at 16 frequency points across a 100 Hz to 400 Hz analysis spectrum. Of note is that this spectrum is considered as dominant in the acoustic response of a large power transformer.

The procedures employed in this thesis have been discussed in detail in the previous chapters. A summary of the methodology employed for predicting the vibration and acoustic characteristics of a transformer during the design process is given as follows:

i) Develop a vibro-acoustic numerical model of the studied power transformer employing the finite element method with the active part, the insulation oil and the transformer tank included in the model;

ii) Determine the vibration characteristics of the active part through a structural modal analysis, noting that the added-mass and viscous damping effects of the insulation fluid may be accounted for through analytical correction of the assembly's natural frequencies;

iii) From the modal analysis conducted in step *ii* analyse the modal mass participation factors of the active part to gain a qualitative prediction of noise levels over the studied frequency spectrum;

iv) Apply excitation forces to the numerical model of the complete transformer (which incorporates the active part, the insulation oil and the transformer tank), with the applied forces simulating the electromagnetic and magnetostrictive forces acting on the active part;

v) Map the vibration velocity of the tank structure, as calculated in step *iv*, to an external acoustic body that replicates the test or operating surrounds of the transformer and hence calculate the radiated sound pressure levels;

vi) Repeat steps *iv* and *v* at frequency points spaced over the frequency spectrum of interest; and

vii) Calculate of the operational acoustic emissions through the combination of sound pressure levels determined at each of the three dominant harmonics of the electromagnetic and magnetostrictive forces (noting that step *vii* has not been performed in this thesis).

The procedures detailed above are nonspecific and may be applied to any transformer. In addition to these generic procedures this thesis has: validated the vibro-acoustic numerical methodology; identified the key vibration characteristics of the transformer studied; conducted a sensitivity analysis of the key design parameters influencing a transformer's acoustic behaviour; and detailed a novel damping estimation methodology. Concluding remarks applicable to these studies are as follows:

i) Validation of the vibro-acoustic methodology was conducted through the comparison of numerical and experimental results. Both a structural and an acoustic validation of the model was performed, noting:
   - Numerical and experimental modal results showed a high level of correlation with the average difference between the natural frequencies of the first six comparable modes found to be 2.9 %;
   - The acoustic validation of the numerical model was conducted over a 100 Hz to 400 Hz spectrum and illustrated that the applied methodology identified both the transformer's global and local acoustic behaviour. The accuracy of the sound pressure level predictions was shown to be in line with comparable preceding studies.

ii) Analyses conducted with the validated vibro-acoustic model showed that the vibration characteristics of the active part significantly influence the overall acoustic response of a transformer. The numerical model also illustrated how the frequency overlap of active part and tank modes can result in increased noise levels.

iii) The sensitivity analysis conducted in this thesis concluded that the stiffness of the active part is the parameter best suited to optimise a transformer's acoustic behaviour. Specifically, increasing the active part's stiffness is shown to produce a more linear acoustic spectrum with lower sound pressure levels.

iv) A novel damping estimation technique was presented to determine the modal damping of the complex oil-filled transformer assembly, noting:

- The damping estimation technique methodology estimates modal damping within defined bandwidths as opposed to at natural frequency points, allowing for damping estimates to be computed of complex structures with high modal densities; and
- The partial numerical validation conducted suggests that the methodology is able to provide a good estimate of a complex system's damping characteristics over a wide frequency spectrum.

In summary, the numerical methodology presented in this thesis is shown to identify the acoustic behaviour of a transformer through numerically calculated sound pressure levels. These acoustic emissions result from excitation forces applied to both the core and the windings. Furthermore, the vibro-acoustic modelling scheme and analyses methods, including a modal mass participation factor analysis of the active part, allow for the complex vibration characteristics of a transformer to be identified. An understanding of these vibration characteristics together with sound pressure level predictions will better enable transformer manufacturers to consistently meet acoustic targets while also reducing the costly safety margins in current design practices.

7.2 FUTURE WORK

As presented in the preceding chapters, this thesis has detailed and validated a numerical methodology able to predict the noise and vibration characteristics of a large power transformer. However, areas of further research have also been identified. These future works focus on the assumptions and limitations of the modelling methodology, which are potential sources of error and may account for the discrepancies between predicted and measured values in this thesis. The limited scope of the work presented in this thesis is also to be addressed in future investigations.

It is proposed that the first study to follow this thesis is the application of the modelling methodology to a three-phase large power transformer. This work is seen as significant as three-phase large power transformers are the most commonly utilised class of transformer in transmission networks. The principal challenge of this proposed investigation is the determination and application to the finite element model of the electromagnetic and magnetostrictive forces resulting from three-phase excitation. In this thesis a single-phase unit has been considered which, in comparison to a three-phase transformer, greatly simplified the calculation and application of the excitation mechanisms.

Having validated the numerical modelling methodology in this thesis, it is proposed that a future study determines the total sound pressure levels of a transformer under nominal operating conditions employing the computational scheme presented. This would require the non-linearity of the excitation forces to be accounted for. Specifically, the magnitude of the excitation forces and the first three even harmonics of the network would need to be determined and applied to the numerical model. Estimation of a transformer's acoustic emissions under nominal operating conditions would then be made through the combination of the sound pressure levels determined at the aforementioned harmonics.

As previously discussed in this thesis, the vibration characteristics of the active part are a significant factor in the acoustic behaviour of a transformer. However, no explicit experimental modal analysis of the active part was conducted within this thesis. Conducting a detailed EMA to validate the numerical modelling of the active part in future works is therefore of importance, with a focus on experimental modal measurements of:

- The windings blocks – to validate the homogeneous body employed to simulate the windings within the finite element model; and
- The core – to validate modal mass participation factors and mode shapes resulting from the numerical modal analysis of the active part.

Within this thesis all thermal effects on the vibration and subsequent acoustic characteristics of a transformer have been disregarded. However, assuming that the thermal environs and operating temperatures do not affect the sound emissions of a transformer is not valid. Future works may therefore consider how thermal factors (i) affect and (ii) may be accounted for within the numerical modelling of power transformer noise.

In addition to finite element modelling procedures, the damping estimation technique presented in this thesis to determine the modal damping characteristics of the transformer tank may be improved upon and further validated. In particular, it has been noted previously that the primary source of error associated with the methodology is considered to result from taking the IFFT of the FRF signal. However, within this thesis no steps have been made to correct this purported error. Furthermore, the damping estimation technique may be further validated through a detailed analytical study aimed at describing the statistical properties of the proposed estimators.

As noted in the assumptions detailed at the beginning of this work, the excitation forces employed in this thesis were determined analytically and provided by Siemens AG. Although it may not improve the accuracy of the vibro-acoustic predictions, the numerical methodology presented in this thesis may be extended to incorporate a coupled electromagnetic finite element calculation. The primary advantage of the coupled electromagnetic simulation would be the detailed force distribution of the excitation mechanisms to the structural finite element model. Accounting for all excitation mechanisms within a numerical multi-physics simulation to predict transformer noise would amount to a significant body of research.

REFERENCES

[1] "Large Power Transformers and the U.S. Electric Grid," U. S. D. o. E. Office of Electricity Delivery and Energy Reliability, Ed., ed. [online], 2012.

[2] W. Passchier-Vermeer and W. F. Passchier, "Noise exposure and public health," *Environmental health perspectives,* vol. 108, p. 123, 2000.

[3] M. Rausch, M. Kaltenbacher, H. Landes, and R. Lerch, "Numerical computation of the emitted noise of power transformers," *COMPEL - The international journal for computation and mathematics in electrical and electronic engineering,* vol. 20, pp. 636-649, 2001.

[4] M. Kavasoglu, *Load controlled noise of power transformers: 3D modelling of interior and exterior sound pressure field*: KTH Royal Institute of Technology, School of Computer Science and Communication, 2010.

[5] P. Shuai and J. Biela, "Investigation of acoustic noise sources in medium frequency, medium voltage transformers," in *Power Electronics and Applications (EPE'14-ECCE Europe), 2014 16th European Conference on*, 2014, pp. 1-11.

[6] B. García, J. C. Burgos, and Á. Alonso, "Winding deformations detection in power transformers by tank vibrations monitoring," *Electric Power Systems Research,* vol. 74, pp. 129-138, 4// 2005.

[7] S. V. Kulkarni and S. Khaparde, *Transformer engineering: design and practice* vol. 25: CRC Press, 2004.

[8] P. S. Georgilakis, *Spotlight on modern transformer design*: Springer Science & Business Media, 2009.

[9] R. S. Girgis, M. Bernesjo, and J. Anger, "Comprehensive analysis of load noise of power transformers," in *Power & Energy Society General Meeting, 2009. PES '09. IEEE*, 2009, pp. 1-7.

[10] A. J. Moses, P. I. Anderson, T. Phophongviwat, and S. Tabrizi, "Contribution of magnetostriction to transformer noise," in *Universities Power Engineering Conference (UPEC), 2010 45th International*, 2010, pp. 1-5.

[11] D. Miljković, "Active reduction of power transformer noise based on synchronous averaging of the residual noise signal," in *MIPRO, 2012 Proceedings of the 35th International Convention*, 2012, pp. 875-880.

[12] M. H. T. Chaudhuri, G. Kmita, M. Kozupa, P. Stefanuti and R. Zannol, "Noise Management in Transformers," in *Cigre SC A2 & C4 Joint Colloquiun 2013*, Zurich, Switzerland, 2013.

[13] J. W. Pan, J.; Jin, M., "Structural vibration of a transformer," presented at the Proceeding of the 17th International Congress of Sound and Vibration, Cairo, 2010.

[14] M. P. Jin, J.; Huang, H.; Zhou, J., "Transmission of vibration of a power transformer from the internal structures to the tank," *Proceedings of Acoustics,* vol. 34, 2012.

[15] M. Jin and J. Pan, "Vibration transmission from internal structures to the tank of an oil-filled power transformer," *Applied Acoustics,* vol. 113, pp. 1-6, 2016.

[16] J.-F. Sigrist, "Structural Dynamics with Fluid–Structure Interaction," in *Fluid-Structure Interaction*, ed: John Wiley & Sons, Ltd, 2015, pp. 225-280.

[17] B. S. H. Cazzolato, C. Q., "Introduction to Damped Acoustic Systems," in *Acoustic Analyses Using Matlab and Ansys*, ed: CRC Press, 2014, pp. 255-319.

[18] W. Heylen and P. Sas, *Modal analysis theory and testing*: Katholieke Universteit Leuven, Departement Werktuigkunde, 2006.

[19] Y.-D. Kim, J.-M. Shim, K.-S. Park, Y.-M. Jeong, and D.-D. Lee, "Structure Vibration Analysis by Active Noise Control of Power Transformer," in *Computer Applications for Security, Control and System Engineering*, ed: Springer, 2012, pp. 234-244.

[20] A. Shen, "Optimised Reduction of the Radiated Noise from the Casing of a Constant Speed Gearbox," The University of New South Wales Australia, 2008.

[21] J. Helsen, F. Vanhollebeke, B. Marrant, D. Vandepitte, and W. Desmet, "Multibody modelling of varying complexity for modal behaviour analysis of wind turbine gearboxes," *Renewable Energy,* vol. 36, pp. 3098-3113, 2011.

[22] A. Seybert, T. Wu, and X. Wu, "Experimental Validation of Finite Element and Boundary Element Methods for Predicting Structural Vibration and Radiated Noise," DTIC Document1994.

[23] J. Mao, Z.-y. Hao, K. Zheng, and G.-x. Jing, "Experimental validation of sound quality simulation and optimization of a four-cylinder diesel engine," *Journal of Zhejiang University SCIENCE A,* vol. 14, pp. 341-352, 2013.

[24] I. L. Ver, D. W. Andersen, M. M. Myles, and A. M. Teplitzky, "Field Study of Sound Radiation by Power Transformers," *Power Engineering Review, IEEE,* vol. PER-1, pp. 51-51, 1981.

[25] C. G. Gordon, "A Method for Predicting the Audible Noise Emissions from Large Outdoors Power Transformers," *Power Apparatus and Systems, IEEE Transactions on,* vol. PAS-98, pp. 1109-1112, 1979.

[26] G. O. Usry, P. Saha, J. Hadden, and A. Pierce, "Prediction of Far Field Sound Radiation from Transformers," *Power Apparatus and Systems, IEEE Transactions on,* vol. PAS-99, pp. 358-364, 1980.

[27] E. Reiplinger, "Assessment of grain-oriented transformer sheets with respect to transformer noise," *Journal of Magnetism and Magnetic Materials,* vol. 21, pp. 257-261, 10// 1980.

[28] A. J. Moses, "Measurement of magnetostriction and vibration with regard to transformer noise," *Magnetics, IEEE Transactions on,* vol. 10, pp. 154-156, 1974.

[29] B. Weiser, H. Pfutzner, and J. Anger, "Relevance of magnetostriction and forces for the generation of audible noise of transformer cores," *Magnetics, IEEE Transactions on,* vol. 36, pp. 3759-3777, 2000.

[30] Y. Wang, J. Pan, and M. Jin, "Finite element modeling of the vibration of a power transformer," *The University of Western Australia,* 2011.

[31] E. I. Amoiralis, M. A. Tsili, and A. G. Kladas, "Transformer Design and Optimization: A Literature Survey," *Power Delivery, IEEE Transactions on,* vol. 24, pp. 1999-2024, 2009.

[32] M. Kaltenbacher, *Numerical simulation of mechatronic sensors and actuators* vol. 2: Springer, 2007.

[33] T. R. Chandrupatla, A. D. Belegundu, T. Ramesh, and C. Ray, *Introduction to finite elements in engineering*: Prentice Hall Upper Saddle River, 1997.

[34] E. Wang and T. Nelson, "Structural Dynamic Capabilities of ANSYS," in *ANSYS 2002 Conference, Pittsburg, Pennsylvania, USA*, 2002.

[35] H. Fukusho, T. Koseki, and T. Sugimoto, "Control of a straight line motion for a two-link robot arm using coordinate transform of bi-articular simultaneous drive," in *2010 11th IEEE International Workshop on Advanced Motion Control (AMC)*, 2010, pp. 786-791.

[36] (2015, Introduction to Acoustics: Acoustics ATCx Extension R160.

[37] M. Gad-el-Hak, "Questions in Fluid Mechanics: Stokes' Hypothesis for a Newtonian, Isotropic Fluid," *Journal of Fluids Engineering,* vol. 117, pp. 3-5, 1995.

[38] G. Dhatt, E. Lefrançois, and G. Touzot, *Finite element method*: John Wiley & Sons, 2012.

[39] C. Q. Howard and B. S. Cazzolato, *Acoustic Analyses Using Matlab® and Ansys®*: CRC Press, 2014.

[40] P. Hamberger, A. Hauck, M. Kaltenbacher, F. Bachinger, M. Dibold, H. Irschik*, et al.*, "3d-fem simulation for investigation of load noise of power transformers verified by measurements," in *Electrical Machines, 2008. ICEM 2008. 18th International Conference on*, 2008, pp. 1-4.

[41] M. Ertl and H. Landes, "Investigation of load noise generation of large power transformer by means of coupled 3D FEM analysis," *COMPEL - The international journal for computation and mathematics in electrical and electronic engineering,* vol. 26, pp. 788-799, 2007.

[42] Y. Chen, Y. Li, Y. Peng, and L. Luo, "Vibration modal analysis and calculation of a new HVDC converter transformer with inductive filtering method," in *2015 5th International Conference on Electric Utility Deregulation and Restructuring and Power Technologies (DRPT)*, 2015, pp. 1683-1688.

[43] R. Haettel, M. Kavasoglu, A. Daneryd, and C. Ploetner, "Prediction of Transformer Core Noise."

[44] R. S. Masti, W. Desmet, and W. Heylen, "On the influence of core laminations upon power transformer noise," in *Proceedings of ISMA*, 2004, pp. 3851-3862.

[45] H.-S. Liu, L. Ma, Y.-T. GU, and S. Nielsen, "Numerical investigation of mechanical and thermal dynamic properties of the industrial transformer," *International Journal of Computational Methods,* vol. 11, p. 1344012, 2014.

[46] Y.-D. Kim, J.-M. Shim, K.-S. Park, Y.-M. Jeong, and D.-D. Lee, "Structure Vibration Analysis and Active Noise Control of a Power Transformer by Mobility Measurement," in *Control and Automation, and Energy System Engineering*. vol. 256, T.-h. Kim, H. Adeli, A. Stoica, and B.-H. Kang, Eds., ed: Springer Berlin Heidelberg, 2011, pp. 322-332.

[47] M. Kaltenbacher, H. Landes, and R. Lerch, "An efficient calculation scheme for the numerical simulation of coupled magnetomechanical systems," *Magnetics, IEEE Transactions on,* vol. 33, pp. 1646-1649, 1997.

[48] M. Kaltenbacher, K. Ettinger, R. Lerch, and B. Tittmann, "Finite element analysis of coupled electromagnetic acoustic systems," *Magnetics, IEEE Transactions on,* vol. 35, pp. 1610-1613, 1999.

[49] R. Girgis, M. Bernesjö, S. Thomas, J. Anger, D. Chu, and H. Moore, "Development of ultra—Low noise transformer technology," in *2011 IEEE Power and Energy Society General Meeting*, 2011, pp. 1-8.

[50] W. Kitagawa, Y. Ishihara, T. Todaka, and A. Nakasaka, "Analysis of structural deformation and vibration of a transformer core by using magnetic property of magnetostriction," *Electrical Engineering in Japan,* vol. 172, pp. 19-26, 2010.

[51] M. Mizokami, M. Yabumoto, and Y. Okazaki, "Vibration analysis of a 3tructural deformation and vibrat*Electrical engineering in Japan,* vol. 119, pp. 1-8, 1997.

[52] M. J. Heathcote and D. P. Franklin, *The J & P transformer book : a practical technology of the power transformer*, 13th ed. Burlington, MA: Newnes, 2007.

[53] M. Rausch, M. Kaltenbacher, H. Landes, R. Lerch, J. Anger, J. Gerth*, et al.*, "Combination of Finite and Boundary Element Methods in Investigation and Prediction of Load-Controlled Noise of Power Transformers," *Journal of Sound and Vibration,* vol. 250, pp. 323-338, 2/14/ 2002.

[54] M. Kavasoglu, R. Haettel, and C. Ploetner, "Prediction of Transformer Load Noise," in *Proceedings of the COMSOL Conference*, 2010.

[55] O. Dossing, "Structural Testing Part II: Modal Analysis and Simulation," *Naerum: Bruel & Kjaer,* 1988.

[56] D. J. Ewins, *Modal testing: theory and practice* vol. 15.

[57] R. Randall, G. Zurita, and T. Wardrop, "Extraction of Modal Parameters from Response Measurements."

[58] N. Thrane, J. Wismer, H. Konstantin-Hansen, and S. Gade, "Practical use of the Hilbert transform," *B&K Application Note No. bo0437-11,* 1999.

[59] R. B. Randall, *Frequency analysis*: Brül & Kjor, 1987.

[60] R. J. Allemang, "The modal assurance criterion–twenty years of use and abuse," *Sound and vibration,* vol. 37, pp. 14-23, 2003.

[61] S. Rad, "Methods for Updating Numerical Models in Structural Dynamics," Department of Mechanical Engineering, University of London: London, England, 1997.

[62] S. Ibrahim, "Correlation and updating methods: finite element dynamic model and vibration test data," in *International Conference on Structural Dynamics Modelling, Test, Analysis and Correlation*, 1993, pp. 323-347.

[63] R. Pascual, J. Golinval, and M. Razeto, "Testing of FRF based model updating methods using a general finite element program," *ISMA 21,* pp. 1933-1945, 1996.

[64] J. Winders, *Power transformers: principles and applications*: CrC Press, 2002.

[65] J. Turowski and M. Turowski, *Engineering Electrodynamics: Electric Machine, Transformer, and Power Equipment Design*: CRC Press, 2014.

[66] O. Vogel and J. Ulm, "Theory of Proportional Solenoids and Magnetic Force Calculation Using COMSOL Multiphysics," in *Proceedings of the 2011 COMSOL Conference in Stuttgart*, 2011.

[67] T. Stirl, J. Harthun, and F. Hofmann, "New Trends in Noise Reduction of Power Transformers," presented at the 21st International Conference on Electricity Distribution, Frankfurt, 2011.

[68] B. García, J. C. Burgos, and Á. M. Alonso, "Transformer tank vibration modeling as a method of detecting winding deformations-part I: theoretical foundation," *IEEE Transactions on Power Delivery,* vol. 21, pp. 157-163, 2006.

[69] R. Ming, J. Pan, M. Norton, S. Wende, and H. Huang, "The sound-field characterisation of a power transformer," *Applied Acoustics,* vol. 56, pp. 257-272, 1999.

[70] G. Shilyashki, H. Pfützner, F. Hofbauer, D. Sabic, and V. Galabov, "Magnetostriction distribution in a model transformer core," *J. Electr. Eng,* vol. 61, pp. 130-132, 2010.

[71] H. Herlufsen, "Modal Analysis using Multi-reference and Multiple-Input Multiple-Output Techniques," *Brüel & Kjær, Application Note,* 2004.

[72] T. Carne and E. Stasiunas, "Lessons learned in modal testing—part 3: Transient excitation for modal testing, more than just hammer impacts," *Experimental Techniques,* vol. 30, pp. 69-79, 2006.

[73] A. M. Iglesias, "Investigating various modal analysis extraction techniques to estimate damping ratio," 2000.

[74] D. Atherton, *Control engineering*: Bookboon, 2009.

[75] P. Danguang, "An optimization solution for Rayleigh damping coefficients in seismic response analysis," *Engineering Mechanics,* vol. 30, pp. 15-20, 2013.

[76] IEC, "Power Transformers " in *Part 10: Determination of Sound Levels*, ed: International Electrotechnical Commission, 2001.

[77] T. Irvine, "Effective modal mass and modal participation factors," *Available on the web on site:* http://www*. vibrationdata.com/tutorials2/ModalMass.pdf (last access on march 7 2016),* 2013.

[78] C. P. Green and J. E. Sader, "Torsional frequency response of cantilever beams immersed in viscous fluids with applications to the atomic force microscope," *Journal of applied physics,* vol. 92, pp. 6262-6274, 2002.

[79] C. A. van Eysden and J. E. Sader, "Frequency Response of Cantilever Beams Immersed in Viscous Fluids," *Resonant MEMS: Fundamentals, Implementation, and Application,* 2015.

[80] "Intel Solid-State Drives Increase Productivity of Product Design and Simulation," ed: Intel Corporation, 2013.

[81] K. Inoue, M. Yamanaka, and M. Kihara, "Optimum stiffener layout for the reduction of vibration and noise of gearbox housing," *Journal of Mechanical Design,* vol. 124, pp. 518-523, 2002.

[82] D. Gueorguiev, J. G. McDaniel, P. DuPont, and L. B. Felsen, "Analysis of floquet wave generation and propagation in a plate with multiple arrays of line attachments," *Journal of sound and vibration,* vol. 234, pp. 819-840, 2000.

[83] A. Shen, R. Randall, and C. Maury, "Minimisation of the Noise Radiation of Constant Speed Gearboxes," in *Proceedings of the Twelvth International Congress on Sound and Vibration*, 2005.

[84] W.-C. Xie and R. Z.-H. Chen, "Vibration mode localization in rib-stiffened plates with misplaced stiffeners in one direction," *Chaos, Solitons & Fractals,* vol. 14, pp. 311-333, 2002.